TECHNISCHE UNIVERSITÄT MÜNCHEN
LUDWIG-MAXIMILIANS-UNIVERSITÄT MÜNCHEN

THEORETICAL ELEMENTARY PARTICLE PHYSICS T30D

BOSON STARS: STRUCTURE, EVOLUTION AND DETECTION. A THEORETICAL PROPOSAL

MASTER THESIS IN
THEORETICAL AND MATHEMATICAL PHYSICS

AUTHOR:

BORIS BETANCOURT KAMENETSKAIA

THESIS ADVISOR:

PROF. DR. ALEJANDRO IBARRA

Munich 2021

First referee: Prof. Dr. Alejandro Ibarra

Second referee: Prof. Dr. Elisa Resconi

Day of the defense: Friday the 24th of September, 2021

Моему дяде Игорю.
Вечная память

Abstract

Ever since the first hints of the existence of dark matter, the scientific community has tried to understand its properties. One such effort showed that it is likely that self-interacting bosonic dark matter may be able to form invisible compact objects, known as self-interacting boson stars, with masses and sizes similar to those of neutron stars. In light of this prospect, as well as inspired by the work done on the effect of dark matter capture in stars, I consider the effect that the capture of Standard Model matter could have on this type of exotic celestial bodies and if it could lead to visible signals, which would open a new path for their detection, other than gravitational searches.

After an introduction to the subject of dark matter and motivation of the present work, the structure of self-interacting boson stars in the context of General Relativity is determined. With this information, the rate of capture of baryons, namely protons, by such a compact object is calculated. This baryonic population is then considered to ascertain the radiation mechanisms available and which signals are expected from them. The question of their detectability by modern observational efforts is then addressed in terms of the assumptions and parameters of the boson star model.

Acknowledgements

First I would like to thank the main supervisor of this thesis Prof. Dr. Alejandro Ibarra, who generously dedicated his time to me, offering me the possibility of having his invaluable experience and enlightening advice close at hand at all times.

Secondly, I thank Prof. Dr. Elisa Resconi for her patience and the time invested in the revision of this thesis, in addition to her pertinent observations.

Subsequently, I extend my gratitude to Anja Brenner for important discussions and references, which helped to make considerable advancements towards the understanding of the subject matter.

Furthermore, I am grateful to Dr. Chris Kouvaris from the National Technical University of Athens, for very helpful and insightful discussions, which were crucial for the final chapter of this thesis.

I also extend my thanks to Dr. Robert C. Helling, manager of the TMP Master program, for his time and help with all official procedures.

I am also grateful to Renate Pfister, Christl Jarius and Herta Rogg for their hospitality, company and care during my stay in their beautiful country.

Finally, I extend my deepest gratitude to my parents, Carlos Betancourt Cid and Sofía Kamenetskaia Kotseruba, for all their support and advice, which have proven invaluable my whole life and especially during this Master's degree.

I thank the Consejo Nacional de Ciencia y Tecnología, CONACYT/Gobierno de México (National Council of Science and Technology/Mexican Government) and the Deutscher Akademischer Austauschdienst, DAAD (German Academic Exchange Service) for granting me a scholarship under the Convocatoria Becas al Extranjero Convenios DAAD 2019 - 1. Without their financial suport this Master's degree and the present work would not have been achieved.

Contents

List of Figures

Acronyms

AMS	**A**lpha **M**agnetic **S**pectrometer
BBN	**B**ig **B**ang **N**ucleosynthesis
BS	**B**oson **S**tar
CMB	**C**osmic **M**icrowave **B**ackground
DM	**D**ark **M**atter
ISM	**I**nter**s**tellar **M**edium
ΛCDM	**L**ambda **C**old **D**ark **M**atter
LHC	**L**arge **H**adron **C**ollider
MACHO	**Ma**ssive **C**ompact **H**alo **O**bject
MOND	**Mo**dified **N**ewtonian **D**ynamics
RAQUAL	**R**elativistic **AQUA**dratic **L**agrangian
SM	**S**tandard **M**odel
SIBEC	**S**elf-**I**nteracting **B**ose-**E**instein **C**ondensate
TeVeS	**Te**nsor-**Ve**ctor-**S**calar
WIMP	**W**eakly **I**nteracting **M**assive **P**article

1. Introduction

Previous research has given reason to believe that self-interacting dark matter may be able to form compact objects in a manner analogous to that of baryonic matter. These exotic bodies have been appropriately named as dark stars. Motivated by the scientific effort towards the detection of dark matter (from now on abbreviated as DM) based on its capture by stars, this thesis considers the inverse case, that is the capture of Standard Model particles by compact objects made up entirely of DM and its consequences on the dark star's evolution and observational features.

This work intends to give a general introduction to the problem of DM by discussing the efforts that have been historically made to tackle it and the models that have been designed to explain it. Making use of this theoretical background, I will proceed to calculate the equations governing the structure of a dark star, specifically a star made up of bosonic DM, hereafter named as boson star (and abbreviated as BS). I will also discuss the effects that baryonic matter would have on the evolution of these exotic compact objects and if they could emit signals that could be observed.

In summary, the main objectives of the present thesis are to establish the theoretical model for the treatment of the structure of stars formed by bosonic DM. Given their structure, the capture of visible matter by these compact objects will be estimated and their effect on the star will be discussed.

To fulfill this goal, it will be assumed that DM is a particle and it is bosonic in nature, it is able to form compact objects and it couples to protons. The hypothesis is that these stars will be able to gather enough baryonic matter, such that thermal electromagnetic radiation may be emitted. It is expected that this radiation will be able to be detected by modern observational efforts, which will set limits on microphysical parameters of DM.

This thesis is organized as follows: in Chapter 2, I offer a brief historical overview on the theoretical and experimental efforts on DM and link the relevant research avenues with this thesis. Then, in Chapter 3, the structure of a BS will be derived in terms of microphysical parameters such as the DM particle mass and its self-interaction coupling constant. Subsequently, in Chapter 4, using the previously derived results, the capture rate of protons by the star will be calculated. Afterwards, in Chapter 5, the consequences of the acquisition of these protons on the evolution of the BS will be discussed, in the context of detectable signals. In closing this chapter, the validity of the results and the assumptions that went into them are discussed. Finally, Chapter 6, summarizes this thesis, discusses how the work could be refined and possible research avenues that could be pursued in the future.

2. Dark Matter?

This chapter begins with a brief historical overview on the subject of DM and the work done towards its understanding. Afterwards, some observational evidence is touched upon with more detail, namely the observations of the Cosmic Microwave Background and the Bullet Cluster. Subsequently, the contemporary approaches to the detection of DM in the form of particles are commented on, as well as theoretical estimates in the case of DM capture in stars. Finally, the main objective of this thesis is introduced in relation to the previous subjects.

2.1. Why Dark Matter?

2.1.1. Introduction

The Standard Model (hereafter abbreviated as SM) of particle physics has been one of the greatest achievements of modern physics. Based on arguments of gauge symmetry it has been able to describe three of the four elemental forces of nature (the electromagnetic, strong and weak interactions) and classify all particles that take part in these processes. But despite its astounding success in providing experimental predictions that have withstood decades of tests at numerous ground-based accelerators and satellite-based observatories, the SM does not describe all phenomena in the Universe.

Cosmological observations have shed light on the energy content of the Universe and recent measurements (Planck Collaboration *et al.*, 2020b) have shown that today it consists approximately of 32% matter and 68% dark energy, which is the name given to the component of the material content of the Universe that varies only slowly with time and space and so acts like Einstein's cosmological constant Λ (Peebles and Ratra, 2003). The matter content is further divided into baryonic matter (5% of the total energy content) and DM (27% of the total energy content). The SM of particle physics has been greatly successful at accounting for the interactions of the baryonic matter, but has left questions about the nature of the dark component unanswered.

Nevertheless, the existence of DM (or invisible, as it was first called) has been presumed since much earlier (see Bertone and Hooper, 2018 for a very precise chronology). This presumption dates as far back as the middle of the 19th century with the work of the mathematician Friederich Bessel, who argued that the proper motion of the stars Sirius and Procyon could only be explained by the presence of invisible stars. Astronomers of the time also considered invisible matter in the form of dark clouds or "dark nebulae" and in the early 20th century Lord Kelvin and Henri Poincaré made a dynamical estimate of DM in the Milky Way. Poincaré's article from 1906 was one of the first instances where the words "dark matter" were explicitly mentioned ("matière obscure" in French) and in it he concluded that its amount was likely to be less than or similar to that of visible matter (Poincaré, 1906).

Approximately 30 years later, in the famous article from 1933, the astronomer Fritz Zwicky employed Poincaré's ideas of applying the virial theorem to determine the mass of the Coma cluster; a cluster of galaxies that presented a large velocity dispersion (up to the order of 1000 $\frac{\mathrm{km}}{\mathrm{s}}$) between eight of its galaxies. He estimated the mass of the cluster as the product of its number of observed galaxies (800) with the average mass of a galaxy. Then, he approximated the potential energy of the system with an estimate of its physical size to obtain its potential energy. With these calculations, he roughly estimated the average kinetic energy and a velocity dispersion. His findings showed that the velocity dispersion of the 800 galaxies that conformed this cluster should be around 80 $\frac{\mathrm{km}}{\mathrm{s}}$. Given the large discrepancy between his theoretical estimation and the observations, as the individual galaxies were moving too fast to be gravitationally bound only to luminous matter, Zwicky concluded that DM is present in greater amount than luminous matter (Zwicky, 1933).

This conclusion would be met with skepticism from the astronomical community and numerous explanations would be provided to account for the galaxies that presented such a large velocity dispersion. One such possibility was that these galaxies were temporary, that is, not bound to the gravitational potential of the cluster and that they had simply fallen into it (Holmberg, 1940). Other researchers doubted the validity of the virial theorem that Zwicky had applied and argued that clusters were unstable and rapidly expanding systems, but this reasoning was in contradiction with the estimated ages of galaxies, as it implied that the age of the cluster would be less than that of its galaxies (Burbidge and Burbidge, 1959).

Another key observation that played an important role in the problem of DM, but at a smaller scale than that of clusters, were the rotation curves of galaxies, namely the circular velocity profile of the stars and gas in a galaxy, as a function of their distance from the galactic center. Rotation curves can be applied to obtain the mass distribution of galaxies, thus providing another tool for the calculation of the so-called “mass-to-light ratio”. Another reason why this observation is important is the profile itself, as exemplified by Figure 2.1:

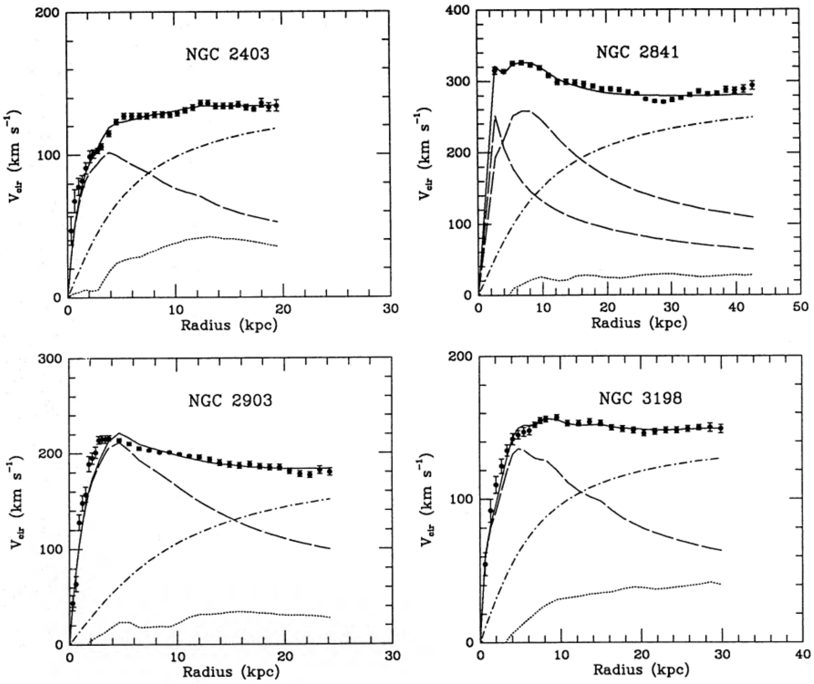

Figure 2.1.: Some examples of rotation curves of some galaxies. The dotted, dashed and dash-dotted lines are the contributions of gas, disk and DM, respectively. Begeman, Broeils, and Sanders, 1991

Today, it is expected that rotation curves exhibit a characteristic flat behavior at large distances. Using a Newtonian analysis, one obtains that the circular velocity should be

$$v(r) = \sqrt{\frac{GM(r)}{r}}, \tag{2.1}$$

where the mass is defined as $M(r) = 4\pi \int r^2 \rho(r) dr$ with $\rho(r)$ the mass density profile. Outside of the galaxy ($r > R$, where R is the radius of the galaxy's optical disc) it would be expected that the mass reaches its maximum and remains constant, which would lead to a circular velocity proportional to $1/\sqrt{r}$. This disagrees with measurements, however, as illustrated by the data points of Figure 2.1, where a behavior with a constant rotation curve for large radii is observed. A non-changing circular velocity would imply a scaling of the mass as $M(r) \propto r$, which in turn would mean a density scaling $\rho(r) \propto 1/r^2$, a result consistent with invisible particles behaving as an ideal gas.

Such rotation curves were obtained in the early 20th century, with one prominent example given in 1939 by Babcock, 1939, who calculated the mass distribution of the Andromeda galaxy using this approach, and he recognized that the rotation curve at large radii implied the existence of large amounts of mass in the outer parts of the galaxy. Nevertheless, his conclusion was conservative, as he assigned the invisibility of this surplus of mass in the furthest regions to absorption effects or "new dynamical considerations" which affected the baryonic mass distribution of the galaxy.

The scientific community would find itself in a state of confusion for the subsequent 40 years after Zwicky's and Babcock's articles, as following research would measure the masses and luminosities of several astrophysical objects, as well as the rotation curves for several galaxies, and find their mass-to-light ratio to be larger than 1 (which was the assumption at the time), often times by several orders of magnitude (one such example given by Schwarzschild, 1954), with no explanation provided by baryonic matter.

It is worth to mention the work performed by Vera Rubin and Kent Ford during this time frame. They performed spectroscopic observations of the Andromeda galaxy (Rubin and Ford, 1970) which, compared to Babcock's earlier work, extended further away from the galaxy's center (120 arcminutes) and were of much better quality. Their analysis showed a flattening of the rotation curve at large radii, which was in line with 21-cm line observations performed previously. They took their work further in the years following this publication and applied their methods to 21 galaxies with a large range of luminosities and radii (Rubin, Ford, and Thonnard, 1980). Their findings showed that the flattening of the curve was not unique to the Andromeda galaxy, rather it was a general feature of their analyzed dataset. As such, they were able to strongly conclude that it "is inescapable that non-luminous matter exists beyond the optical galaxy".

It was until the 1970's that the community started to accept the idea of a mass discrepancy in galaxies. This was exemplified by Freeman, 1970 who analyzed data from the galaxies NGC 300 and M33 and concluded that, if they were correct, there must be undetected matter in both galaxies, whose mass must be as large as the detected mass, but with a very different distribution. Such an analysis was repeated by several authors for different sets of galaxies. An example of such exponents were Roberts and Rots, 1973, who analyzed the galaxies M31, M101, and M81 and concluded, much like Freeman, that a significant unseen mass density was implied at large distances.

Further articles tackled this issue (Ostriker, Peebles, and Yahil, 1974; Einasto, Kaasik, and Saar, 1974). They accounted for the mass excess with different models, such as intermediate and late dwarf M stars or the presence of large amounts of gas in the outer parts of galaxies. Such models were further expanded and many others were introduced by subsequent papers throughout the decade. It was around this time when the scientific community began to theorize and discuss the composition of the additional material and its nature.

The first candidates came from a link with cosmological results, like in the work from Szalay and Marx, 1976 where the authors connected the missing mass density of the Universe (more on this in Section 2.1.2) with the missing mass phenomenon in galactic clusters. They were inspired by previous work on the subject, such as the article by Gershtein and Zel'dovich, 1966, in which they treated the freeze-out of massive thermal relics due to the expansion of the Universe, and discussed the upper limit on neutrino masses. Szalay and Marx proposed relict cosmological neutrinos, produced in the hot era after the Big Bang, as an explanation to the excess mass in the scale of cosmology and galactic clusters. Neutrinos had been a sensible choice for this missing mass, as within the known particles in the SM, they were the only stable, electrically neutral, and not strongly interacting examples that the theory naturally provided.

Nevertheless, the nature of neutrinos as relativistic (hot), collisionless particles implied a "top-down" formation in the history in the Universe, that is, that big structures formed first in the Universe. In the mid 1980's, research in a similar line as the one of Peebles, 1984 found, however, groups and clusters that were younger than the galaxies they contained, a so called "bottom-up" process of structure formation. Therefore neutrinos lost strength as a viable DM candidate.

As such, it became accepted that SM neutrinos could not make up the largest part of the DM in the Universe, but they led to the discussion of other "unknown" particles with characteristics similar to those of the neutrino that were not considered by the SM.

One such effort, that began in the 1970's and has maintained traction up to recent days, is the case of "supersymmetry". Supersymmetry lies in the possibility that nature may contain a space-time symmetry relating fermions to bosons. Such a symmetry requires that for every fermion, a boson must exist with the same quantum numbers (the fermion's "superpartner"), and vice versa. As such, this theory leads to the existence of several non-SM particles which, like the neutrino, are electrically neutral and non-strongly interacting. A few examples are the superpartners of the neutrinos, Z boson, photon, Higgs boson, and graviton. In the case that any of these new particles was stable, it would be a strong candidate to explain the cosmological abundance and the missing mass in smaller scales. Such has been the point of view of supersymmetric research since the 1980's, as exemplified by the work of Ellis *et al.*, 1984.

The reason why supersymmetry has had the staying power to remain an active field of study today, is that the theory does not only provide several DM candidates (the lightest neutralino, in particular), but it also has the ability to solve the electroweak hierarchy problem, and to enable gauge coupling unification, so it is also an interesting point of research, even outside the DM problem.

In spite of that, supersymmetric particles were not the only strong contenders in particle physics that emerged as a possible solution to the missing mass problem. Wilczek, 1978 suggested the “axion” based on a mechanism by Peccei and Quinn, 1977 to solve the strong CP-problem. The axion is a very light and very feebly interacting particle, as was concluded by Kim, 1979 and Dine, Fischler, and Srednicki, 1981. As such, being stable over cosmological timescales, any axions produced in the early Universe would survive and, if sufficiently numerous, could constitute the DM.

The axion and supersymmetric particles remain the most popular candidates today, but alternatives had also been proposed from the astrophysical side of the spectrum. Two important ideas were: massive compact halo objects (hereafter abbreviated as MACHOs) and Modified Newtonian Dynamics (from now on abbreviated as MOND).

MACHOs are astronomical bodies that emit little to no radiation and are composed of SM matter. Examples of bodies that conform the MACHOs are black holes, neutron stars, faint stars and planets. Their search method is the fairly recent technique of gravitational microlensing. The main idea behind it rests on the prediction from General Relativity that, if a massive object lies directly on the line of sight to a much more distant star, then the light emitted from the star will be bent. Microlensing searches examine huge numbers of stars in nearby galaxies and look for variations of light consistent with this bending. The duration of the variation measures a combination of the intermediate object’s mass (the expected MACHO, which is also named as lens in this scenario), its velocity perpendicular to the observer’s line of sight, its distance and the light-emitting object’s separation from the observer. This last quantity can be determined since it is visible, but the other three physical parameters cannot. However, statistically, one can use information about the halo density and velocity distribution, to gain information about the MACHO masses.

The results from early microlensing searches is that the mass of the objects is above the brown dwarf limit 0.1 $M_{\odot}$ and the galactic halo MACHO fraction is around 0.5 (Griest, 2002), but more recent analyses have shed doubt on the validity of these observations (Hawkins, 2015). However, the plausibility of a Galactic halo composed entirely of compact bodies has not been ruled out.

The MACHO proposal was more in line with the ideas of the 1930’s about the composition of DM. Unfortunately, it encountered problems since its creation. On the one hand, several arguments were presented to expect detectable signals from such objects, such as those given by Hegyi and Olive, 1983. On the other hand, the theory of Big Bang Nucleosynthesis (from now on abbreviated as BBN) suggested that the number of baryons in the Universe was just enough to constitute a small fraction of the total DM (Reeves *et al.*, 1973). More recent observations from microlensing surveys such as EROS-2 were able to confirm this last counterargument and found that MACHOs could, at most, account for only 8% of the galactic DM (Tisserand *et al.*, 2007).

The other astrophysical alternative was that of MOND, proposed by Mordehai Milgrom in 1982 and published in three articles in 1983 (Milgrom, 1983c; Milgrom, 1983a; Milgrom, 1983b). The heart of Milgrom's proposal was that Newtonian dynamics were modified when the acceleration of a particle was smaller than a value a_0 of order $\mathscr{O}(10^{-10}\ \frac{\mathrm{m}}{\mathrm{s}^2})$, that is, that Newton's second law had to be modified for small accelerations to be of the form $F = m\frac{a}{a_0^2}$. Milgrom argued that all past astronomical observations that had led to the mass problem, which in turn made way for the ideas of DM, were instead a discovery of evidence for a new framework of dynamics and gravity.

Immediately there were some concerns with Milgrom's proposal, as the excruciatingly tested theory of General Relativity reduced to Newton's laws in the weak field limit and not to MOND. Milgrom and collaborators worked to embed MOND in a relativistic framework in the so-called Relativistic AQUAdratic Lagrangian theory (RAQUAL). Unfortunately, there were still observational issues, in particular that the modifications needed to explain galactic scale observations did not simultaneously explain phenomena on cluster scales.

Despite these difficulties MOND-like theories kept being worked on, until the appearance of Tensor-Vector-Scalar gravity (hereafter abbreviated as TeVeS), a theory developed by Bekenstein, 2004, which has become the leading theory of MOND. The theory contains, beyond those of General Relativity, two additional fields, three free parameters and one free function. The addition of these new mathematical structures made TeVeS limited in its predictive power, but flexible enough to account for astrophysical observations. The success was short lived, however, as in 2006 Douglas Clowe and collaborators (Clowe *et al.*, 2006) analyzed the previously discovered Bullet Cluster (Tucker, Tananbaum, and Remillard, 1995), and showed that it had a behavior that could not be described by MOND, but could be naturally be explained by the existence of DM (more on this in Section 2.1.3).

Rather unexpectedly, instead of bringing MOND-like theories to an end, the observations of the Bullet Cluster have attracted significant attention to such mechanisms. Amusingly enough, some authors have noticed that the astrophysical observations could be explained by TeVeS if some of the additional degrees of freedom of the theory behaved much like cold DM (Skordis, 2008), a possibility that contradicts the original idea of MOND.

By the end of the 1980's a numerous amount of models had been proposed as a solution to the missing mass problem, but observational evidence provided strong arguments against modifications of gravity, baryonic objects and even SM particles. Therefore, cold DM in the form of some unknown particle became the leading line of work, with compelling motivation in particular towards supersymmetric models and the axion. This paradigm shift led to a diverse list of exotic models of particles outside of the SM, such as Kaluza-Klein states, Q-balls, mirror particles, to name a few. I refer to the work of Bertone, Hooper, and Silk, 2005 and references therein for a more extensive overview of the models.

Yet, despite the huge amount of DM particle candidates, some of which are presented in Figure 2.2, there was a striking common characteristic between many of the proposals. It was that the particle could not be too light (roughly heavier than $\sim$1-100 keV). This constraint came from cosmological arguments, as a lighter particle species would not be able to freeze-out of thermal equilibrium in the early Universe and become a cold relic, much like the neutrinos.

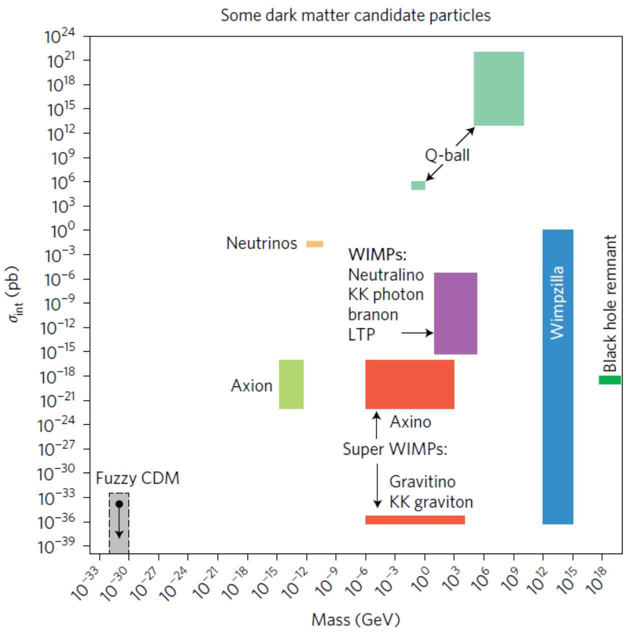

Figure 2.2.: DM candidates indicating the interdependence of the interaction cross-section and particle mass (Conrad and Reimer, 2017).

As an astonishing consequence, in order for the predicted cold relic abundance to match the observed cosmological DM density, the annihilation cross-section of the new proposed particles had to be of the order $\langle \sigma v \rangle \simeq 3 \times 10^{-26}$ cm^{3}s^{-1} (where v is the relative velocity between the annihilating particles). The reason why this result was surprising is that this value is very close to the cross section of weak force interactions. This curious coincidence, combined with theoretical arguments in favor of the electroweak scale being a natural place for the appearance of new physics birthed a paradigm that became known as the Weakly Interacting Massive Particle (subsequently abbreviated as WIMP), and has since become the leading class of particle DM candidates.

Investigation on the subject has continued until this day and DM presents one of the most important areas of research in the field of astrophysics and particle physics.

2.1.2. Cosmic Microwave Background

In the previous section it was discussed that astrophysical measurements on the scales of galaxies and clusters of galaxies were compelling evidence for the existence of DM. In spite of this, these observations did not shed light on the total amount of DM in the Universe. Such information is provided by measurements on the cosmological scale and can be extracted from the analysis of the so-called Cosmic Microwave Background (hereafter abbreviated as CMB).

The CMB is background electromagnetic radiation that permeates the Universe which originated from the propagation of photons in the early Universe after they decoupled from matter around 370,000 years after the Big Bang. It was first measured by McKellar, 1941 using spectrographic observations of CN stellar absorption lines performed by W. S. Adams. Later theoretical work by Gamow, 1948 with some later corrections performed by Alpher and Herman, 1948 showed the need of CMB for consistency with early cosmological models. It was finally rediscovered and brought attention to years later by Penzias and Wilson, 1965 with theoretical explanations provided as a companion article by Dicke *et al.*, 1965.

At the time of photon decoupling, the universe was filled with a hot, opaque plasma of protons, electrons and photons. During this epoch free electrons became bound to protons to form hydrogen atoms in an excited state. When the atoms transitioned to the ground state, they emitted photons which were not recaptured by other hydrogen atoms and were free to propagate freely. The light produced from these reactions was mostly in the visible and ultraviolet energy ranges, but the expansion of the Universe has redshifted this radiation toward longer wavelengths; as such today it appears in the microwave band.

The primordial plasma at the time was almost completely uniform, but it did have slight deviations, namely spots that were slightly (1 part in 100,000) more or less dense. These fluctuations are reflected in temperature fluctuations. The slight changes in the intensity of the CMB across the sky are able to give a map of the Universe at these early times, such as the one from Figure 2.3.

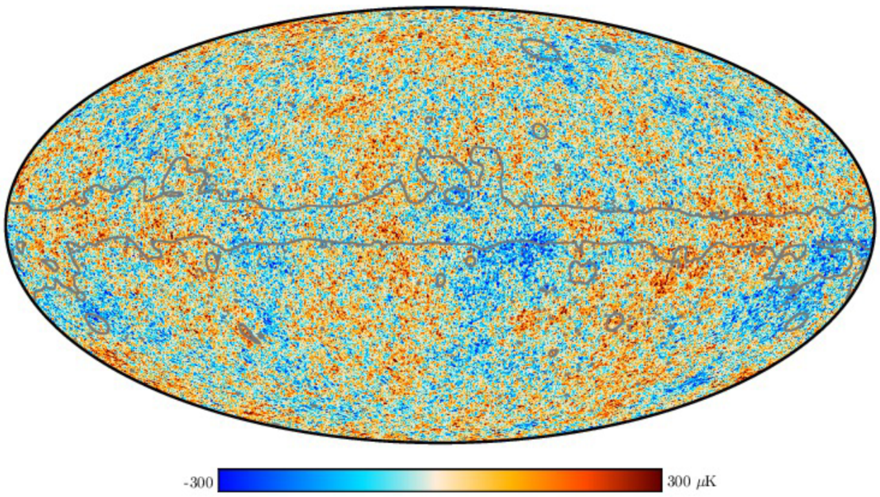

Figure 2.3.: The anisotropies of the Cosmic microwave background as observed by Planck. Planck Collaboration *et al.*, 2020a

The CMB is almost perfectly isotropic (it has tiny temperature fluctuations of the order $\frac{\delta T}{T} := \theta(\vec{n}) \sim \mathscr{O}(10^{-5})$, for a position $\vec{n}$ in the CMB map) and emits with a black body spectrum with a temperature $T = 2.725$ K $= 2.3 \times 10^{-4}$ eV. The structure of these fluctuations has been analyzed using the correlation of two measurements separated by some angle ϕ and expanded in terms of spherical harmonics as

$$\langle \theta(\vec{n})\theta(\vec{n}') \rangle = \sum_l \frac{2l+1}{4\pi} D_l^{TT} P_l(cos\phi), \tag{2.2}$$

where the angular coefficient D_l^{TT} is the angular temperature power spectrum, $P_l(cos\phi)$ are the Legendre polynomials and l are the multipole elements, related to a specific angle by $\phi_l \sim \frac{2\pi}{l}$.

Most of the cosmological information that is obtained from the CMB is found by studying different angular power spectra. These are plots of the amount of fluctuation in quantities from the CMB at different angular scales on the sky. The main quantities that are considered are the temperature (as mentioned above), but other measurements of interest are the temperature-polarization cross-spectrum, the E mode of polarization, and the lensing potential. Figure 2.4 shows measurements of the temperature power spectrum reported by the Planck collaboration. Large angular scales are at the left of the plot, while smaller sky features contribute to the right of the plot.

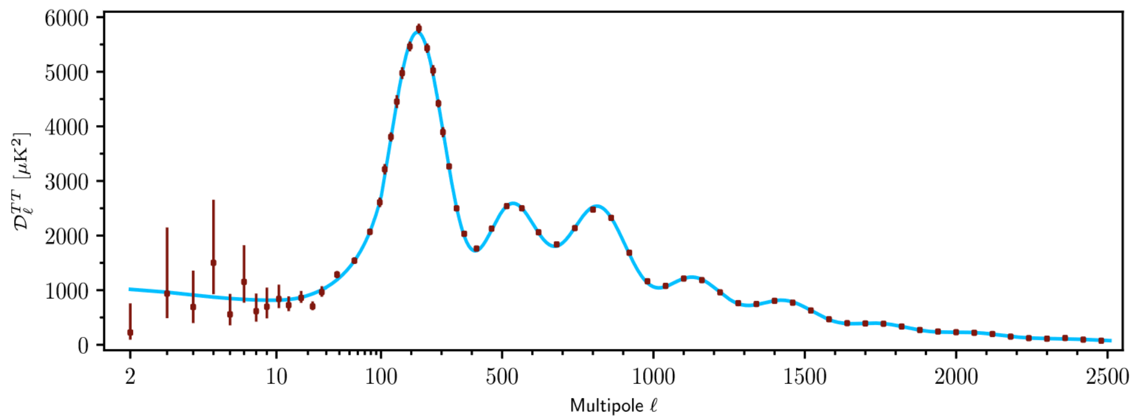

Figure 2.4.: The angular power spectrum for temperature as reported by Planck. Planck Collaboration *et al.*, 2020a

The shape of this power spectrum is determined by oscillations in the hot gas of the early universe, and the resonant frequencies and amplitudes of these oscillations are determined by its composition. The properties of the oscillating gas can be computed by studying the positions and relative sizes of the peaks in the power spectrum. The position of the first peak, for instance, gives information about the curvature of the universe, while the ratio of heights between the first and second peaks shed light on how much of the matter is baryonic and how much is DM. As such, fits to the spectrum using the ΛCDM model (Λ Cold Dark Matter) are able to tell with incredible accuracy how large the total amount of DM in the Universe is, which according to recent measurements, is about ten times higher than the amount of baryonic matter (Hu and Dodelson, 2002).

2.1.3. The Bullet Cluster

The galaxy cluster 1E 0657-56, also known as the "bullet cluster" was first detected by the Imaging Proportional Counter (IPC) aboard the *Einstein* (HEAO 2) X-Ray Observatory during its 3 years of lifetime from November 12, 1978 to April, 1981 (Editor NASA HEASARC, 2020). It was discovered by Tucker, Tananbaum, and Remillard, 1995 in the *Einstein* Imaging Proportional Counter (IPC) during their search for "failed clusters", that is large clouds of hot gas with no visible galaxies. In their article, the authors were able to eliminate 1E 0657-56 as a "failed cluster". This cluster was revisited by Tucker *et al.*, 1997 aided by X-ray data obtained with the *ROSAT* HRI and *ASCA*. They were able to identify the source with a previously unknown cluster of galaxies at redshift $z = 0.296$ and measure its temperature $kT = 17.4 \pm 2.5$ keV, which made it a contender for the hottest cluster known and also one of the most luminous.

Given its unusual properties, the cluster garnered attention from the astronomical community and it was later analyzed by Markevitch *et al.*, 2002 with help of previous X-ray observations and newer ones provided by the *Chandra* X-ray Observatory. The new *Chandra* image revealed a "bow shock propagating in front of a bullet-like gas cloud just exiting the disrupted cluster core". The authors noted that this behaviour presented an opportunity to test the collisional nature of DM based on the location of the smaller subcluster's DM density peak. They expanded further on this point in Clowe *et al.*, 2006 where they compared the X-ray image with an optical image and noticed the offset between the galaxies and the gas, as shown in Figure 2.5:

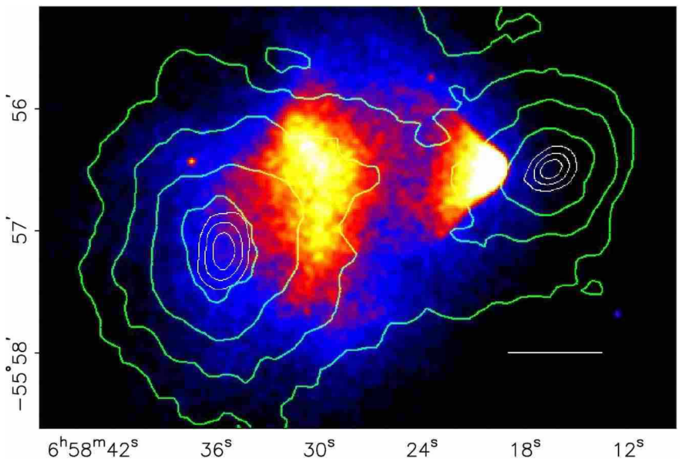

Figure 2.5.: The merging cluster 1E0657-558. The bullet cluster (shown on the right) has traversed the larger cluster. The colors indicate the X-ray temperature of the plasma: blue is coolest and white is hottest. The green contours are the weak lensing reconstruction of the gravitational potential of the cluster. Clowe *et al.*, 2006

The explanation of the phenomenon takes into account the two predominant types of baryonic matter found in galaxy clusters: the stars and gas consisting of mostly hydrogen, helium, protons and electrons. In a collision, the two components have different behaviors. The stars, that although numerous, have a small probability of colliding with other stars, and as such propagate unhindered; on the other hand, the gas experiences large electromagnetic friction, it is stopped and heated in the collision point with associated X-ray emission. In clusters with only baryonic matter and Newtonian gravity, the majority of gravitational lensing of background light should trace the gas, as this component is far more massive than the stars.

Figure 2.5 shows the collision of two clusters; as expected, the dissipationless stellar component and the fluid-like X-ray emitting plasma are spatially segregated. However, the Figure shows that the gravitational potential does not trace the plasma distribution, the dominant baryonic mass component, but rather approximately traces the distribution of the stars. An 8σ significance spatial offset of the center of the total mass from the center of the baryonic mass peaks proves that the majority of the matter in the system is unseen. It also sheds light on characteristics of this matter, given that it traces the star distribution, which propagates freely. This is consistent with the hypothesis that DM is a collisionless fluid surrounding galaxies.

It is however, inconsistent with an alteration of the gravitational force law, as motivated by MOND. As argued by Clowe, Gonzalez, and Markevitch, 2004, in a purely baryonic MOND universe there would still be a separation between the X-ray and galaxy centroids due to the collisionless behavior of the stars. However, in the absence of DM the vast majority, $\sim 85-90\%$, of the mass of the subclump would be with the X-ray gas because the X-ray halo is the dominant mass component of the visible baryons in the cluster, in the absence of a dark mass component . Thus, any direct method to measure the mass of the system would detect a higher mass about the X-ray halo than around the galaxies, which went against their observations.

A later analysis by the same authors (Markevitch *et al.*, 2004) attempted to use their observations to constrain the collisional nature of DM, namely they found that $\frac{\sigma}{m} < 5\ \mathrm{cm}^2\ \mathrm{g}^{-1}$, where σ is the DM collision cross section and m is the particle mass. This result was derived from limits on the size of any potential offset between the DM and stars in the Bullet Cluster. Following the discovery of the Bullet Cluster, other colliding clusters have been found and methods similar to those of Markevitch *et al.*, 2004 have been used to obtain and refine constraints for DM interaction. The strongest currently existing constraint on self-interacting DM from colliding cluster observations is $\frac{\sigma}{m} \lesssim 0.47\ \mathrm{cm}^2\ \mathrm{g}^{-1}$ (Harvey *et al.*, 2015), who averaged the DM-galaxy offsets in a sample of 72 merging galaxy clusters. Even so, this result is not agreed upon by the entire community and the accepted limits are relaxed to $\frac{\sigma}{m} \lesssim 2\ \mathrm{cm}^2\ \mathrm{g}^{-1}$ (Wittman, Golovich, and Dawson, 2018).

2.2. Contemporary Efforts for the Detection of Weakly Interacting Particle Dark Matter

The existence of DM has been made clear by several observations on various different scales, as summarized in the previous sections. Its nature as particles akin to the ones enclosed by the SM has also been accepted, however until today no DM particle has been observed by any experiment. Despite this apparent impossibility, the scientific community has not refrained from conducting studies in this line.

The standard experimental techniques employed to discover particle physics in the dark sector, namely those of the WIMP paradigm, are summarized in Figure 2.6. There are three main lines of work and each one assumes an interaction between DM and the SM.

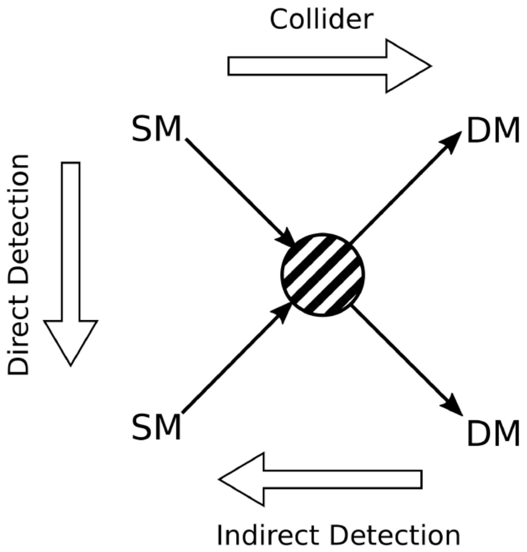

Figure 2.6.: Different DM detection channels. Giagu, 2019

Following the diagram from left to right denotes processes where SM particles and antiparticles annihilate at high energies to possibly create DM. This technique is dubbed *collider production* and it looks for DM as missing energy that leaves the detector.

Reading the diagram from top to bottom signifies scatterings between SM particles and DM. This avenue is called *direct detection* and it searches for galactic DM particles recoiling on terrestrial nuclei (or electrons).

Finally, following the diagram from right to left corresponds to DM annihilating into SM particles. Searches which make use of this interaction are called *indirect detection*. Such experiments are mainly astrophysical with telescopes that focus on regions where there is a high concentration of DM, for example, the core of the Milky Way galaxy.

2.2.1. Collider Production

Collider searches for DM assume that SM particles may annihilate into DM at very high energies. Unfortunately, if such an annihilation were to take place, it would not produce a visible signal like in other collider experiments due to the extremely weak interaction between the DM and the SM particles which constitute the detectors. Instead, the presence of DM particles could be inferred using transverse momentum conservation, as shown in the schematic drawing in Figure 2.7:

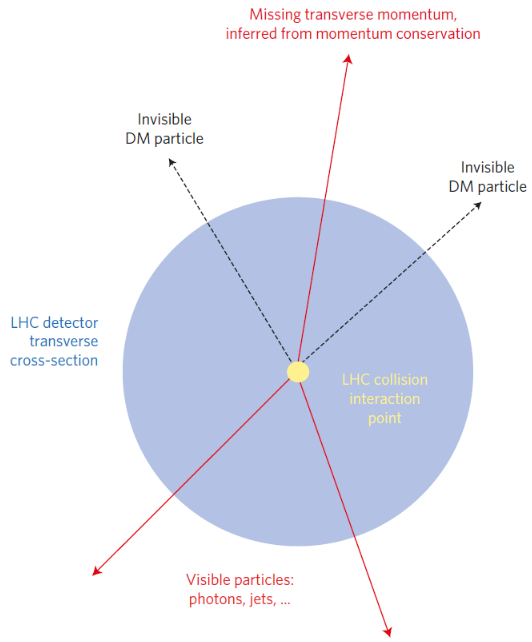

Figure 2.7.: Missing transverse momentum from DM production in an LHC detector (Buchmueller, Doglioni, and Wang, 2017).

It relies on the basis of momentum conservation, which states that the net momentum in the plane perpendicular to the colliding beams must be zero before and after the collision has taken place. The vector sum of the transverse momenta of all detected particles is calculated and, if an imbalance in this plane would be obtained, this would be the main signal for direct production of DM at colliders. This quantity is termed "missing transverse momentum" or "missing transverse energy" ($E_{\mathrm{T}}^{\mathrm{m}iss}$).

The missing transverse momentum is the basis for two types of searches at particle colliders. The first targets specific new physics models, such as supersymmetry, and it allows to set limits on the parameters that enter such theories. On the other hand, the second type of search focuses on the simplest, most general models. The basic idea behind this search is that DM could be produced as pairs alongside one or more highly energetic SM particles. Then, the existence of the DM pair could be inferred from the $E_{\mathrm{T}}^{\mathrm{m}iss}$ as it recoils against the energetic SM particles, named "mono-object". This search is sometimes called "monojet-X search" and has become a standard at particle colliders.

Collider searches for DM have been performed by several high energy colliders, including the Large Electron Positron Collider at CERN and the Tevatron at Fermilab. So far, no experimental evidence for DM or specific new models of physics has been found. Notwithstanding, the expectations for detection remain high and the experiment with the greatest hopes at the time is the currently operating Large Hadron Collider (LHC), given that it provides the largest sensitivity to rare processes and gives access to the highest energy scales for new phenomena, including DM.

2.2.2. Direct Detection

Another avenue of observation of DM is that of direct detection, which follows from the assumption that SM particles and DM go through scattering processes, which may hopefully be detected in ultra-sensitive low-background experiments (for a recent, general review, I refer to the work of Schumann, 2019). In particular, this avenue searches for signatures of scattering of DM off a target nucleus. Unfortunately, such scattering processes are expected to be extremely rare leaving only tiny signatures. Therefore, a good grasp on the background of the detector is crucial in order to confirm or refute a signal.

Using the same principle of momentum conservation as collider production searches, indirect detection relies on the momentum transferred from an incoming DM particle to a nucleus. Interaction with a nucleus instead of a surrounding electron is of particular importance, given that the typical kinetic energy after the energy transfer is $\frac{1}{2}m\beta^2$, where m is the mass of the SM matter interacting with the DM and $\beta = \frac{v}{c} \sim 10^{-3}$ is the incoming DM particle's speed, so nuclei of mass similar to that of the DM particles are the best choice in terms of kinematics.

Once the energy transfer occurs, various signal channels are expected, such as scintillation light, phonon signals, ionization signals, and bubble generation. The appearance of multiple manifestations proves advantageous for reducing various types of common background, such as the one caused by gamma rays. Unfortunately, despite the experimental efforts there is an irreducible background for direct searches due to the fact that coherent neutrino-nucleus scattering leads to the same hypothesized signature as DM-nucleus interactions. This lower limit is know as the "neutrino floor" and is shown in Figure 2.8 alongside parameter space traversed by several different direct detection searches.

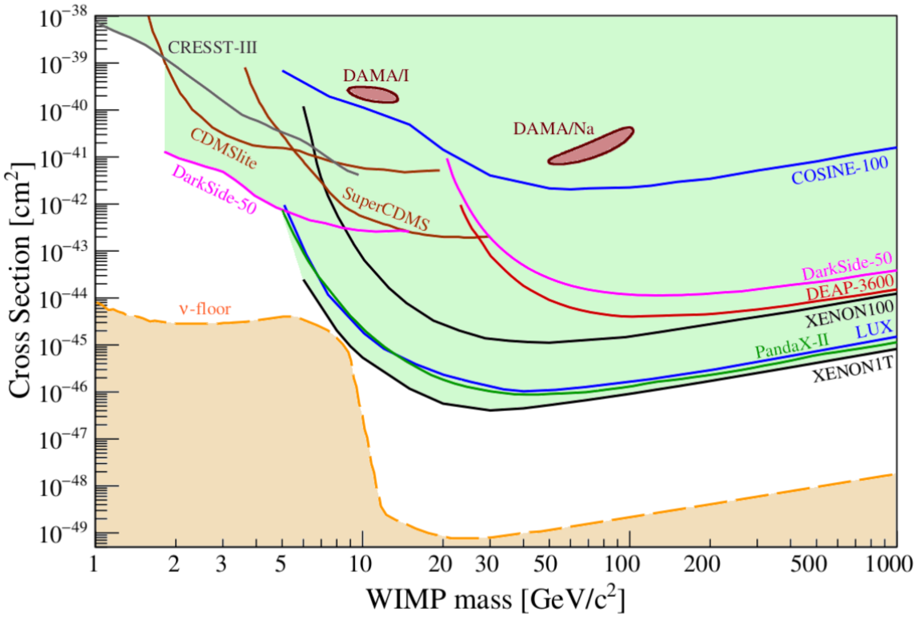

Figure 2.8.: The current experimental parameter space for spin-independent WIMP-nucleon cross sections. The lower brown are corresponds to the limit due to the neutrino floor (Schumann, 2019).

Despite all efforts, the DM particle remains elusive in direct detection experiments, but there is still hope for detection as several regions of parameter space above the neutrino floor are still unexplored. Of special recent importance is the reported low-energy excess above the background in the XENON1T experiment, which may be due to an unconsidered source of background or the more positive explanation, the detection of axions from the Sun. The significance of this measurement, however, is consistent with the data, so the detection of an excess is still inconclusive.

2.2.3. Indirect Detection

Finally, indirect DM searches rely on the prediction that DM annihilates or decays into SM particles, leaving behind distinct signatures in gamma rays, neutrinos and antiparticles such as positrons and antiprotons. Such signals are expected from regions where DM densities are significantly enhanced around clumps of gravitational matter, such as in the Sun or in the center of the galaxy. For a recent and more in depth review, I refer to the work of Conrad and Reimer, 2017.

A detection of DM annihilation through indirect methods would establish its nature as a particle and yield further information about its microscopic properties; in particular, it would allow for the estimation of the annihilation cross-section and DM mass. On the other hand, the non-detection leads to constraints and limits which are of use for future experiments.

An advantage of indirect methods is their non-specialization. Indirect DM searches rarely constitute the one and only scientific objective of experiments designed to observe cosmic rays or photons at the upper end of the electromagnetic spectrum. Therefore, the amount of observatories that can conduct research in this line is considerable and, in turn, reported findings can very easily be strengthened or refuted by the wide array of experiments. Another pro is that the signature in gamma- and cosmic-ray observations is determined by the composition of SM particles that the DM annihilates into. As such, a detection would provide information to determine which DM models to neglect, which are still viable and whether new ones have to be built.

This method of observation is not without challenges, however. It requires a profound understanding of the astrophysical background. A lack of it leads to two main difficulties: the first is origin confusion, as astrophysical sources, such as pulsars, can mimic sources of DM annihilation. The second is poorly determined backgrounds, which mark the difference between the detection or non-detection of anomalies. Uncertainties of the DM model also lead to difficulties, as the flux of gamma- or cosmic-rays depends on the annihilation cross-section and the particle mass. Another variable of great importance into the calculation of the flux is the spatial distribution of DM, which until now is still uncertain. The expected flux is proportional to the integral (traditionally referred to as the "J-factor") of this DM density over the line of sight and solid angle subtended by the observation.

There are also channel-specific difficulties. While anti-matter is usually not produced in astrophysical processes and an excess of anti-nuclei would point to DM, the fact that cosmic-rays are charged makes their propagation complicated and the determination of their origin problematic. On the other hand, neutrino observatories struggle with the very weak interaction of neutrinos themselves.

2.2.4. Capture of Particles by Stars

As mentioned in Section 2.2.3, stars can be used as laboratories to study DM, given that their self-annihilation within these compact objects is enhanced. On the other hand, capture of DM can also affect stellar evolution, which provides a different testing ground for probing the dark particle's nature. Examples of such consequences have been studied, for instance, by Raen *et al.*, 2021, who considered asymmetric DM with spin-dependent interactions with the star's nuclei. They studied the effects of energy transport in stars of masses $0.9M_{\odot} \leq M \leq 5M_{\odot}$ living in a variety of DM environments. They found that DM does indeed play a role in their evolution, for example the stars' temperature profiles were flattened, which led to different burning rates and stellar structures. This, in turn, changed the main sequence lifetimes; for low mass stars ($M \leq 1.3M_{\odot}$) they were increased by 20%, while for high mass stars they were reduced by as much as 40%.

The authors also speculated that these effects could be observed in surveys of dwarf galaxies with very large mass-to-light ratios. Their models suggested that the hottest main sequence stars of such a galaxy should be slightly hotter or colder if no DM was present depending on population's age, and assured that such a measurement is possible for contemporary experiments.

2.3. Relation to the Present Work

Jumping off from the theoretical and experimental efforts on MACHOs and DM capture in stars is where I motivate the work that was done in this thesis. According to the example set by MACHOs of close to invisible celestial bodies, I assumed that DM itself may form compact objects, more specifically BSs made up of asymmetric DM, which could be detected by microlensing searches. If DM was only self-interacting, then objects of this type could only be detected by gravitational searches, however the research on DM capture provides a different viewpoint. If it is possible for a normal star to capture DM, then there exists an interaction between the invisible and visible sectors, so the inverse case could also be viable, namely that BSs could capture baryons from the ISM, which could then emit radiation according to well known emission mechanisms. As such, this opens a new path for detection of dark compact objects through non-gravitational searches. The expected signals from this capture and effects on the BS's evolution are the focus of this thesis.

3. Structure of Boson Stars

In order to figure out whether baryons captured by a BS are able to emit signals with possibility of detection, it proves crucial to understand the environment which contains them. This means that the first step is to understand the structure of BSs. This chapter focuses on tackling this problem. I begin with the standard treatment for modeling a compact object under general relativistic effects, which is summed up by the relativistic equations for stellar structure. Afterwards, in order to apply them to the particular case of BSs, I derive the system of differential equations which governs the metric components of a compact object made up of self-interacting bosons. These equations are solved numerically and some results are exposed before proceeding to take the limit of strong self-interactions. In this limit, the equations for stellar structure are applied and solved, which leads to critical information about the star, which will be used in the following chapters.

3.1. Stellar Structure

3.1.1. The Metric of a Stellar Interior

The majority of observable stars are not dense enough for general relativistic effects to play a big role in their interior. Nevertheless, such effects are important in the case of compact objects with extremely high densities, such as a neutron star. There is also reason to believe that stars made up of DM will exhibit densities in the range of those exhibited by neutron stars. As such, general relativistic methods must be taken in order to figure out their structure. In the following section I will develop this approach for a general compact object. In Section 3.2 it will be applied to the case of BSs.

In the following sections, unless mentioned otherwise, units will be used where $c = 1$. Assuming spherical symmetry and a static matter distribution the line element is given in Schwarzschild coordinates by

$$ds^2 = B(r)dt^2 - A(r)dr^2 - r^2(d\theta^2 + \sin^2\theta d\varphi^2). \tag{3.1}$$

The Schwarzschild metric is then obtained by solving Einstein's field equations in vacuum $R_{\mu\nu} = 0$, but as the interior of a star is not empty, the general form of the equations is taken:

$$R_{\mu\nu} = -\kappa\left(T_{\mu\nu} - \frac{1}{2}Tg_{\mu\nu}\right),\ \kappa = 8\pi G. \tag{3.2}$$

The interior of the star is modeled as being a perfect fluid, whose energy-momentum tensor is of the form

$$T_{\mu\nu} = (\rho + p)u_\mu u_\nu - pg_{\mu\nu}, \tag{3.3}$$

and its trace is

$$T := T^\mu_\mu = T(\rho + p)u^\mu u_\mu - p\delta^\mu_\mu = \rho(r) - 3p(r), \tag{3.4}$$

where the result $u^\mu u_\mu = 1$ has been used. As such the field equations may be rewritten for this case as

$$R_{\mu\nu} = -\kappa\left[\rho(r)\left(u_\mu u_\nu - \frac{1}{2}g_{\mu\nu}\right) + p(r)\left(\frac{1}{2}g_{\mu\nu} + u_\mu u_\nu\right)\right]. \tag{3.5}$$

From the line element (3.1), the non-zero Christoffel symbols may be derived. The non-zero components are given by

$$\begin{aligned}
&{\Gamma^0}_{01} = \frac{B'}{2B}, && {\Gamma^1}_{00} = \frac{B'}{2A}, && {\Gamma^1}_{11} = \frac{A'}{2A},\\
&{\Gamma^1}_{22} = -\frac{r}{A}, && {\Gamma^1}_{33} = -\frac{r\sin^2\theta}{A}, && {\Gamma^2}_{12} = {\Gamma^2}_{21} = \frac{1}{r},\\
&{\Gamma^2}_{33} = -\sin\theta\cos\theta, && {\Gamma^3}_{13} = {\Gamma^3}_{31} = \frac{1}{r}, && {\Gamma^3}_{23} = {\Gamma^3}_{32} = \cot\theta,
\end{aligned} \tag{3.6}$$

where the prime denotes derivative with respect to r. With these symbols, the diagonal elements of the Ricci tensor are calculated:

$$\begin{aligned}
R_{00} &= -\frac{B''}{2A} + \frac{B'}{4A}\left(\frac{B'}{B} + \frac{A'}{A}\right) - \frac{B'}{rA},\\
R_{11} &= \frac{B''}{B} - \frac{B'}{4B}\left(\frac{B'}{B} + \frac{A'}{A}\right) - \frac{A'}{rA},\\
R_{22} &= \frac{1}{A} - 1 + \frac{r}{2A}\left(\frac{B'}{B} - \frac{A'}{A}\right),\\
R_{33} &= R_{22}\sin^2\theta.
\end{aligned} \tag{3.7}$$

By comparison of equations (3.5) with (3.7), the system of differential equations governing the metric of the interior of the compact object are obtained. Nevertheless, it proves easier to first consider the consequences of the non-vanishing Ricci components

$$0 = R_{0\mathrm{i}} = -\kappa u_0 u_\mathrm{i}(\rho(r) + p(r)) \implies u_0 u_\mathrm{i} = 0. \tag{3.8}$$

The velocity 4-vector is written as $u^\mu = \gamma(1, \vec{v})$, so the covariant 0-component is expressed as $u_0 = g_{0\nu}u^\nu = B(r)\gamma \neq 0$. Given that $u_0 u_\mathrm{i} = 0$ and $u_0 \neq 0$, then $u_\mathrm{i} = 0\ \forall\ \mathrm{i} \in \{1,2,3\}$. As such, the covariant velocity 4-vector is of the form $u_\mu = (u_0, \vec{0})$. Finally, by using the fact that $1 = u_\mu u^\mu = g^{\mu\nu}u_\mu u_\nu = \frac{u_0^2}{B(r)}$, then $u_0 = \sqrt{B(r)}$, so the 4-vector can be expressed as

$$u_\mu = \sqrt{B(r)}(1,0,0,0), \tag{3.9}$$

thus the 3-velocity of the fluid must vanish everywhere. This means that the matter distribution itself is static and the compact object is in a state of hydrostatic equilibrium. With this knowledge, the non-vanishing Ricci components given by equation (3.5) may be simplified and written as

$$\begin{aligned} R_{00} &= -\frac{\kappa}{2}B(r)\left[\rho(r) + 3p(r)\right], \\ R_{11} &= -\frac{\kappa}{2}A(r)\left[\rho(r) - p(r)\right], \\ R_{22} &= -\frac{\kappa}{2}r^2\left[\rho(r) - p(r)\right], \\ R_{33} &= R_{22}\sin^2\theta. \end{aligned} \tag{3.10}$$

By adding the equations above, the following expression is obtained:

$$\frac{R_{00}}{B} + \frac{R_{11}}{A} + \frac{2R_{22}}{r^2} = -2\kappa\rho, \tag{3.11}$$

and upon substitution of the Ricci components by the expressions from (3.7) and simplification the equation is rewritten as

$$\left(1 - \frac{1}{A}\right) + \frac{A'}{A^2}r = \kappa\rho r^2. \tag{3.12}$$

The left-hand side of this equation can be expressed as a total derivative $\frac{d}{dr}\left[r\left(1 - \frac{1}{A}\right)\right]$, so the whole equation can be integrated as

$$\int d\left[r\left(1-\frac{1}{A}\right)\right] = \kappa\int_0^r r^2\rho(r)dr, \tag{3.13}$$

where the associated constant of integration for the left-hand side must be zero in order for $A(r)$ to be non-zero at the origin, which is demanded by the expression $\frac{1}{A(r)}$ from equation (3.12). At this point, the familiar definition

$$m(r) = 4\pi\int_0^r r^2\rho(r)dr, \tag{3.14}$$

may be used to write the solution of the differential equation for $A(r)$ as

$$A(r) = \left[1-\frac{\kappa m(r)}{4\pi r}\right]^{-1} = \left[1-\frac{2Gm(r)}{r}\right]^{-1}. \tag{3.15}$$

Despite the familiar definition of equation (3.14), $m(r)$ is not the enclosed mass. The enclosed mass is obtained with the volume element (proper spatial volume) of the metric (3.1), which reads, $d^3V = \sqrt{A(r)}r^2\sin\theta dr d\theta d\phi$. So the proper integrated mass is written as

$$\bar{m}(r) = 4\pi\int_0^r \sqrt{A(r)}r^2\rho(r)dr = 4\pi\int_0^r\left[1-\frac{2Gm(r)}{r}\right]^{-\frac{1}{2}} r^2\rho(r)dr. \tag{3.16}$$

The difference between both masses is the gravitational binding energy of the compact object. Let R be its radius and $M := m(R)$, $\bar{M} := \bar{m}(R)$, then this energy is given by $E_{\text{binding}} = \bar{M} - M$.

To find the equation for the metric component $B(r)$, it proves convenient to use the conservation equation $\nabla_\mu T^{\mu\nu} = 0$. Inserting (3.3) for $T^{\mu\nu}$, one obtains

$$\begin{aligned} 0 &= \nabla_\mu\left((\rho+p)u^\mu u^\nu - pg^{\mu\nu}\right) \\ &= \frac{1}{\sqrt{-g}}\partial_\mu\left[(\rho+p)u^\mu u^\nu\right] + (\rho+p)\Gamma^\nu{}_{\sigma\mu}u^\mu u^\sigma - g^{\mu\nu}\partial_\mu p. \end{aligned} \tag{3.17}$$

By using (3.9) and the explicit form of the Christoffel symbol $\Gamma^\nu{}_{00} = -\frac{1}{2}g^{\mu\nu}\partial_\mu B$, (3.17) may be simplified as

$$0 = \nabla_\mu T^{\mu\nu} = g^{\mu\nu}(\partial_\mu B)\left(\frac{\rho+p}{2B}\right) + g^{\mu\nu}\partial_\mu p, \tag{3.18}$$

and then multiplication by $g_{\sigma\nu}$ yields the differential equation

$$\frac{dB}{dr} = -\frac{2B(r)}{\rho(r)+p(r)}\frac{dp}{dr}. \tag{3.19}$$

One then finally concludes with the system of equations for the metric components

$$A(r) = \left[1 - \frac{2Gm(r)}{r}\right]^{-1}, \tag{3.20a}$$

$$\frac{dB}{B} = -\frac{2}{\rho(r)+p(r)}\frac{dp}{dr}dr, \tag{3.20b}$$

$$m(r) = 4\pi \int_0^r r^2 \rho(r) dr, \tag{3.20c}$$

which are solvable as long as equations for $p(r)$ and $\rho(r)$ are provided.

3.1.2. Relativistic Equations for Stellar Structure

To learn about the structure of the star one prefers to know the density and pressure profiles of the object instead of the metric components. As such, the equations for stellar structure are different from those given by (3.20). The first one, though, is equation (3.20c) in its differential form, mainly

$$\frac{dm}{dr} = 4\pi r^2 \rho(r). \tag{3.21}$$

The second equation is obtained from the 22-component of the Ricci tensor. By equating the relevant expressions from (3.7) with the ones from (3.10), one obtains

$$\frac{1}{A} - 1 + \frac{r}{2A}\left(\frac{B'}{B} - \frac{A'}{A}\right) = R_{22} = -\frac{\kappa}{2} r^2 \left[\rho(r) - p(r)\right]. \tag{3.22}$$

Upon substitution of (3.20a) and (3.20b) and simplification, the second equation of stellar structure (also known as the Oppenheimer-Volkoff equation) is obtained:

$$\frac{dp}{dr} = -\frac{1}{r^2}\left[4\pi G p(r) r^3 + G m(r)\right]\left[\rho(r) + p(r)\right]\left(1 - \frac{2Gm(r)}{r}\right)^{-1}. \tag{3.23}$$

The third and final equation of stellar structure is the equation of state:

$$p = p(\rho) = K\rho^{\alpha}, \tag{3.24}$$

where the last equality represents the polytropic equation of state (K and α are constants), which is valid for several astrophysical systems. So, the system of equations governing the structure of a compact object is

$$\frac{dm}{dr} = 4\pi r^2 \rho(r), \tag{3.25a}$$

$$\frac{dp}{dr} = -\frac{1}{r^2}\left[4\pi G p(r) r^3 + G m(r)\right]\left[\rho(r) + p(r)\right]\left(1 - \frac{2Gm(r)}{r}\right)^{-1}, \tag{3.25b}$$

$$p = p(\rho). \tag{3.25c}$$

The three equations consist of two coupled ordinary differential equations and one algebraic equation. Thus, two boundary conditions are required. The usual choice is

$$m(0) = 0, \quad p(0) = p_0 \text{ (or equivalently } \rho(0) = \rho_0), \tag{3.26}$$

that is, enclosed mass and pressure (or density) at the core. Given an equation of state and the equations of stellar structure, the mass, density and pressure profiles of the star can be obtained. This is what will be done in the following section for a dark star made up of bosonic DM.

3.2. Boson Stars

3.2.1. Noninteracting Boson fields

The case of BSs with non-interacting bosons, that is, BSs bound only by gravity was first analyzed by Kaup, 1968. In his work Kaup considered a complex scalar field theory in a spacetime background curved due to self-gravity. Such objects are macroscopic quantum states, that are only prevented from collapsing gravitationally by the Heisenberg uncertainty principle. The equations of motion were solved numerically[1] and he found that the maximum mass of these solutions was $M_{\max} = 0.633\frac{M_{\mathrm{Pl}}^2}{m}$, the often called Kaup limit,[2] where m is the mass of the DM particle. This result is generally much smaller than the Chandrasekhar mass, $M_{\mathrm{Chandra}} \propto \frac{M_{\mathrm{Pl}}^3}{m^2}$, characteristic of marginally relativistic fermion stars.

[1] The equations that were solved were the system 3.43 in the limit $\Lambda \to 0$.

[2] Later derived by Ruffini and Bonazzola, 1969 using a different method by taking expectation values of the equations of motion in an N-particle quantum state. As such, it is also known as the Kaup-Ruffini-Bonazzola limit.

3.2.2. Interacting Boson Fields

In this work, I focus on the case of BSs with repulsive self-interactions. This problem was first treated by Colpi, Shapiro, and Wasserman, 1986 by solving the equations of motion in a similar manner to that of Kaup. In the following I will develop this method of solution, where from here onward, except explicitly stated, I will work in units where $\hbar = 1, c = 1$.

The DM particles are assumed to be produced by a self-interacting complex scalar field with a quartic interaction given by the potential

$$V(\phi) = \frac{\lambda}{4}|\phi|^4, \tag{3.27}$$

where λ is a dimensionless coupling constant.

In the interacting case $\lambda \neq 0$, the importance of the interaction potential is given by the ratio of the interaction energy to the kinetic energy

$$\frac{V(\phi)}{m^2\phi^2} \sim \frac{\lambda|\phi|^4}{m^2|\phi|^2} \sim \frac{\lambda|\phi|^2}{m^2} \sim \lambda\left(\frac{\mathrm{M_{Pl}}}{m}\right)^2.$$

Thus, self-interaction may only be ignored if the coupling is sufficiently small, that is

$$\lambda << \left(\frac{m}{\mathrm{M_{Pl}}}\right)^2 = (6.71\times10^{-39}\ \mathrm{GeV}^{-2})m^2. \tag{3.28}$$

In order to parametrize the different solutions which depend on the DM mass and the coupling of the self-interaction in the theory, one introduces the dimensionless parameter

$$\Lambda := \frac{\lambda}{4\pi}\left(\frac{\mathrm{M_{Pl}}}{m}\right)^2, \tag{3.29}$$

which allows one to easily differentiate between the non-interacting and interacting cases by considering $\Lambda << 4\pi$ and $\Lambda >> 4\pi$, respectively.

The starting point of the calculation are Einstein's equations. One considers spherically symmetric, time-independent solutions of Einstein's field equations

$$G^{\mu}_{\nu} := R^{\mu}_{\nu} - \frac{1}{2}\delta^{\mu}_{\nu}R = -8\pi G T^{\mu}_{\nu}, \tag{3.30}$$

with a spherically symmetric line element given in Schwarzschild coordinates

$$ds^2 = B(r)dt^2 - A(r)dr^2 - r^2(d\theta^2 + \sin^2\theta d\varphi^2). \tag{3.31}$$

With this line element the Christoffel symbols and components of the Ricci tensor were derived in equations (3.6) and (3.7). For the following, one is also interested in the Ricci scalar, given by

$$R = -\frac{B''}{AB} + \frac{B'}{2AB}\left(\frac{B'}{B} + \frac{A'}{A}\right) - \frac{2B'}{rAB} + \frac{2A'}{rA^2} - \frac{2}{Ar^2} + \frac{2}{r^2}. \tag{3.32}$$

Finally, by making use of equations (3.7) and (3.32), one obtains the following components of Einstein's tensor:

$$\begin{aligned} G_0^0 &= \frac{1}{r^2}\left(\frac{1}{A} - 1\right) - \frac{A'}{rA^2}, \\ G_1^1 &= \frac{1}{r^2}\left(\frac{1}{A} - 1\right) + \frac{B'}{rAB}, \\ G_2^2 &= \frac{B''}{2AB} + \frac{1}{2Ar}\left(\frac{B'}{B} - \frac{A'}{A}\right) - \frac{B'}{4AB}\left(\frac{B'}{B} + \frac{A'}{A}\right). \end{aligned} \tag{3.33}$$

According to (3.30), one must equate the components from (3.33) to the ones from the energy-momentum tensor. To find them, one first considers the scalar field Lagrangian with quartic interaction

$$\mathscr{L} = \frac{1}{2}g^{\mu\nu}\partial_\mu\phi^*\partial_\nu\phi - \frac{1}{2}m^2|\phi|^2 - \frac{\lambda}{4}|\phi|^4, \tag{3.34}$$

and its respective energy-momentum tensor

$$T_\nu^\mu = \frac{\partial\mathscr{L}}{\partial(\partial_\mu\phi)}\partial_\nu\phi + \frac{\partial\mathscr{L}}{\partial(\partial_\mu\phi^*)}\partial_\nu\phi^* - \delta_\nu^\mu\mathscr{L}, \tag{3.35}$$

which is written explicitly in terms of the field:

$$T_\nu^\mu = \frac{1}{2}g^{\mu\sigma}\left(\partial_\sigma\phi^*\partial_\nu\phi + \partial_\sigma\phi\partial_\nu\phi^*\right) - \frac{1}{2}\delta_\nu^\mu\left(g^{\alpha\sigma}\partial_\alpha\phi^*\partial_\sigma\phi - m^2|\phi|^2 - \frac{\lambda}{2}|\phi|^4\right). \tag{3.36}$$

For spherically symmetric, time independent solutions to exist one requires:

$$\phi(r,t) = \Phi(r)\mathrm{e}^{-i\omega t}, \tag{3.37}$$

where $\Phi(r)$ is a real function. With this substitution, one finds the first three diagonal components of the energy-momentum tensor to be

$$
\begin{aligned}
T_0^0 &= \frac{1}{2}\left[\left(\frac{\omega^2}{B}+m^2\right)\Phi^2+\frac{(\Phi')^2}{A}+\frac{\lambda}{2}\Phi^4\right],\\
T_1^1 &= -\frac{1}{2}\left[\left(\frac{\omega^2}{B}-m^2\right)\Phi^2+\frac{(\Phi')^2}{A}-\frac{\lambda}{2}\Phi^4\right],\\
T_2^2 &= -\frac{1}{2}\left[\left(\frac{\omega^2}{B}-m^2\right)\Phi^2-\frac{(\Phi')^2}{A}-\frac{\lambda}{2}\Phi^4\right].
\end{aligned}
\tag{3.38}
$$

Before equating (3.33) with (3.38) it is convenient to rewrite both sets of equations with the following proposal:

$$
x := mr, \quad \sigma := \sqrt{4\pi G}\Phi, \quad G^{\frac{1}{2}} = \mathrm{M}_{\mathrm{Pl}}^{-1}, \quad \Omega := \frac{\omega}{m},
\tag{3.39}
$$

where for the following development, the primes will denote $\frac{d}{dx}$, instead of $\frac{d}{dr}$. It is worth noting that, given the choice of units $c = 1$ and $\hbar = 1$, both x and Ω are dimensionless. Under this rescaling, equations (3.33) and (3.38) are rewritten as

$$
\begin{aligned}
G_0^0 &= \left(\frac{m}{x}\right)^2\left[\left(\frac{1}{A}-1\right)-\frac{A'}{A^2}x\right],\\
G_1^1 &= \left(\frac{m}{x}\right)^2\left[\left(\frac{1}{A}-1\right)+\frac{B'}{AB}x\right],\\
G_2^2 &= m^2\left[\frac{B''}{2AB}+\frac{1}{2Ax}\left(\frac{B'}{B}-\frac{A'}{A}\right)-\frac{B'}{4AB}\left(\frac{B'}{B}+\frac{A'}{A}\right)\right],
\end{aligned}
\tag{3.40}
$$

and

$$
\begin{aligned}
-8\pi G T_0^0 &= -m^2\left[\left(\frac{\Omega^2}{B}+1\right)\sigma^2+\frac{\Lambda}{2}\sigma^4+\frac{(\sigma')^2}{A}\right],\\
-8\pi G T_1^1 &= m^2\left[\left(\frac{\Omega^2}{B}-1\right)\sigma^2-\frac{\Lambda}{2}\sigma^4+\frac{(\sigma')^2}{A}\right],\\
-8\pi G T_2^2 &= m^2\left[\left(\frac{\Omega^2}{B}-1\right)\sigma^2-\frac{\Lambda}{2}\sigma^4-\frac{(\sigma')^2}{A}\right],
\end{aligned}
\tag{3.41}
$$

respectively.

By equating (3.40) with (3.41) by the field equations (3.30), one concludes with the equations

$$
\begin{aligned}
&\frac{A'}{A^2 x}+\frac{1}{x^2}\left(1-\frac{1}{A}\right)=\left(\frac{\Omega^2}{B}+1\right)\sigma^2+\frac{\Lambda}{2}\sigma^4+\frac{(\sigma')^2}{A},\\
&\frac{B'}{ABx}-\frac{1}{x^2}\left(1-\frac{1}{A}\right)=\left(\frac{\Omega^2}{B}-1\right)\sigma^2-\frac{\Lambda}{2}\sigma^4+\frac{(\sigma')^2}{A},\\
&\frac{B''}{2AB}+\frac{1}{2Ax}\left(\frac{B'}{B}-\frac{A'}{A}\right)-\frac{B'}{4AB}\left(\frac{B'}{B}+\frac{A'}{A}\right)=\left(\frac{\Omega^2}{B}-1\right)\sigma^2-\frac{\Lambda}{2}\sigma^4-\frac{(\sigma')^2}{A}.
\end{aligned}
\tag{3.42}
$$

To solve the system, one usually replaces the third equation with an additional equation for the evolution of σ. It is obtained by making use of the conservation equation $\nabla_\mu T^{\mu\nu}=0$ for $\nu=1$ and the rescaling given by (3.39). Finally, the system of equations that describe the form of the metric for the interior of the dark star is

$$
\frac{A'}{A^2 x}+\frac{1}{x^2}\left(1-\frac{1}{A}\right)=\left(\frac{\Omega^2}{B}+1\right)\sigma^2+\frac{\Lambda}{2}\sigma^4+\frac{(\sigma')^2}{A}, \tag{3.43a}
$$

$$
\frac{B'}{ABx}-\frac{1}{x^2}\left(1-\frac{1}{A}\right)=\left(\frac{\Omega^2}{B}-1\right)\sigma^2-\frac{\Lambda}{2}\sigma^4+\frac{(\sigma')^2}{A}, \tag{3.43b}
$$

$$
\sigma''+\left(\frac{2}{x}+\frac{B'}{2B}-\frac{A'}{2A}\right)\sigma'+A\left[\left(\frac{\Omega^2}{B}-1\right)\sigma-\Lambda\sigma^3\right]=0. \tag{3.43c}
$$

A further redefinition may be made to extract the mass of the BS. One defines the mass parameter $\mathscr{M}$ implicitly by

$$
A(x):=\left[1-\frac{2\mathscr{M}(x)}{x}\right]^{-1}, \tag{3.44}
$$

where emphasis is made on the fact that this is not the enclosed mass, but the mass parameter in agreement with the discussion of Section 3.1.1, and that the real enclosed mass is found analogously as argued in this section. One may replace equation (3.43a) by the according equation for the mass parameter $\mathscr{M}$:

$$
\mathscr{M}'(x)=x^2\left[\frac{1}{2}\left(\frac{\Omega^2}{B}+1\right)\sigma^2+\frac{\Lambda}{4}\sigma^4+\frac{1}{2}\frac{(\sigma')^2}{A}\right], \tag{3.45}
$$

and replace the variable A in (3.43a) and (3.43b) in favor of $\mathscr{M}$. In order to solve the system of equations, it proves useful to redefine $B_*(x) := \frac{B(x)}{\Omega^2}$, to obtain the system

$$\begin{aligned}
\frac{d\mathscr{M}}{dx} &= x^2 \left[\frac{1}{2}\left(\frac{1}{B_*}+1\right)\sigma^2 + \frac{\Lambda}{4}\sigma^4 + \frac{1}{2}\frac{(x-2\mathscr{M})(\sigma')^2}{x} \right], \\
\frac{dB_*}{dx} &= \frac{2\mathscr{M}B_*}{x(x-2\mathscr{M})} + \frac{x^2 B_*}{x-2\mathscr{M}} \left[\left(\frac{1}{B_*}-1\right)\sigma^2 - \frac{\Lambda}{2}\sigma^4 + \frac{(x-2\mathscr{M})(\sigma')^2}{x} \right], \\
\frac{d^2\sigma}{dx^2} &= -\left(\frac{2}{x} + \frac{B_*'}{2B_*} - \frac{x\mathscr{M}'-\mathscr{M}}{x(x-2\mathscr{M})}\right)\sigma' - \frac{x}{x-2\mathscr{M}} \left[\left(\frac{1}{B_*}-1\right)\sigma - \Lambda\sigma^3 \right].
\end{aligned} \tag{3.46}$$

To solve, the following boundary conditions are imposed: $\mathscr{M}(0) = 0$, $\sigma'(0) = 0$ (regularity at the origin), $B(\infty) = 1$ (asymptotic flatness at infinity) and $\sigma(0) = \sigma_c$ and the further constraint that $\sigma(x)$ is a function that has no nodes. The $\sigma(0) = \sigma_c$ condition is arbitrary, but one may find a value of σ_c which maximizes the mass of the BS, maintaining all other parameters fixed.

To find the value of σ_c which maximizes the total mass of the BS, several mass parameter profiles have been plotted with different values of Λ in Figure 3.1a. As one can observe, an increase in Λ leads to a decrease in the σ_c which maximizes the mass parameter. For the non-interacting case ($\Lambda < 4\pi$) it is approximately $\sigma_c = 0.2$, while for the interacting case ($\Lambda > 4\pi$) it lies in the range $\sigma_c \in (0, 0.2)$. Also hinted by this Figure is that the maximum mass parameter increases for higher Λ. This behavior is made clearer in Figure 3.1b.

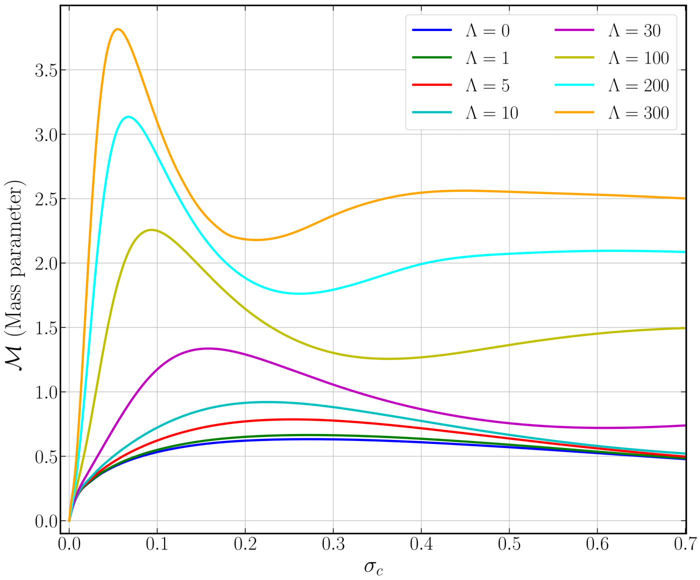

(a) Mass parameter $\mathscr{M}$ as a function of $\sigma_c = \sqrt{4\pi G}\Phi_c$ for different values of Λ.

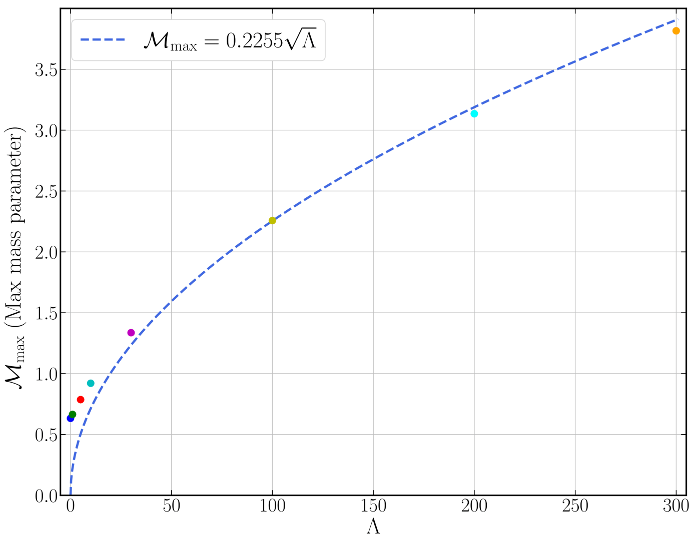

(b) Maximum value of the mass parameter $\mathscr{M}_{\max}$ as a function of Λ for the same values of Λ as in Figure 3.1a. The dashed curve is the fit.

Figure 3.1.: Behavior of the mass parameter and its maximum for different values of σ_c and Λ.

In Figure 3.1b the maximum mass parameter has been plotted against Λ. The behavior has been approximately fitted by a square-root function of the form $\mathscr{M}_{\max} = 0.2255\sqrt{\Lambda}$.

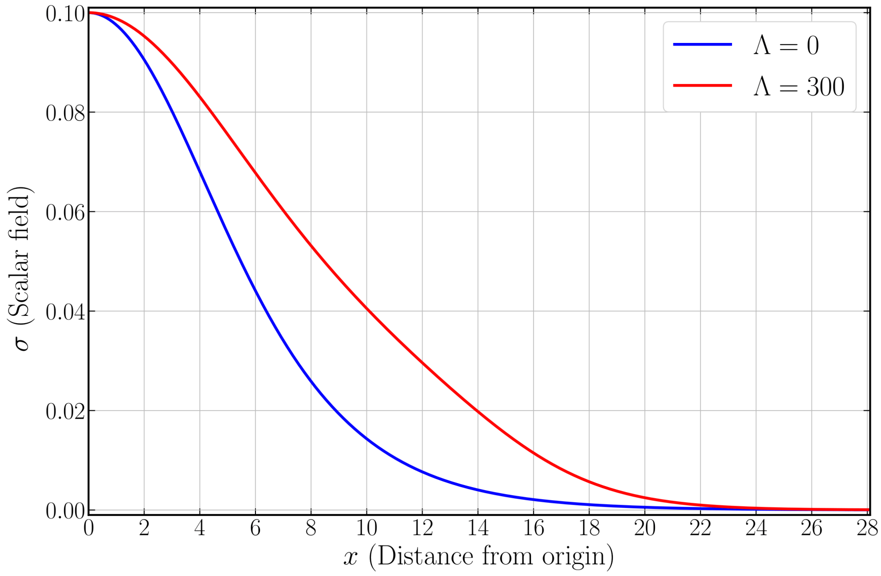

(a) Scalar field σ as a function of the dimensionless radius x for $\Lambda = 0, 300$.

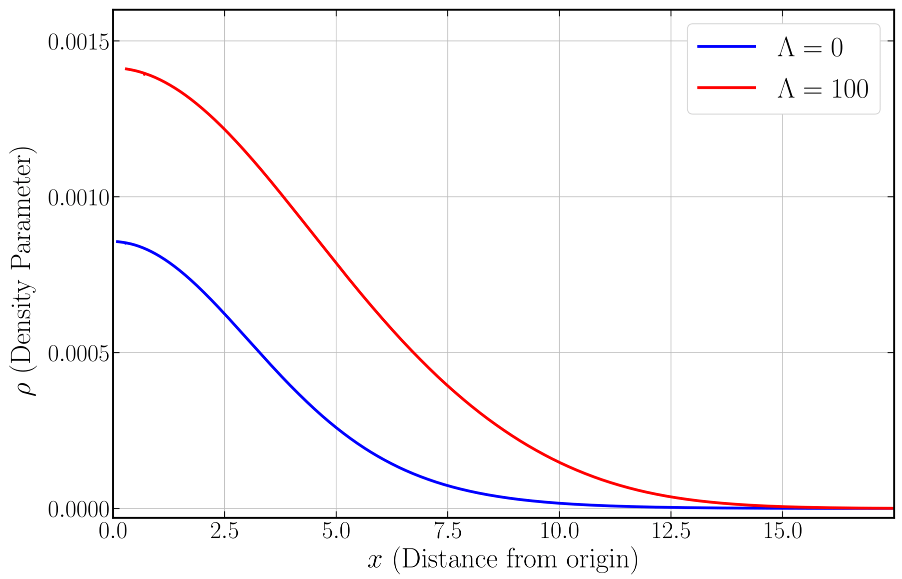

(b) Comparison between the density profiles for $\Lambda = 0$ and $\Lambda = 100$ for $\sigma_c = 0.1$.

Figure 3.2.: Comparison of the field and density profiles in the interacting and non-interacting cases.

As another comparison, Figure 3.2a shows the difference in the profiles of the scalar field σ for the non-interacting and interacting cases. Both profiles used the condition $\sigma(0) = \sigma_c = 0.1$ and exemplify the constraint that the field has no nodes and approaches zero asymptotically at infinity. Figure 3.2b on the other hand, compares the density profiles, where the density parameter has been defined implicitly from the comparison between equations (3.25a) and (3.45) as

$$\rho := \frac{1}{4\pi}\left[\frac{1}{2}\left(\frac{\Omega^2}{B}+1\right)\sigma^2 + \frac{\Lambda}{4}\sigma^4 + \frac{1}{2}\frac{(\sigma')^2}{A}\right]. \tag{3.47}$$

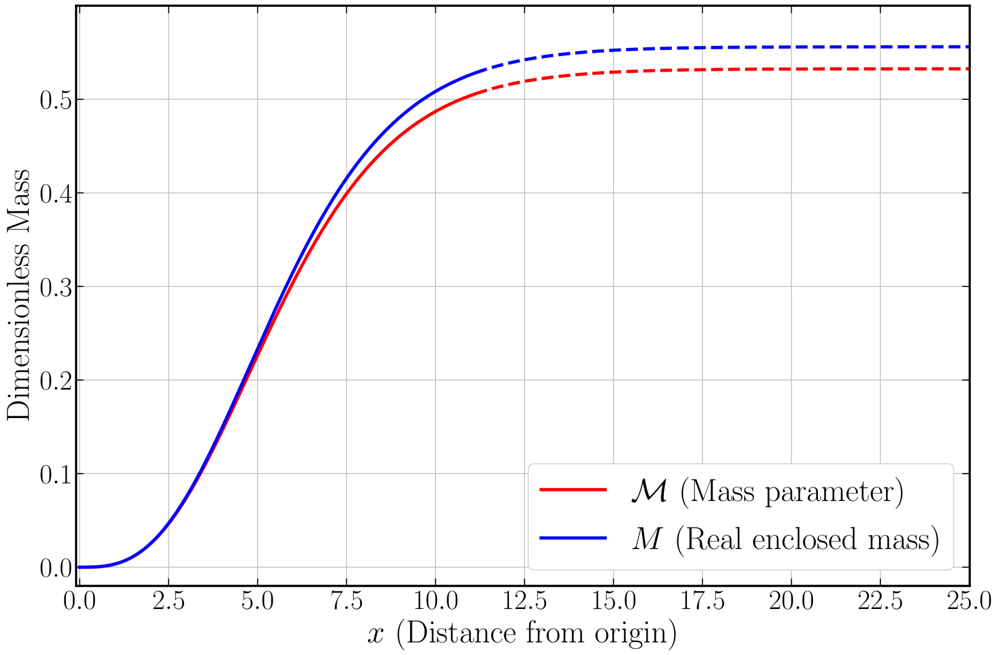

Figure 3.3.: Comparison between the mass parameter and dimensionless mass profiles for $\Lambda = 0$ and $\sigma_c = 0.1$.

So far the discussion has taken into account the mass parameter of the BS, without taking into account its real enclosed mass. The difference between their behaviors is shown in Figure 3.3. Here, the radial profiles for both quantities are plotted; the solid lines represent the mass profile until 95% of the total mass is reached, which is what I define as the star's rescaled radius $X = mR$. The dashed lines show the asymptotic behavior of the profiles as the radial coordinate goes to infinity. From this Figure it is noticed that the enclosed mass is greater than the mass parameter, but their overall behavior is the same which means that the radius of the star is independent of which mass is considered.

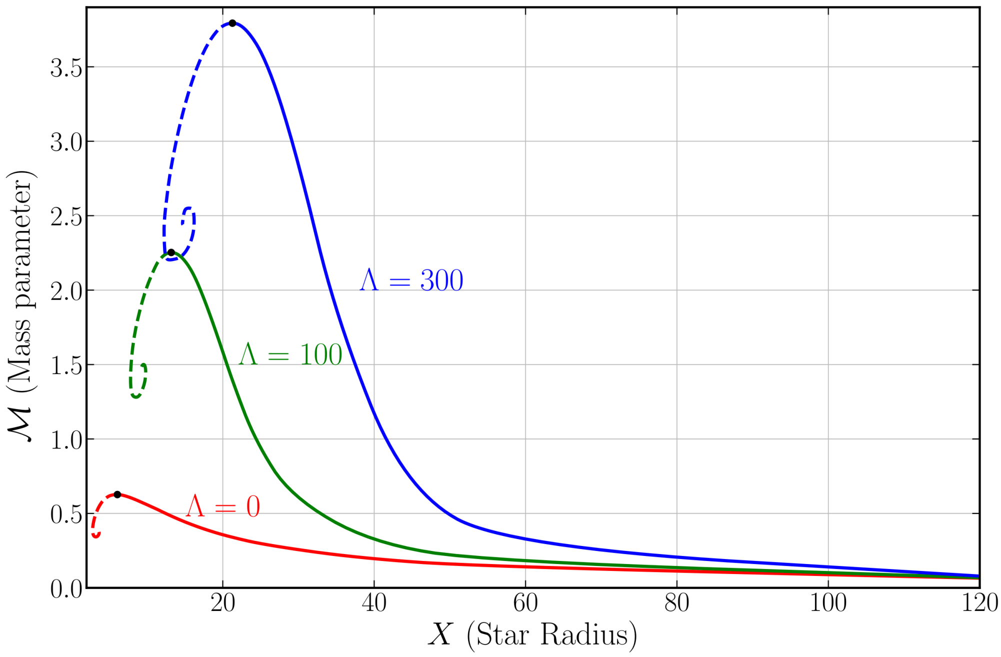

Figure 3.4.: Mass-radius relation for three values of Λ.

In Figure 3.4 the total mass parameter of the BS is plotted against the star's radius for the non-interacting ($\Lambda = 0$) and interacting cases ($\Lambda = 100, 300$). A dot has also been plotted to mark the maximum total mass parameter and its associated radius. It also labels the separation between the dashed and solid lines for each profile. The dashed lines represent unstable equilibria, where the ground state energy is higher than the equilibrium on the solid branch with the same number of particles.

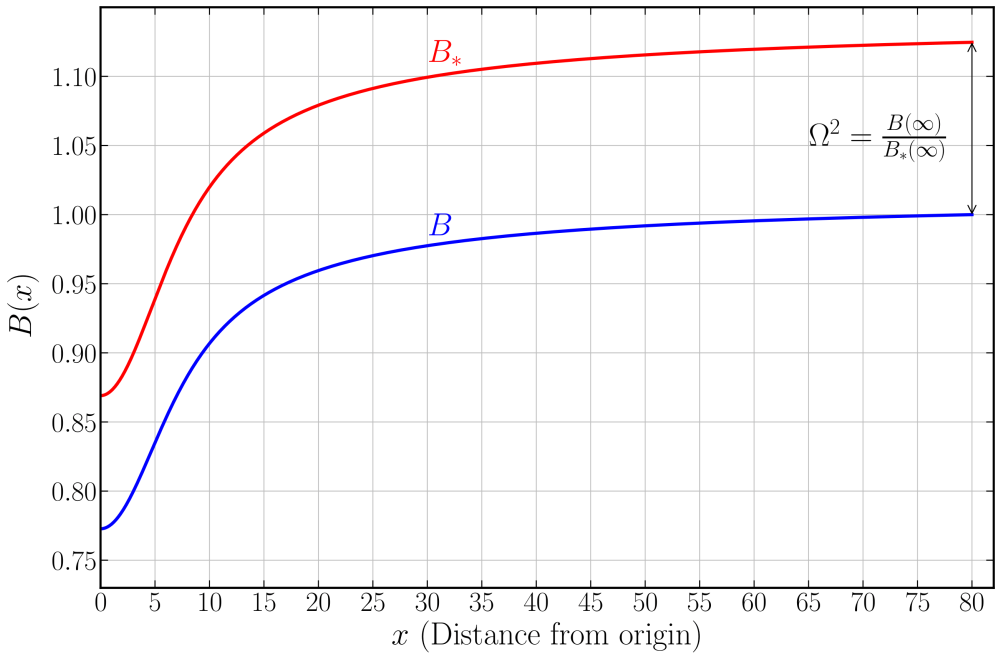

Figure 3.5.: Behaviour of the metric element B and B_* and calculation of Ω^2.

Figure 3.5 shows the behavior of the metric component B and its relation with the quantity used in computational calculations B_*. It also tells how to obtain the square of the particle energy divided by its mass $\Omega = \frac{\omega}{m} = \sqrt{\frac{B(\infty)}{B_*(\infty)}}$.

3.2.3. Strong Self-Interactions: the High Λ Limit

In the limit of large Λ, σ_c is no longer required. To see this a further redefinition of the variables is necessary:

$$x_* := x\Lambda^{-\frac{1}{2}} \quad \sigma_* := \sigma\Lambda^{\frac{1}{2}} \quad \mathscr{M}_* := \mathscr{M}\Lambda^{-\frac{1}{2}}. \tag{3.48}$$

Once again, these are dimensionless as Λ is itself dimensionless. In the following the primes will denote $\frac{d}{dx_*}$, instead of $\frac{d}{dx}$. Under this redefinition, equation (3.43c) becomes

$$\frac{1}{\Lambda}\sigma_*'' + \frac{1}{\sqrt{\Lambda}}\left(\frac{1}{\sqrt{\Lambda}}\frac{2}{x_*} + \frac{B'}{2B} - \frac{A'}{2A}\right)\sigma_*' + A\left[\left(\frac{\Omega^2}{B} - 1\right)\sigma_* - \sigma_*^3\right] = 0, \tag{3.49}$$

which in the limit $\Lambda \to \infty$ goes to

$$\sigma_* = \left(\frac{\Omega^2}{B} - 1\right)^{\frac{1}{2}}, \tag{3.50}$$

that is, σ_* is completely defined by $B(x_*)$ and Ω. Under the redefinitions above, the system to solve becomes

$$\mathscr{M}_*'(x_*) = x_*^2\left[\frac{1}{2}\left(\frac{\Omega^2}{B} + 1\right)\sigma_*^2 + \frac{1}{4}\sigma_*^4 + \frac{1}{2\Lambda}\frac{(\sigma')^2}{A}\right], \tag{3.51a}$$

$$\frac{B'}{ABx_*} - \frac{1}{x_*^2}\left(1 - \frac{1}{A}\right) = \left(\frac{\Omega^2}{B} - 1\right)\sigma_*^2 - \frac{1}{2}\sigma_*^4 + \frac{1}{\Lambda}\frac{(\sigma_*')^2}{A}. \tag{3.51b}$$

In the limit $\Lambda \to \infty$, the system may be written as

$$\mathscr{M}_*'(x_*) = 4\pi x_*^2 \rho_*\,, \tag{3.52a}$$

$$\frac{B_*'}{AB_*x_*} - \frac{1}{x_*^2}\left(1 - \frac{1}{A}\right) = 8\pi p_*\,, \tag{3.52b}$$

with the newly defined dimensionless pressure (p_*) and density (ρ_*):

$$\rho_* = \frac{1}{16\pi}\left(\frac{3}{B_*}+1\right)\left(\frac{1}{B_*}-1\right), \tag{3.53a}$$

$$p_* = \frac{1}{16\pi}\left(\frac{1}{B_*}-1\right)^2, \tag{3.53b}$$

$$B_*(x_*) = \frac{B(x_*)}{\Omega^2}. \tag{3.53c}$$

From the system above one may obtain an effective equation of state that gives p_* as a function of ρ_*. From the equation (3.53a) one finds $\frac{1}{B_*}$ expressed as

$$\frac{1}{B_*} = \frac{1}{3}\left(1+2\sqrt{1+12\pi\rho_*}\right). \tag{3.54}$$

Upon substitution into (3.53b), the equation of state reads

$$p_* = \frac{1}{16\pi}\frac{4}{9}\left(\sqrt{1+12\pi\rho_*}-1\right)^2. \tag{3.55}$$

The goal here is now to obtain the Oppenheimer-Volkoff equation (3.23) in terms of the newly defined dimensionless variables, which will shed light on the reason why they were called the pressure and density. By analyzing the structure of the Oppenheimer-Volkoff equation, it is hinted that the expression $\rho_* + p_*$ should be calculated in terms of only one quantity (either ρ_* or p_*) by use of the equation of state. By choosing to only use the pressure, one obtains:

$$\rho_* + p_* = \frac{1}{18\pi}\left[1+24-\sqrt{1+12\pi\rho_*}\right]. \tag{3.56}$$

To fulfill the goal, one rewrites equation (3.52b) by substitution of A in terms of the mass parameter $\mathscr{M}_*$, that is

$$A(x_*) = \left(1-\frac{2\mathscr{M}_*}{x_*}\right)^{-1}, \tag{3.57}$$

which leads to:

$$\frac{B_*'}{B_*} = \frac{2\mathscr{M}_*}{x_*^2}\left(1+\frac{4\pi p_* x_*^3}{\mathscr{M}_*}\right)\left(1-\frac{2\mathscr{M}_*}{x_*}\right)^{-1}. \tag{3.58}$$

From (3.53b), the rescaled metric component B_* may be expressed in terms of the pressure as

$$B_* = \left(1 + \sqrt{16\pi p_*}\right)^{-1}. \tag{3.59}$$

Using this fact, one can rewrite the equation above in terms of only the pressure. Upon insertion of this expression, the left hand side is turned into

$$\frac{B'_*}{B_*} = -\frac{36\pi p'_*}{1 + 24\pi\rho_* - \sqrt{1 + 12\pi\rho*}}, \tag{3.60}$$

and here is where the hint from equation (3.56) comes into play. By comparison of these two equations, one obtains:

$$\frac{B'_*}{B_*} = -\frac{2p'_*}{\rho_* + p_*} = \frac{2\mathscr{M}_*}{x_*^2}\left(1 + \frac{4\pi p_* x_*^3}{\mathscr{M}_*}\right)\left(1 - \frac{2\mathscr{M}_*}{x_*}\right)^{-1}. \tag{3.61}$$

After isolation of the derivative of the pressure, the final expression takes the form

$$\frac{dp_*}{dx_*} = -\frac{1}{x_*^2}\left(4\pi p_* x_*^3 + \mathscr{M}_*\right)\left(\rho_* + p_*\right)\left(1 - \frac{2\mathscr{M}_*}{x_*}\right)^{-1}, \tag{3.62}$$

which is precisely the Oppenheimer-Volkoff equation in terms of dimensionless quantities and variables.

Before applying the equations of stellar structure (3.25), one must reformulate the Oppenheimer-Volkoff equation (3.62) in terms of the derivative of the density by using the equation of state (3.55) and making the substitution

$$\frac{dp_*}{dx_*} = \frac{dp_*}{d\rho_*}\frac{d\rho_*}{dx_*} = \frac{1}{3}\frac{\sqrt{1 + 12\pi\rho_*} - 1}{\sqrt{1 + 12\pi\rho_*}}\frac{d\rho_*}{dx_*}.$$

Thus, the system of equations for the stellar structure of a BS in the high Λ limit is expressed as

$$\frac{d\mathscr{M}_*}{dx_*} = 4\pi x_*^2 \rho_*(x_*), \tag{3.63a}$$

$$\frac{d\tilde{\mathscr{M}}_*}{dx_*} = \frac{d\mathscr{M}_*}{dx_*}\sqrt{A(x_*)} = \frac{d\mathscr{M}_*}{dx_*}\left[1 - \frac{2\mathscr{M}_*}{x_*}\right]^{-\frac{1}{2}}, \tag{3.63b}$$

$$\frac{d\rho_*}{dx_*} = -\frac{3}{x_*^2}\left(\rho_* + p_*(\rho_*)\right)\left(\frac{\sqrt{1+12\pi\rho_*}}{\sqrt{1+12\pi\rho_*}-1}\right)\left(\mathscr{M}_* + 4\pi P_* x_*^3\right)\left(1 - \frac{2\mathscr{M}_*}{x_*}\right)^{-1}, \tag{3.63c}$$

$$p_*(\rho_*) = \frac{1}{36\pi}\left[\sqrt{1+12\pi\rho_*} - 1\right]^2, \tag{3.63d}$$

where $\tilde{\mathscr{M}}_*$ denotes the real enclosed mass in dimensionless units, as hinted by equation (3.16). It is also of interest to obtain the behaviour of the metric components from equations (3.57), (3.59):

$$A(x_*) = \left(1 - \frac{2\mathscr{M}_*(x_*)}{x_*}\right)^{-1}, \tag{3.64a}$$

$$B_*(x_*) = \left(1 + \sqrt{16\pi p_*(x_*)}\right)^{-1}. \tag{3.64b}$$

In Figure 3.6, three density and mass profiles are plotted in dimensionless units. The red curve corresponds to the stable configuration with the largest total mass. The blue and green profiles serve as examples that suggest that the max radius of the star is inversely proportional to its mass.

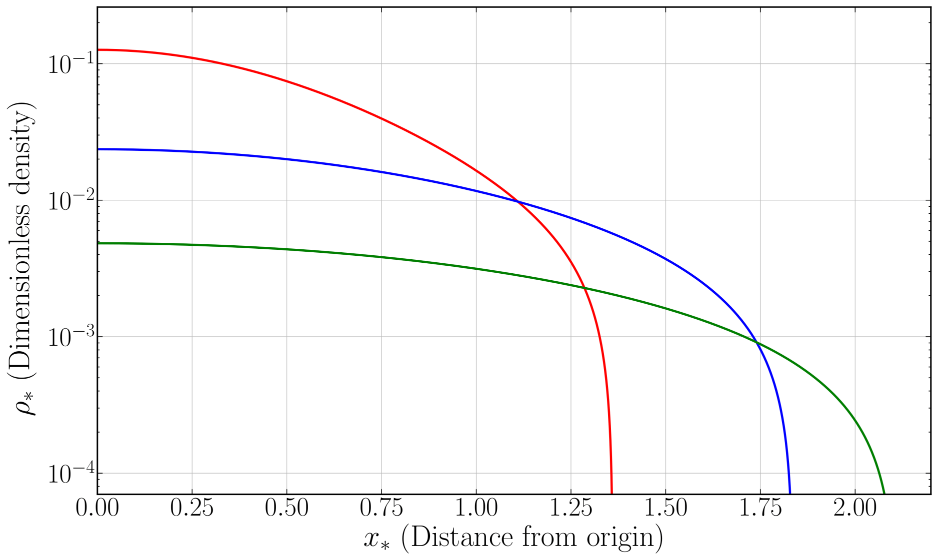

(a) Density profiles.

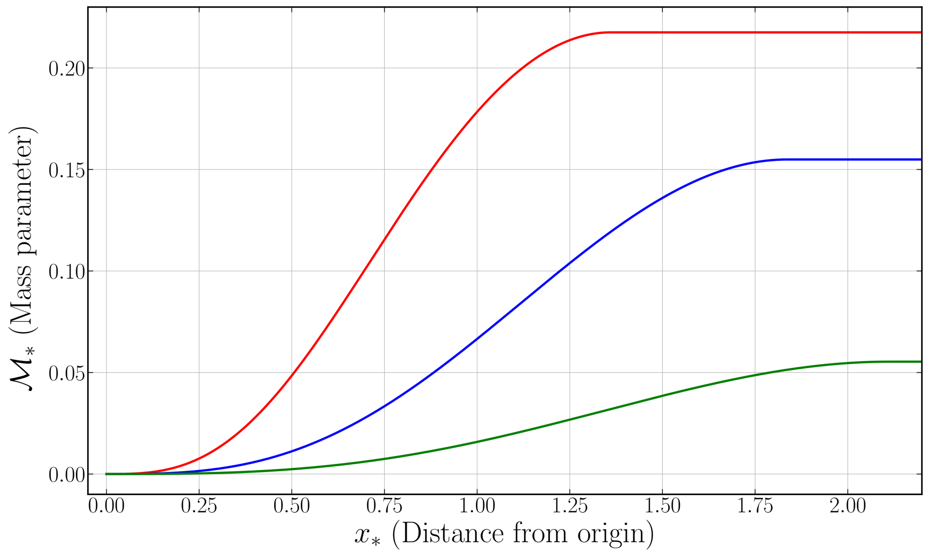

(b) Mass profiles.

Figure 3.6.: Three examples of density and their corresponding mass profiles in the high Λ limit. The red profile corresponds to the maximum mass equilibrium.

The total mass-radius relation is shown in Figure 3.7. The solid line corresponds to the stable configurations, while the dashed line represents the set of unstable equilibria; both branches are separated by the configuration with the largest total mass. The colored dots correspond to the profiles plotted in Figure 3.6. The behavior of the stable branch of the curve makes evident that the size of the compact object grows inversely to its mass.

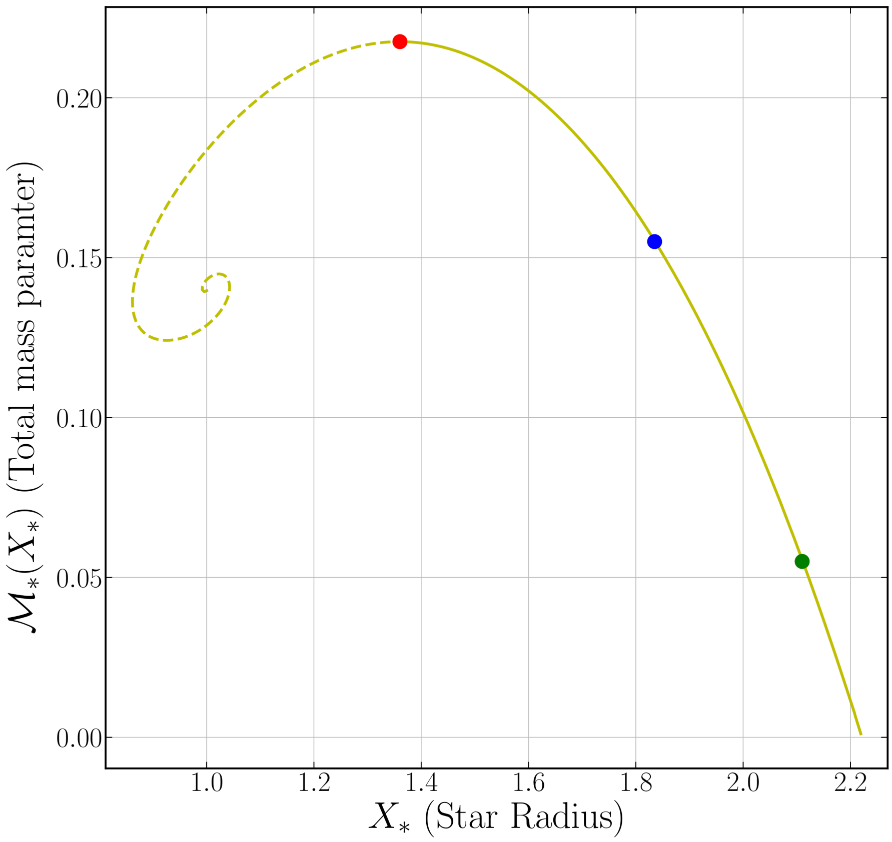

Figure 3.7.: The mass-radius relation for a BS in the high Λ limit. The 3 circles correspond to the density profiles in Figure 3.6.

In Figure 3.8 the behavior of the metric element B is shown for the largest-mass configuration. The size of this object in dimensionless units is read from the red profile of Figure 3.7 to be around $X_* = 1.36$. After this radius, the metric element behaves as the analog for the Schwarzschild metric and, as exemplified by the Figure, it approaches unity at infinity.

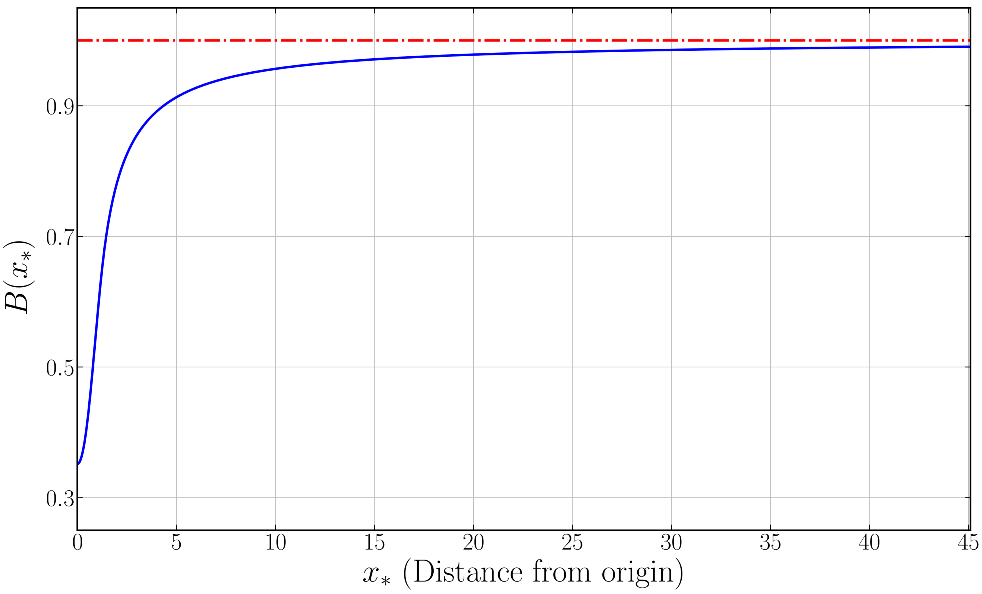

Figure 3.8.: Behavior of the metric element B in the high Λ limit.

Given the profiles for the structure of the star, its temperature profile may also be calculated as proposed by Balberg, Shapiro, and Inagaki, 2002; Masuda, Hatsuda, and Takatsuka, 2016 for the cases of a DM halo and a neutron star, respectively. They related the squared velocity dispersion of the particles which form the star in terms of the pressure and density as $p = \rho v^2$, which can then be associated with the temperature by use of the equipartition theorem by $k_B T = mv^2$. As such, in terms of the variables of this section, the dimensionless square velocity dispersion is given by

$$v_*^2(x_*) = \frac{p_*}{\rho_*} = \frac{1 - B_*(x_*)}{3 + B_*(x_*)}, \tag{3.65}$$

from which the temperature profile can be obtained to be

$$T(x_*) = \frac{m}{k_B}\frac{p}{\rho} = (1.17 \times 10^{13}\ \mathrm{K})\left(\frac{m}{1\ \mathrm{GeV}}\right) v_*^2(x_*) = (1004.52\ \mathrm{MeV})\left(\frac{m}{1\ \mathrm{GeV}}\right) v_*^2(x_*), \tag{3.66}$$

where, hinted by the equation above, the dimensionless temperature is defined as $T_* := \frac{p_*}{\rho_*}$. In Figure 3.9, the temperature profiles for the three color-coded configurations of Figure 3.7 are plotted in terms of the newly defined dimensionless variables. This Figure demonstrates, after the appropriate conversion to SI units (see A), that dark stars of interacting bosons are fairly small (with a radius of the order of 1 km) and that their core temperatures are in the same order of magnitude of newly formed neutron stars (10^{12} K).

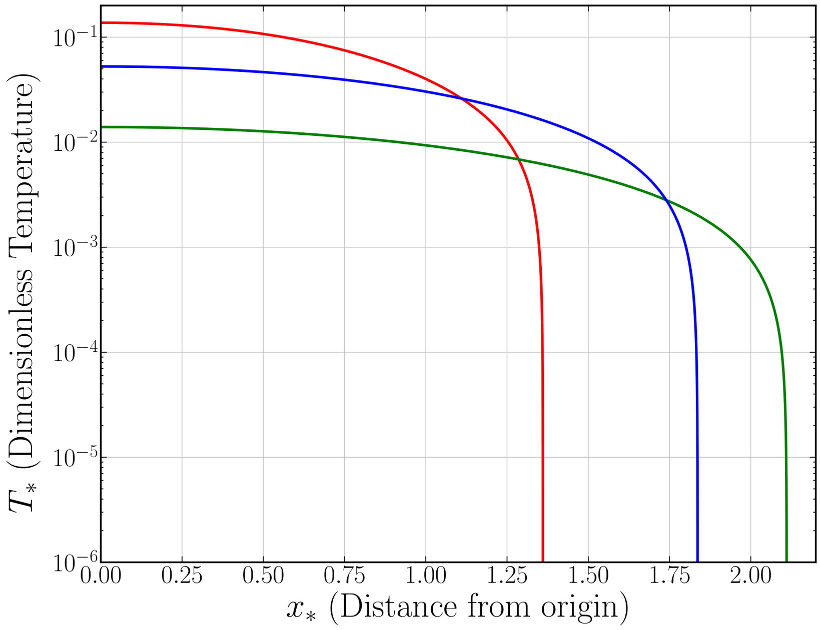

Figure 3.9.: Temperature profile in the high Λ limit assuming $m = 1$ GeV.

Finally, some values that will be used in following calculations are presented in Table 3.1, which correspond to dimensionless quantities for the BS with the greatest mass possible, namely the red point from Figure 3.7. Their transformation to SI units can be obtained from A.

Dimensionless quantity	**Value**
$\mathscr{M}_*$	0.217
X_*	1.358
ρ_*	0.058
p_*	0.007
T_*	0.082
$\rho_{*,\text{core}}$	0.126
$p_{*,\text{core}}$	0.017
$T_{*,\text{core}}$	0.137

Table 3.1.: Dimensionless quantities for the BS with the greatest mass in the high Λ limit. The first row corresponds to the averages over the star's interior, while the second presents the values at the core.

4. Capture of Visible Matter by Boson Stars

Given the structure of BSs, which has been investigated in the previous chapter, the next step towards answering the question of whether baryons captured by a BS are able to emit detectable signals is to tackle the capture itself. The goal of this chapter is to first give a brief presentation of the likely environment which encompasses a BS, as this dictates the amount of baryons available for capture. After getting a grasp on this surrounding medium, taking only gravitational effects, some first naive calculations of the amount of baryons captured by a general compact object per second (the capture rate) are performed. They serve as order of magnitude estimations and introduction to the related symbols and nomenclature. Afterwards, assuming that there is an interaction between DM particles and baryons, namely protons, the equation for the rate of capture of DM particles by celestial bodies is derived by using the widely used formalism introduced in the late 80s by Andrew Gould. Subsequently, this is applied to the particular case of this thesis: the capture rate of protons by a BS.

4.1. The Interstellar Medium

The goal of this section is to calculate the amount of SM matter that a theoretical self-interacting BS will be able to gather in time. This information will later be used to analyze whether such a star filled with known matter will be able to radiate, in hopes of being able to detect it and set limits on the DM mass and the interaction cross section between baryonic matter and DM.

Firstly, one must understand what kinds of matter would be available for the star to gather in its surrounding medium. The stars of a galaxy are embedded in a medium with several different constituents such as ordinary SM matter, relativistic charged particles (cosmic rays) and magnetic fields. All these components are called the interstellar medium (hereafter abbreviated as ISM) and, in the particular case of our Milky Way galaxy, their physical and chemical properties are inferred from a broad range of observations. For a comprehensive review, consider the work of Ferrière, 2001.

The interstellar matter, which accounts for $\sim 10 - 15\%$ of the total mass of the Galactic disk, exists in the form of gas (atoms, molecules, ions and electrons) and dust (tiny solid particles). The distribution of this mass is very inhomogeneous at small scales. Half of the mass distribution is found in clouds which occupy roughly 2% of the interstellar volume. The other half, which is spread out between the clouds, is freely distributed in the sense that it doesn't conglomerate with other particles.

The interstellar matter is usually classified as a function of its temperature, and how good they are at blocking the light from nearby stars. For the case of interstellar clouds, they are divided into three types: the dark clouds, which are made up of very cold molecular gas ($T \sim$ 10 K) and block off the light from the stars, diffuse clouds that consist of cold atomic gas ($T \sim$ 100 K) and are almost transparent to starlight except at a number of specific wavelengths which are crucial for their detection, and translucent clouds, which are made up of molecular and atomic gases and have different absorption wavelengths as the diffuse clouds.

On the other hand, the spread-out interstellar matter is divided into warm atomic (neutral), warm ionized and hot ionized, where warm refers to a temperature $\sim 10^4$ K and hot to $\sim 10^6$ K.

As mentioned before, the number density of each of these types of interstellar matter varies greatly between each of them, with the clouds being the densest (dark clouds have densities $n \sim 10^2 - 10^6$ cm^{-3}) and the free matter the least concentrated (hot ionized matter has a density $n \sim 0.0065$ cm^{-3}). The relevant quantities are summarized in Table 4.1:

Component	**Temperature** (K)	**Number density** (cm^{-3})	**Mass** ($10^9\ M_\odot$)
Molecular	10-20	$10^2 - 10^6$	1.3-2.5
Cold atomic	50-100	20-50	Cold and warm
Warm atomic	6000-10000	0.2-0.5	atomic $\gtrsim 6.0$
Warm ionized	$\sim$8000	0.2-0.5	$\gtrsim 1.6$
Hot ionized	$\sim 10^6$	~ 0.0065	$10^{-4} - 10^{-2}$

Table 4.1.: Parameters of the different components of the interstellar matter. The number density is that of hydrogen nuclei near the Sun and the mass is the one contained in the entire Milky Way.

The composition of the interstellar matter by its number of constituents is 90.8% of hydrogen, 9.1% of helium, and 0.12% of heavier elements, from which the most common are carbon, nitrogen and oxygen. On average, the density of the interstellar matter rounds up to one hydrogen atom per cubic centimeter in the Milky Way.

Another of the constituents of the ISM are magnetic fields. Their origin is still unknown (Widrow, 2002), but their features have been analyzed and they are believed to be present in all galaxies and galaxy clusters. They are characterized by a modest strength ($\sim 10^{-7} - 10^{-5}$ G) and a huge spatial scale ($\lesssim 1$ Mpc). They contribute significantly to the total pressure which balances the ISM against gravity and they may affect the gas flows in spiral arms, around bars and in galaxy halos.

The final component of the ISM are cosmic rays. They are highly energetic charged particles that traverse the Galaxy at speeds close to the speed of light. They are composed of protons ($\sim 90\%$), helium nuclei ($\sim 10\%$), heavier nuclei ($\sim 1\%$), electrons ($\sim 2\%$), and smaller amounts of positrons and antiprotons.

Given that cosmic rays are electrically charged, they are deflected by magnetic fields, and their directions are randomized, so it is impossible to localize their sources. Nevertheless, the elemental composition of these rays has led to two different kinds of possible sources. On the one hand, the similarity with the elemental composition of solar energetic particles, suggests that Galactic cosmic rays originate in unevolved late-type stars, and are injected into the surrounding ISM via flares out of their corona. On the other hand, highly energetic cosmic rays must be produced by supernova explosions, as these are the only events that both provide the required energy (10^{51} ergs) and explain the overabundance of heavy nuclei, namely iron, element which is only present in very evolved early-type stars.

The field of study of cosmic rays and their origins is a hot topic in the astrophysical community and recent observations, such as the one by the Alpha Magnetic Spectrometer (AMS-02) related to positrons (Aguilar *et al.*, 2013) has led several researchers to suggest new, "exotic" cosmic ray sources such as astrophysical accelerators (namely pulsars) and annihilating or decaying DM.

4.2. Distribution of Hydrogen in the Galaxy

Hydrogen is the most abundant element in the ISM, and is most commonly found in cold, diffuse clouds. It emits radiation due to a magnetic dipole transition from two very closely spaced energy levels in the ground state of the neutral hydrogen atom (HI). This transition comes about when a slightly more energetic parallel spin configuration between proton and electron drops to a less energetic anti-parallel ground state. The energy difference between both states is approximately 6 μeV, which by the Planck equation corresponds to an emitted photon with a wavelength $\lambda = \frac{hc}{\Delta E} \approx 21$ cm, as such this line is often called the "21 cm line".

Magnetic dipole emission is a "forbidden" transition, which means that its probability is extremely low; in fact, the lifetime of the excited state is approximately 11 million years. Such a phenomenon is practically impossible to be observed in a laboratory because collisions between the particles will de-excite the aligned spin well before there has been a spontaneous transition. Despite this fact, as mentioned in Section 4.1, the ISM has very small number densities, while still having a huge amount of neutral hydrogen. In this context, the 21 cm line holds great observational value, as its low probability becomes an advantage, since the radiation can traverse HI gas without being reabsorbed and its long wavelength avoids it from being blocked by dust.

It is precisely this 21 cm line and its Doppler shift that is observed by astronomers to determine the distance to and amount of HI in the Milky Way galaxy. The problem is, however, not trivial and enjoys interest from the astrophysical community. Such efforts are introduced in the review by Kalberla and Kerp, 2009.

The HI distribution in the Milky Way has been studied from three different perspectives:

- From a quasi-static, large-scale approach. This is the so-called global picture of the HI distribution.
- From a dynamical, small-scale point of view, known as the violent ISM.
- From the observed physical state of the neutral HI distribution, which can be characterized by a cold, cloud or by a warm, diffuse medium. Here the multiphase structure of the ISM is considered.

The global structure of HI in the galaxy can be traced far beyond the stellar population, radially but also perpendicular to the galactic disk. The outer part is only slightly affected by the stellar disk but it sheds light on influences from the intergalactic medium on the Milky Way and its star formation (Kalberla and Dedes, 2008). The properties of the large scale HI distribution depend on the shape of the Galactic rotation curve, as the distribution must be consistent with the density profile used in the fit of the rotation curve, as mentioned in Section 2.1.1. There is a general consensus that the most likely rotation curve is flat at large distances with $v_{\text{rot}} \sim 220\ \frac{\text{km}}{\text{s}}$, as demonstrated by observations, like the example shown in Figure 4.1:

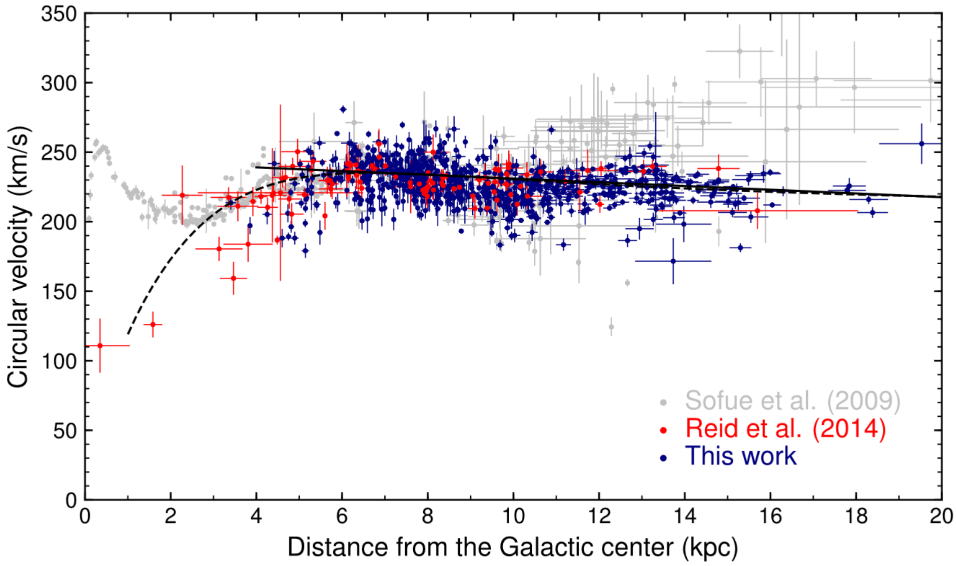

Figure 4.1.: Rotation Curve of the Milky Way from a study using Cepheids by Mróz *et al.*, 2019.

The hydrogen distribution on this large scale drops with distance from the Galactic center. The distribution inside the solar circle is ambiguous, but for galactocentric radii larger than the Sun's ($R > R_{\odot} \approx 8$ kpc), it is exponential with a radial scale length of $R_s = 3.15$ kpc, as presented in Figure 4.2. The HI disk of the Milky Way follows the exponential distribution until $R \sim 35$ kpc. At the outskirts ($40 \lesssim R \lesssim 60$ kpc), the behavior of the hydrogen gas turns turbulent and it is best described by a different exponential with scale length $R_s = 7.5$ kpc and a velocity dispersion of 74 $\frac{\text{km}}{\text{s}}$.

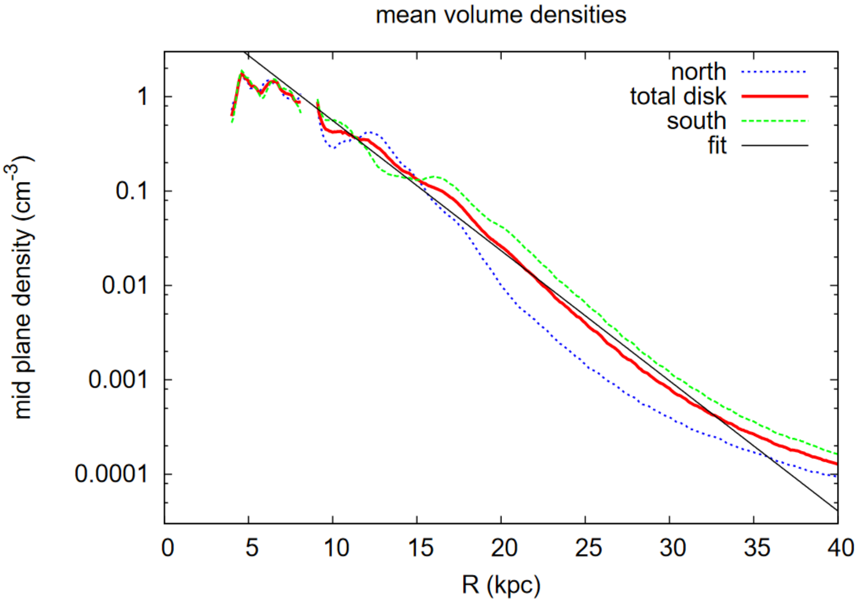

Figure 4.2.: Density distribution of neutral hydrogen in the Milky Way (Kalberla and Dedes, 2008).

The HI distribution presents small-scale structure at all galactocentric distances in the form of filaments, shells, spurs and chimneys. These types of structures are created by intense stellar winds and violent supernova explosions, and are the most prominent tracers of the Galactic "ecosystem" and its magnetic fields, as these formations are preferentially aligned with the magnetic field. The distribution of the shell substructures, for example, also follows an exponential with a scale length of $2 \lesssim R_s \lesssim 5$ kpc, but given that the small-scale arrangements depend on individual supernovae their position tends to be randomized. Nonetheless, it has been shown that this component of the ISM is dominated by cool, dense media (Peek and Clark, 2019).

The HI gas is found in mainly two states: in a cold, cloud structure or in a warm, diffuse distribution. Both types coexist in pressure equilibrium with stable phases at the temperatures given in Table 4.1. Gas at intermediate temperatures is considered unstable and it tends to one of the other two.

4.3. First Estimations of the Capture Rate

4.3.1. Geometrical Cross Section

To calculate the amount of particles that a compact object can gather, the strength of the interaction between the incoming particles and the targets that make up the celestial body plays a fundamental role, as it gives a measure of the amount of scatterings that incoming particles can have with the ones that make up the capturing object. The more interactions possible, the higher the probability of capture. As such, it proves useful to determine the interaction cross section that maximizes this probability, namely that it guarantees capture. This is the geometrical cross section and it serves as the "best case scenario" and sets the upper limit on the rate of capture for a compact object. To calculate it one considers a celestial body of radius R and mass M, henceforth referred to as a star, as that is the case of interest. The classical picture is taken and it is assumed that it is filled with identical spherical particles each of mass m and radius r, as exemplified by Figure 4.3:

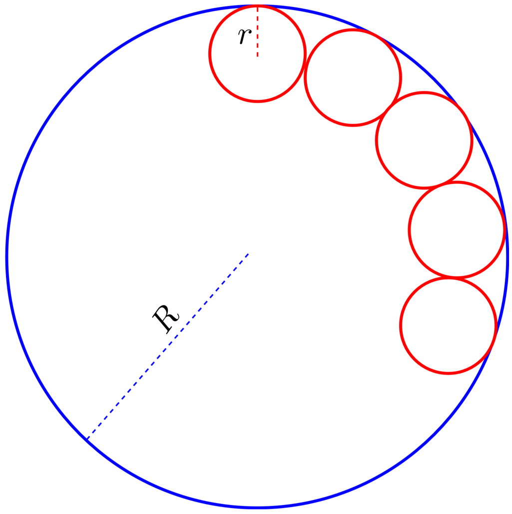

Figure 4.3.: Schematical view of a star filled with spherical particles.

The relation between the masses and volumes of the star and the particles is given by

$$M = Nm \implies N = \frac{M}{m}, \tag{4.1a}$$

$$V_{\text{star}} = \frac{4\pi}{3}R^3 = NV_{\text{particle}} = N\frac{4\pi}{3}r^3 \implies r = RN^{-\frac{1}{3}}. \tag{4.1b}$$

In the classical limit, one may assume that the cross section of each particle is

$$\sigma_{\text{geo}} = \pi r^2 = \pi R^2 N^{-\frac{2}{3}} = \pi R^2 \left(\frac{m}{M}\right)^{\frac{2}{3}}. \tag{4.2}$$

Equation (4.2) is the geometrical cross section and it is the upper limit on the cross section of the $\chi p \to \chi p$ scattering process. In terms of quantities obtained in the high Λ limit of Section 3.2.3:

$$\sigma_{geo} = (2.26 \times 10^{-28}\ \text{cm}^2)\lambda^{\frac{2}{3}} \left(\frac{1\ \text{GeV}}{m}\right)^2 \frac{X_*^2}{\mathscr{M}_*^{\frac{2}{3}}}. \tag{4.3}$$

From here, the expected geometrical capture rate may be calculated as dictated by the relation $C_{\text{geo}} = N\sigma_{\text{geo}}v_\infty n$, where v_∞ is the velocity of the approaching protons and n is the surrounding proton number density. Given the information available on the ISM (summarized in the previous sections), both quantities may be estimated as $v_\infty \sim 220\ \frac{\text{km}}{\text{s}}$ and $n \sim 1\ \text{cm}^{-3}$. This gives the solution

$$C_{\text{geo}} \sim (2.54 \times 10^{36}\ \text{s}^{-1})\lambda^{\frac{7}{6}} \left(\frac{1\ \text{GeV}}{m}\right)^5 \mathscr{M}_*^{\frac{1}{3}} X_*^2. \tag{4.4}$$

This first estimation overshoots the value obtained with a more careful treatment, which will be explained in the following sections. This is because the geometrical cross section is much larger than the measured upper limit of the interaction between DM and baryons by several orders of magnitude. In the next section a more accurate treatment of this calculation is performed.

4.3.2. Classical Capture Rate by a Boson Star

In the following sections, the rate of capture of protons by a BS will be formally calculated as it is done in current research. Nevertheless, it proves useful to obtain an order of magnitude estimate of this quantity in the classical regime. This is what is performed in this section.

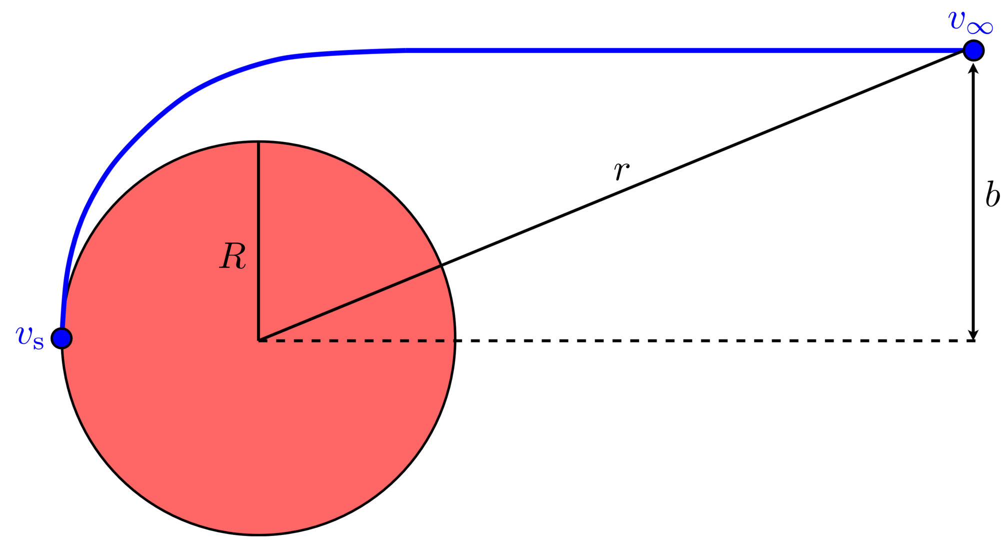

Figure 4.4.: Schematical view of a particle being captured by a star.

One may assume that the star is surrounded by a region of protons with number density n. From the reference frame of the star, the protons approach it with an average velocity v_∞. Then, the classical capture rate can be calculated as

$$C_{\text{classical}} = \pi b^2 v_\infty n, \tag{4.5}$$

where b is the impact parameter as drawn in Figure 4.4. To find an expression for this impact parameter, one uses conservation of energy and angular momentum at two points: infinity and at the point where the particle grazes the star's surface. The energy is given by

$$E = \frac{1}{2}m\dot{r}^2 - \frac{GMm}{r} + \frac{l^2}{2mr^2}, \tag{4.6}$$

where l is the particle's angular momentum. At infinity ($r \to \infty, \dot{r} \to v_\infty$), the energy reads $E = \frac{1}{2}mv_\infty^2$, while for a particle grazing the star ($r = R, \dot{r} = 0$), the energy becomes $E = -\frac{GMm}{R} + \frac{l^2}{2mR^2}$. So, energy conservation allows one to write the square of the angular momentum as

$$l^2 = 2mR^2\left(\frac{1}{2}mv_\infty^2 + \frac{GMm}{R}\right). \tag{4.7}$$

Angular momentum is conserved, and for a particle at infinity it is of the form $l = mv_\infty b$. By equating with (4.7), the impact parameter is found to be

$$b = R\sqrt{1 + \frac{\frac{2GM}{R}}{v_\infty^2}}, \tag{4.8}$$

where $\frac{2GM}{R}$ may be rewritten as the escape velocity at the surface of the star v_s. In the particular case of a BS, the escape velocity at the surface is around 1000 times larger than the assumed velocity of particles at infinity, so the equation above may be approximated to

$$b = R\sqrt{1 + \frac{\frac{2GM}{R}}{v_\infty^2}} \approx R\frac{\sqrt{\frac{2GM}{R}}}{v_\infty} = R\frac{v_s}{v_\infty}. \tag{4.9}$$

Inserting the expression for the impact parameter into equation (4.5), one obtains the classical capture rate

$$C_{\text{classical}} = \pi R^2 \frac{v_s^2}{v_\infty} n = 2\pi G\left(\frac{n}{v_\infty}\right) MR, \tag{4.10}$$

which agrees with the limit when $c \to \infty$ of the result provided by Goldman and Nussinov, 1989. In terms of the expressions from the high Λ limit Section 3.2.3, the classical capture rate is

$$C_{\text{classical}} = \left(2.60 \times 10^{23}\ \frac{\text{m}^4}{\text{s}^2}\right)\left(\frac{n}{v_\infty}\right)\lambda\left(\frac{1\ \text{GeV}}{m}\right)^4 \mathscr{M}_* X_*. \tag{4.11}$$

For $v_\infty \sim 220\ \frac{\text{km}}{\text{s}}$ and $n \sim 1\ \text{cm}^{-3}$, this gives:

$$C_{\text{classical}} \sim \left(1.18 \times 10^{24}\ \text{s}^{-1}\right)\lambda\left(\frac{1\ \text{GeV}}{m}\right)^4 \mathscr{M}_* X_*, \tag{4.12}$$

which is a more conservative result than the one from (4.4), as the square of the impact parameter, which is the analogue to the cross section is much smaller than the number of DM times their geometrical cross section. The result derived here is much closer to the one obtained with the complete formalism, which will be explained in the following section.

4.4. Capture Rate by a Boson Star

4.4.1. Capture Formalism for Dark Matter Particles

The formalism for the calculation of the capture rate of DM particles by celestial bodies such as stars or the Earth was set up in the late 80s and early 90s by Andrew Gould in his two seminal articles (Gould, 1987; Gould, 1992). In this section his work is presented and summarized and in the next it is applied to the case of capture by BSs.

First, the surface of the capturing object is modeled as a thin spherical shell with radius r from its center and thickness dr in a spherically symmetric gravitational field. The escape velocity at the shell is denoted as v_{s} and $\Omega^{-}_{v_{\mathrm{s}}}(w)$ is defined as the rate per unit time that a DM particle with an initial velocity w scatters down to a velocity less than v_{s} while traveling through the shell. The incoming DM particles are assumed to follow an isotropic ($u = \mid \vec{u} \mid$) velocity distribution $f(u)du$ away from the gravitational field.

The next step is to consider a unit surface element located on a sphere of radius $R >> r$, such that the gravitational field is negligible. The spatial number density of incoming DM particles with velocities between u and $u+du$, and with an angle from the normal of the surface element between θ and $\theta + d\theta$ is given by

$$\frac{1}{2} f(u)\, du\, d\cos\theta. \tag{4.13}$$

The differential flux (number per area per time) of such particles going through the surface element is equation (4.13) multiplied by an additional factor $u\cos\theta$, which accounts for velocity of the DM particles perpendicular to the surface. The flux can then be expressed as

$$dF = \frac{1}{4} f(u)\, u\, du\, d\cos^2\theta, \qquad 0 \leq \theta \leq \frac{\pi}{2}. \tag{4.14}$$

Now, the angular momentum per unit mass is considered and variables are changed as:

$$J = Ru\sin\theta, \qquad d\cos^2\theta = \frac{dJ^2}{R^2u^2}, \tag{4.15}$$

such that the flux over all the differential area elements of the surface may be rewritten as

$$dF_{\text{area}} = 4\pi R^2 \frac{1}{4} f(u)\, u\, du \frac{dJ^2}{R^2u^2} = \pi \frac{f(u)}{u} du\, dJ^2. \tag{4.16}$$

A DM particle whose velocity at infinity is u will be accelerated by the gravitational potential and will have a velocity at the shell at radius r of w, where

$$w = \sqrt{u^2 + v_{\text{s}}(r)^2}. \tag{4.17}$$

For the DM particle to be captured by the celestial body, it must interact and scatter to a velocity smaller than $v_{\text{s}}(r)$. The probability of this happening is the product of total time that the particle spends within the shell with the previously defined $\Omega^-_{v_{\text{s}}}(w)$, that is

$$P(w \to w' < v_{\text{s}}(r)) = \Omega^-_{v_{\text{s}}}(w)\, \frac{dl}{w}, \tag{4.18}$$

where $\frac{dl}{w}$ describes the differential time required for the DM particles to traverse the shell. The quantity dl corresponds to the differential distance traveled by the particle within the celestial body.

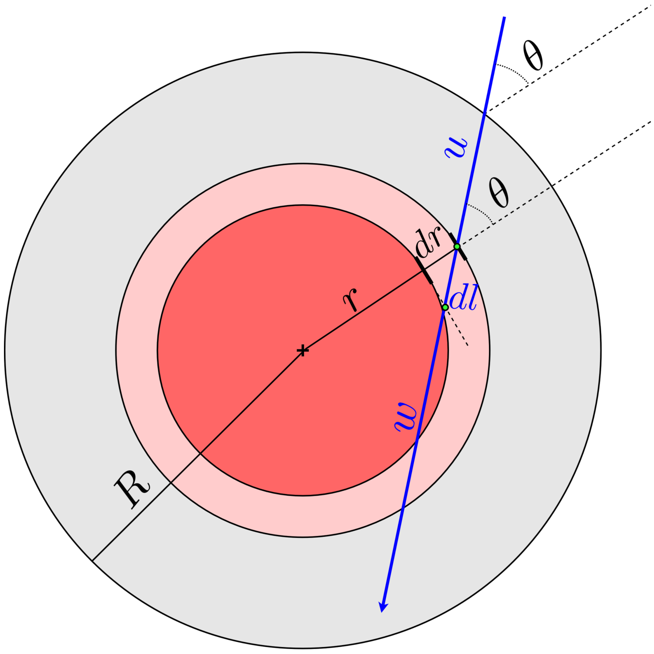

Figure 4.5.: Schematical view of a particle traversing a compact object.

This differential distance can be related to the thickness of the shell through the relation (see Figure 4.5)

$$dl = \frac{dr}{\cos\theta} = \frac{dr}{\sqrt{1 - \frac{J^2}{r^2 w^2}}}, \tag{4.19}$$

where for the last equality the trigonometric function was expressed in terms of the particle's angular momentum per mass by using equation (4.15) and replacing $R \to r$, $u \to w$, which holds within the shell. By applying these transformations, the differential time is rewritten as

$$\frac{dl}{w} = \frac{1}{w}\frac{dr}{\sqrt{1 - \frac{J^2}{r^2 w^2}}} = \frac{1}{w}\left[1 - \left(\frac{J}{rw}\right)^2\right]^{-\frac{1}{2}} dr \times \left[2\mathscr{H}(rw - J)\right], \tag{4.20}$$

where in the last equality the Heaviside step function and a factor of 2 were added by hand. The reason why is that the DM particle intersects the shell twice if the angular momentum is small enough, namely if $J < rw$, or not at all if the converse is true.

Multiplying the differential flux (4.16) with the conditional probability (4.18) with the substitution given by (4.20) and integrating over all angular momenta gives the number of DM particles captured per unit time per unit velocity

$$4\pi r^2 \, dr \frac{f(u)du}{u} w\Omega^-_{v_s}(w), \tag{4.21}$$

from which the capture rate can finally be obtained by integrating (4.21) over the velocity distribution (where w is considered a variable that depends on u explicitly by considering (4.17)) and the capturing body's radius:

$$C = \int_0^R 4\pi r^2 \, dr \int \frac{f(u)du}{u} w\Omega^-_{v_s}(w). \tag{4.22}$$

The last expression to be determined is $\Omega^-_{v_s}(w)$. To do this, one must take a look at the scattering between the incoming DM particle and the particles that make up the capturing body, namely the differential cross section $\frac{d\sigma}{dQ}$, where Q is the energy transfered during the scattering. Assuming that the target particle is at rest before the interaction, kinematic limits on the energy transfer Q can be derived. The minimum is given when no interaction takes place, that is:

$$Q_{\text{minimal}} = 0. \tag{4.23}$$

The maximum, on the other hand, can be quickly derived in the non-relativistic limit by energy and momentum conservation:

$$\begin{aligned} \frac{1}{2}mw^2 =& \frac{1}{2}mv_\chi^2 + \frac{1}{2}m_\mathrm{i}v_\mathrm{i}^2, \\ mw =& mv_\chi + m_\mathrm{i}v_\mathrm{i}, \end{aligned} \tag{4.24}$$

where the subindex i denotes the target particle and v_χ stands for the DM particle's velocity after the interaction. The maximal energy transfer is found to be

$$Q_\mathrm{max} = \frac{1}{2}m(w^2 - v_\chi^2) = \frac{1}{2}mw^2\left(\frac{4m_\mathrm{i}\,m}{(m_\mathrm{i}+m)^2}\right). \tag{4.25}$$

Within this range all energy transfers have the same probability. For a total cross section denoted as σ_tot, the differential cross section can be written as

$$\frac{d\sigma}{dQ} = \frac{1}{Q_\mathrm{max}}\,\sigma_\mathrm{tot}\,\mathscr{H}\,(Q_\mathrm{max} - Q). \tag{4.26}$$

For a DM particle to be captured, it must lose enough energy, so that its velocity is below v_s after the scattering. From this the minimal required energy transfer can be determined to be

$$Q_\mathrm{min} = \frac{1}{2}mw^2 - \frac{1}{2}mv_\mathrm{s}^2 = \frac{1}{2}mu^2, \tag{4.27}$$

where equation (4.17) has been substituted. With the differential cross section and the minimal energy transfer needed for capture $\Omega_{v_\mathrm{s}}^-(w)$ can finally be calculated as

$$\Omega_{v_\mathrm{s}}^-(w) = n_\mathrm{i}(r)w(r)\int_{Q_\mathrm{min}}^{Q_\mathrm{max}} \frac{d\sigma}{dQ}\,dQ = \sigma_\mathrm{tot}\,n_\mathrm{i}(r)\,w(r)\,\frac{Q_\mathrm{max} - Q_\mathrm{min}}{Q_\mathrm{max}}\,\mathscr{H}\,(Q_\mathrm{max} - Q_\mathrm{min}), \tag{4.28}$$

where $n_\mathrm{i}(r)$ is the number density of the target particle i at a distance r from the center of the celestial body. Equation (4.28) presents the total rate of scattering $\sigma_\mathrm{tot}\,n_\mathrm{i}(r)\,w(r)$ multiplied by a factor that stands for the probability that the DM particle has lost enough energy to be captured after its interaction with the target particles.

By introducing (4.28) into (4.22) and multiplying by the number density of DM particles that surround the celestial body, the DM capture rate is finally written as

$$C_{\text{final}} = \int_0^R 4\pi r^2\, dr \int \frac{f(u)\, du}{u} w(r)^2 n_{\text{i}}(r) \sigma_{\text{tot}} \left(\frac{\rho_\chi}{m}\right), \tag{4.29}$$

where it was assumed that all DM particles are captured ($Q_{\text{min}} = Q_{\text{minimal}} = 0$) and ρ_χ stands for the surrounding DM density.

4.4.2. Application to Capture by a Boson Star

In the previous section the capture rate of DM particles by a general celestial body was derived. The formalism for the case of a BS is completely analogous, as such the capture rate of protons by a BS is given by

$$C_{\text{BS}} = \int_0^{R_{\text{BS}}} 4\pi r^2\, dr \int \frac{f(\vec{v})}{v} \omega^2(r,v) n(r) \sigma \left(\frac{\rho_p}{m_p}\right) d^3\vec{v}, \tag{4.30}$$

where $f(\vec{v})$ is the proton velocity distribution, v is the velocity of the proton at infinity with respect to the BS's rest frame. The star's radial number density is expressed as $n(r)$, the surrounding proton density is ρ_p, $\omega = \sqrt{v^2 + v_{\text{esc}}^2(r)}$ is the proton incident velocity at radius r inside the BS, with the escape velocity

$$v_{\text{esc}} = \sqrt{v_c^2 - (v_c^2 - v_s^2)\frac{M(r)}{M_{\text{BS}}}}, \tag{4.31}$$

where $v_s = \sqrt{\frac{2GM_{\text{BS}}}{R_{\text{BS}}}}$ and $v_c = \sqrt{v_s^2 + \frac{2G}{R_{\text{BS}}^3}\int_0^{R_{\text{BS}}} M(r) r\, dr}$ are the escape velocity at the BS's surface and the core, respectively. $M(r)$ is the mass profile of the star, and the velocity-dependent cross section of the proton-DM interaction is $\sigma(\omega)$.

The two proton velocity distributions of interest are the Maxwell-Boltzmann distribution and the delta distribution, given by

$$f(\vec{v}) = \begin{cases} \frac{1}{(\pi v_0^2)^{3/2}} \mathrm{e}^{-\frac{(\vec{v}+\vec{v}_{\text{BS}})^2}{v_0^2}}, & \text{Maxwell} - \text{Boltzmann}, \\ \delta^{(3)}(\vec{v} - \vec{\bar{v}}), & \text{Delta} \end{cases}, \tag{4.32}$$

where v_0 is the velocity dispersion of the distribution, $\vec{v}_{\text{BS}}$ is the BS's velocity relative to the galactic halo and $\vec{\bar{v}}$ is the average velocity of the protons at infinity from the rest frame of the star, and its magnitude can be assumed to be $\bar{v} \approx v_0 = 220\ \frac{\text{km}}{\text{s}}$, as explained in Section 4.2.

Upon insertion of both distributions into equation (4.30), the expression for the capture rate may be expanded as

$$\begin{aligned} C_{\mathrm{BS}} =& \frac{8\pi^2\sigma}{(\pi v_0^2)^{3/2}}\left(\frac{\rho_p}{m_p}\right) R_{\mathrm{BS}}^3 n_{\mathrm{core}} \\ &\times \int_0^1 dx x^2 n_{\mathrm{norm}} \int_0^{v_c}\int_0^{\pi} dv d\theta v \sin(\theta) e^{-\frac{v^2+v_{BS}^2+2vv_{BS}}{v_0^2}} \left[v^2+v_c^2-(v_c^2-v_s^2)\frac{M(x)}{M_{BS}}\right], \end{aligned} \tag{4.33}$$

for the Maxwell-Boltzmann distribution and as

$$\begin{aligned} C_{\mathrm{BS}} =& 4\pi\left(\frac{\rho_p}{m_p}\right)\left(\frac{\sigma}{\bar{v}}\right) R_{\mathrm{BS}}^3 n_{\mathrm{core}} \\ &\times \int_0^1 dx x^2 n_{\mathrm{norm}} \left[\bar{v}^2+v_c^2-(v_c^2-v_s^2)\frac{M(x)}{M_{BS}}\right], \end{aligned} \tag{4.34}$$

for the delta distribution.

For the sake of the simplification of numerical calculation, variables were redefined in terms of dimensionless quantities, namely $x := \frac{r}{R_{\mathrm{BS}}}$ and $n_{\mathrm{norm}} := \frac{n(x)}{n_{\mathrm{core}}}$, where n_{core} is the star's number density at its core. The BS's parameters entering the equations, such as its physical radius and mass, were also converted to the dimensionless analogues defined in Section 3.2.3 by use of the results from A. Further parameter values were set as: $\left(\frac{\rho_p}{m_p}\right) = 1\ \mathrm{cm}^{-3}$, $v_{\mathrm{BS}} = 12\ \frac{\mathrm{km}}{\mathrm{s}} + v_0$. Equations (4.33) and (4.34) don't show the explicit dependence of the capture rate on the DM self-interaction coupling constant and DM mass. Given that these are the only two free parameters of the BS model presented in this work, it proves useful to keep them in mind, so their proportions are

$$C_{\mathrm{BS}} \propto \lambda^{\frac{1}{2}}\left(\frac{m}{1\ \mathrm{GeV}}\right)^{-3}.$$

Using the mass and number density profiles in the high Λ limit, the capture rate can be calculated. Setting $\sigma = 10^{-45}\ \mathrm{cm}^2$ (a value a couple of orders of magnitude below current lower limits on spin-dependent DM interaction (Aprile *et al.*, 2019)), some solutions are plotted in Figure 4.6, where the horizontal axis denotes the dimensionless BS radius defined in Section 3.2.3. For this Figure, the parameters $\lambda = 1$, $m = 1$ GeV were considered and the solutions obtained with the delta distribution were also divided by a factor 10^5. If the geometrical cross section (4.3) is considered instead, the order of magnitude of the capture rate is enhanced by 17 units.

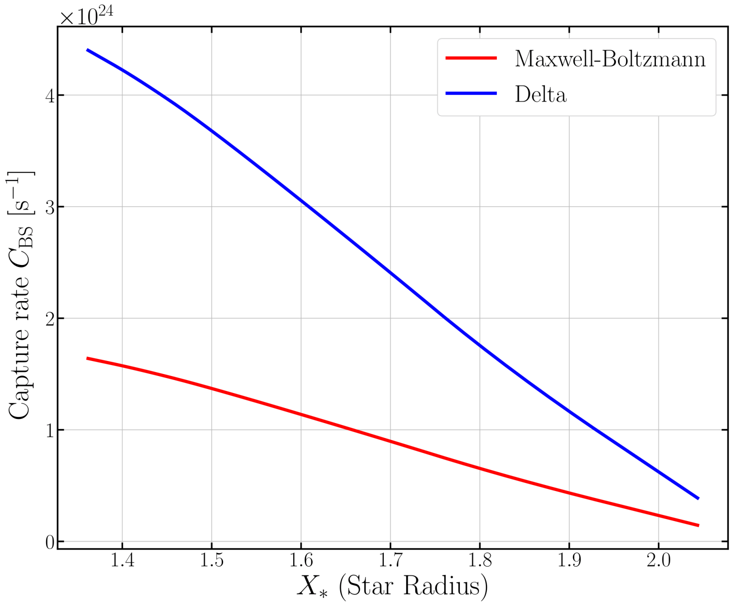

Figure 4.6.: Capture Rate for different solutions in the high Λ limit.

Comparison with the naive calculation for the capture rate (4.10) shows that the values obtained with Gould's formalism are a couple of orders of magnitude larger if the Maxwell-Boltzmann distribution is assumed; while they are larger by seven orders of magnitude if the delta distribution is used. The most important conclusion derived from this Figure is that the BS solution which maximizes capture is the one with the smallest radius. According to Figure 3.7, this corresponds to the red point, which coincides with the stable solution with the greatest enclosed mass. From here on, all calculations will assume this particular solution with the result provided by using the Maxwell-Boltzmann distribution for the incoming protons, which reads

$$C_{\mathrm{BS}} = \left(1.7 \times 10^{24}\,\frac{1}{\mathrm{s}}\right)\left(\frac{\sigma}{10^{-45}\ \mathrm{cm}^2}\right)\lambda^{\frac{1}{2}}\left(\frac{m}{1\ \mathrm{GeV}}\right)^{-3}. \tag{4.35}$$

Assuming that the equation describing the number of protons in a BS takes the simple form

$$\frac{dN_{\mathrm{p}}}{dt} = C_{\mathrm{BS}}, \tag{4.36}$$

that is, neglecting all processes other than capture, then equation (4.35) predicts that the expected amount of protons in the BS after one year will be of the order

$$N_{\mathrm{p}}(1\ \mathrm{year}) = \left(5.4\times10^{31}\ \mathrm{protons}\right)\left(\frac{\sigma}{10^{-45}\ \mathrm{cm}^2}\right)\lambda^{\frac{1}{2}}\left(\frac{m}{1\ \mathrm{GeV}}\right)^{-3}.$$

Such an overabundance of protons would lead to the BS becoming positively charged, which in turn would mean a decrease in the capture due to Coulomb repulsion. However, this also means that negatively charged particles such as electrons will begin to be captured by the BS, which will lead to charge neutrality and a constant capture rate of both protons and electrons given by (4.35). Therefore, the capture rate calculated in this section may be taken as the amount of both protons and electrons gathered by the star per second, or in other words, how much hydrogen it obtains per time, which keeps the star electrically neutral and allows the use of the information from Section 4.2 for the free parameters entering equations (4.33) and (4.34).

5. Radiation from a Boson Star

Armed with the knowledge derived in the previous chapters about the structure of BSs in the limit of strong self-interactions and the amount of protons that such objects gather per unit of time, it is now possible to address the main objective of this work, namely what are the consequences of the eventual baryon population in terms of detectable signals. The strategy, which this chapter follows, is to determine the temperature evolution of the BS, as this variable governs the energy available for the proton population to radiate. To figure this out two ingredients are necessary. The first consists of determining the timescales necessary for the protons to enter thermodynamic equilibrium with the encompassing BS and the spatial region in which they are contained, as this information determines which mechanisms are available for energy dissipation. The second ingredient is to determine the amount of energy needed to produce a change in the star's temperature, which is given by the star's heat capacity.

After the deduction of these two fundamental ingredients, the temperature evolution of the BS is determined, which in turn allows to obtain its luminosity evolution. The derived results are then analyzed and measured against sensitivities of current gamma-ray experiments. The consequences are then discussed.

5.1. Thermalization of Captured Protons

5.1.1. Thermalization Time

Once protons are captured by the BS, they begin to interact with its conforming DM particles through collisions. After sufficient time, they adopt a Maxwell-Boltzmann distribution in the velocity and distance from the center of the star, which is known as thermalization (Kouvaris and Tinyakov, 2011). In order to calculate the energy radiated from these captured protons it is of interest to know how long it would take for them to thermalize, to determine when they start emitting radiation.

Taking off from the assumption that a captured proton moves completely inside the star, the average time between collisions is $\Delta t = \frac{1}{\sigma n v}$, where σ is the proton-DM cross section, n is the BS's number density and v is the proton's velocity from the rest frame of the star. Taking the non-relativistic limit, the proton's velocity can be written as a function of its energy as $v = \sqrt{\frac{2E_\mathrm{p}}{m_\mathrm{p}}}$ and, per collision, it loses approximately $\Delta E_\mathrm{p} = -2\frac{m}{m_p}E_\mathrm{p}$. With this, the energy evolution can be expressed as

$$\frac{dE_\mathrm{p}}{dt} = \frac{\Delta E_\mathrm{p}}{\Delta t} = -2\sqrt{2}\rho\sigma\left(\frac{E_\mathrm{p}}{m_\mathrm{p}}\right)^{\frac{3}{2}}. \tag{5.1}$$

The solution of the differential equation for the thermalization time is

$$t_\mathrm{th} = \frac{m_\mathrm{p}}{\sqrt{2}\rho\sigma c}\left(\sqrt{\frac{m_\mathrm{p}c^2}{E_\mathrm{final}}} - \sqrt{\frac{m_\mathrm{p}c^2}{E_\mathrm{initial}}}\right). \tag{5.2}$$

The initial energy is given by $E_\mathrm{initial} = \frac{1}{2}m_\mathrm{p}v_\mathrm{s}^2 = \frac{GM_\mathrm{BS}m_\mathrm{p}}{R_\mathrm{BS}}$ and the final energy can be obtained from the equipartition theorem as $E_\mathrm{final} = \frac{3}{2}k_BT$. Upon insertion of the quantities from Table 3.1, the thermalization time is

$$t_\mathrm{th} \approx (2.83\times10^{-9}\ \mathrm{s})\left(\frac{10^{-49}\ \mathrm{m}^2}{\sigma}\right)\lambda\left(\frac{1\ \mathrm{GeV}}{m}\right)^4. \tag{5.3}$$

Then, the thermalization occurs in a timescale of nanoseconds, which compared to the star's evolution over millions of years, is negligible. As such, from here on it will be assumed that protons begin emitting radiation as soon as they are captured.

5.1.2. Thermal Radius

After a proton has been captured by the BS and it is gravitationally bound it will interact with its surrounding DM particles. After their thermalization they will concentrate within the thermal radius. This quantity can be calculated by use of the virial theorem with the external potential energy of the BS:

$$\langle E_k\rangle = V_\mathrm{BS}, \tag{5.4}$$

where $\langle E_k\rangle$ is the mean kinetic energy per particle of the proton cloud and V_BS is the external potential per particle due to the BS, which can be calculated as

$$NV_\mathrm{BS} \approx \int_0^{r_\mathrm{th}} \frac{G(4\pi r'^2\rho_\mathrm{core})(\frac{4\pi}{3}r'^3\rho_\mathrm{p})}{r'}dr',$$

where N is the number of captured protons. For ease of calculation the mass density of the BS has been approximated as a constant given by the value at its core ρ_{core}, which is valid given the flat profiles presented in Figure 3.9. After performing the integration, the potential reads

$$V_{\mathrm{BS}} \approx \frac{4\pi}{5} G \rho_{\mathrm{core}} m_{\mathrm{p}} r_{\mathrm{th}}^2, \tag{5.5}$$

where ρ_{p} has been expressed as $\rho_{\mathrm{p}} = \frac{N m_{\mathrm{p}}}{\frac{4\pi}{3} r_{\mathrm{th}}^3}$.

The dependence of the thermal radius can then be obtained by making use of the equipartition theorem to relate the mean kinetic energy per particle with the temperature as $E_k = \frac{3}{2} k_{\mathrm{B}} T$ to give

$$r_{\mathrm{th}} = \sqrt{\frac{15 k_B T}{8\pi G \rho_{\mathrm{core}} m_{\mathrm{p}}}}. \tag{5.6}$$

The thermal radius is a critical quantity which is also used to determine the mechanism with which the protons will emit radiation. Its relationship with the emitted photon's mean free path will be made clear in Section 5.2.

5.2. Boson Star's "Luminosity"

The protons inside of the BS may emit radiation in two different ways. The first one is produced by their deceleration due to the interaction with the BS's particles. This is the bremsstrahlung mechanism, more specifically thermal bremsstrahlung, as made clear in Section 5.1.1, where it was noted that protons thermalize very quickly and their distribution is Maxwellian. The total power per unit volume emitted with this mechanism is given by the emissivity (Rybicki and Lightman, 1986)

$$\varepsilon_{\mathrm{ff}} = \left(\frac{2\pi k_B T}{3 m_{\mathrm{p}}}\right)^{\frac{1}{2}} \frac{2^5 \pi q_{\mathrm{e}}^6}{3 h m_{\mathrm{p}} c^3} Z^2 n_{\mathrm{p}} n_{\mathrm{i}} \bar{g_{\mathrm{B}}} = (1.4 \times 10^{-34} \ \frac{\mathrm{J}}{\mathrm{s\ cm^3}}) \left(\frac{T}{1\ \mathrm{K}}\right)^{\frac{1}{2}} \left(\frac{n_{\mathrm{p}}}{1\ \mathrm{cm^3}}\right)^2 Z^2 \bar{g_{\mathrm{B}}}, \tag{5.7}$$

where the case of hydrogen inside the star was assumed, so $Z = 1$, $n_{\mathrm{p}} = n_{\mathrm{e}} = n_{\mathrm{i}}$ and the correction factor ("Gaunt" factor) $\bar{g_{\mathrm{B}}}$ lies within 1.1 and 1.5. From equation (5.7) the luminosity due to thermal bremsstrahlung can be obtained by multiplying the emissivity by the volume occupied by the protons $V = \frac{4\pi}{3} r_{\mathrm{th}}^3$.

The second mechanism is blackbody radiation in which the radiation itself is in equilibrium. The luminosity for this case is given by the well-known Stefan-Boltzmann law

$$L_{\mathrm{SB}} = 4\pi r_{\mathrm{th}}^2 \sigma_{\mathrm{SB}} T^4, \tag{5.8}$$

where $\sigma_{\mathrm{SB}} = \frac{\pi^2 k_{\mathrm{B}}^4}{60\hbar^3 c^2}$ is the Stefan-Boltzmann constant. The equilibrium condition for the emitted photons is that their mean free path is smaller than the thermal radius, as this allows them to interact several times with the electrons within the thermal radius and thermalize. To summarize, the luminosity due to the radiation of the particles captured by the BS is

$$L_{L\gamma} = \begin{cases} 4\pi r_{\mathrm{th}}^2 \sigma_{\mathrm{SB}} T^4, & \text{if } l_\gamma < r_{\mathrm{th}} \\ V\varepsilon_{\mathrm{ff}}, & \text{if } l_\gamma > r_{\mathrm{th}} \end{cases}, \tag{5.9}$$

where $l_\gamma = \frac{V}{N_{\mathrm{e}}\sigma_{\mathrm{T}}}$ is the photon's mean free path in terms of the volume $V = \frac{4\pi}{3} r_{\mathrm{th}}^3$, the Thomson cross section $\sigma_{\mathrm{T}} = \frac{8\pi}{3}\frac{q_{\mathrm{e}}^4}{c^4 m_{\mathrm{e}}^2}$ and $N_{\mathrm{e}} = N_{\mathrm{p}} = C_{\mathrm{BS}} t$ is the number of protons obtained by the BS at some certain time t from the creation of the star.

Finally, asymmetric BSs have also been studied under the assumption of self-interactions mediated by another invisible particle: the massive dark photon (Maselli, Kouvaris, and Kokkotas, 2019). This opens another path for evacuation of energy for the star analogous to the one for visible photons. In this case, however, the dark photons are assumed to be in thermal equilibrium at the start of the BS's lifetime, so their luminosity is calculated according to the modified Stefan-Boltzmann law

$$L_{D\gamma} = (4\pi R_{\mathrm{DS}}^2 \sigma_{\mathrm{SB}} T^4) \mathrm{e}^{-\frac{m_{D\gamma} c^2}{k_{\mathrm{B}} T}}, \tag{5.10}$$

which incorporates the dark photon's mass $m_{D\gamma}$ as an exponential suppression when the temperature drops below its value.

5.3. Heat Capacity of a Boson Star

The radiation emitted from the BS relies heavily on the star's temperature. As such, it is of importance to understand how it develops over time and what its consequences are on the star's luminosity. After taking into consideration the radiation mechanisms available to the star, the next step to understand the temperature's evolution is to figure out how much energy is needed to produce a change in the star's temperature. This is given by the star's heat capacity, which I calculate in this section.

So far BSs have been modeled as self-gravitating objects made up of bosons with repulsive self-interactions. As such, a correct treatment for the calculation of their heat capacity would be under the formalism of self-interacting Bose-Einstein condensate (hereafter abbreviated as SIBEC) DM, as reviewed by Chavanis, 2015. However, it has been shown that SIBECs present substantial differences from ideal Bose condensates only at extremely low temperatures (Chavanis and Harko, 2012) and, as is made apparent from Figure 3.9, this is not the case for BSs. As such, the results for an ideal Bose gas may be used, namely:

$$\frac{PV}{k_B T} = -\sum_{\varepsilon} \ln(1 - z\mathrm{e}^{-\beta\varepsilon}), \tag{5.11a}$$

$$N = \sum_{\varepsilon} n_{\varepsilon} = \sum_{\varepsilon} \frac{1}{z^{-1}\mathrm{e}^{\beta\varepsilon} - 1}, \tag{5.11b}$$

where, for this section, $\beta := \frac{1}{k_B T}$ and $z := \mathrm{e}^{\frac{\mu}{k_B T}} = \mathrm{e}^{\beta\mu}$ is the fugacity with μ the chemical potential and ε the particle energy. Hereafter the units will be standard, unless explicitly stated, so the thermodynamic quantities are denoted with the standard symbols, as in equations (5.11).

Given that for a large volume V the spectrum of single-particles states is almost continuous, the sums may be replaced by integrals multiplied by the non-relativistic density of states, that is

$$\sum_{\varepsilon} \to \int_0^{\infty} \frac{2\pi V}{h^3} (2m)^{\frac{3}{2}} \varepsilon^{\frac{1}{2}} d\varepsilon,$$

where h is Planck's constant. The non-relativistic density of states is used instead of the relativistic expression as the initial temperature of the star is of the order of $\mathscr{O}(10\text{ MeV})$, which is smaller than the assumed particle DM mass. One further point that has to be taken into account is that the density of states gives a weight of zero to the lowest energy level $\varepsilon = 0$. To be consistent with the assumption that each particle state has a weight of unity, the expressions from equation (5.11) must be rewritten before the introduction of the integrals as

$$\frac{PV}{k_B T} = -\sum_{\varepsilon \neq 0} \ln(1 - z\mathrm{e}^{-\beta\varepsilon}) - \ln(1 - z), \tag{5.12a}$$

$$N = \sum_{\varepsilon \neq 0} \frac{1}{z^{-1}\mathrm{e}^{\beta\varepsilon} - 1} + \frac{z}{1 - z}. \tag{5.12b}$$

Now the integrals may be performed and the expressions rewritten as

$$\frac{P}{k_B T} = -\frac{2\pi}{h^3}(2m)^{\frac{3}{2}} \int_0^\infty \varepsilon^{\frac{1}{2}} \ln(1 - z\mathrm{e}^{-\beta\varepsilon}) d\varepsilon - \frac{1}{V}\ln(1-z), \tag{5.13a}$$

$$\frac{N}{V} = \frac{2\pi}{h^3}(2m)^{\frac{3}{2}} \int_0^\infty \frac{\varepsilon^{\frac{1}{2}} d\varepsilon}{z^{-1}\mathrm{e}^{\beta\varepsilon} - 1} + \frac{1}{V}\frac{z}{1-z}. \tag{5.13b}$$

The last term of (5.13b) is equal to the number of particles in the ground state divided by the volume, that is $\frac{N_0}{V} = \frac{1}{V}\frac{z}{1-z}$, so the fugacity may be expressed as $z = \frac{N_0}{N_0+1}$, which shows that this quantity is bounded as $0 \le z \le 1$. Inserting into the last term of (5.13a) one obtains $-\frac{1}{V}\ln(1-z) = \frac{1}{V}\ln(N_0+1)$, which is at most of order $\mathscr{O}(N^{-1}\ln(N))$, so this term may be safely neglected for a large number of particles. Taking this into account and doing the change of variables $x := \beta\varepsilon$, equation (5.13a) may be rewritten as

$$\frac{P}{k_B T} \approx -\frac{2\pi}{h^3}\left(\frac{2m}{\beta}\right)^{\frac{3}{2}} \int_0^\infty x^{\frac{1}{2}} \ln(1 - z\mathrm{e}^{-x}) dx,$$

which upon integration by parts turns into

$$\frac{P}{k_B T} \approx -\frac{2\pi}{h^3}\left(\frac{2m}{\beta}\right)^{\frac{3}{2}} \left[\frac{2}{3} x^{\frac{3}{2}} \ln(1 - z\mathrm{e}^{-x}) \Big|_0^\infty - \frac{2}{3}\int_0^\infty x^{\frac{3}{2}} \frac{z\mathrm{e}^{-x}}{1 - z\mathrm{e}^{-x}} dx \right].$$

Now, it proves useful to rewrite the result in terms the Bose-Einstein functions:

$$g_\nu(z) := \frac{1}{\Gamma(\nu)} \int_0^\infty \frac{x^{\nu-1}}{z^{-1}\mathrm{e}^x - 1} dx. \tag{5.14}$$

So, the expression becomes

$$\frac{P}{k_B T} \approx \frac{(2\pi m k_B T)^{\frac{3}{2}}}{h^3} g_{\frac{5}{2}}(z).$$

Applying similar steps and redefinitions and substituting $\frac{N_0}{V} = \frac{1}{V}\frac{z}{1-z}$, equation (5.13b) may be rewritten in a similar manner. To summarize:

$$\frac{P}{k_B T} \approx \lambda_{\mathrm{dB}}^{-3} g_{\frac{5}{2}}(z), \tag{5.15a}$$

$$\frac{N - N_0}{V} = \lambda_{\mathrm{dB}}^{-3} g_{\frac{3}{2}}(z), \tag{5.15b}$$

where $\lambda_{\text{dB}} = \frac{h}{\sqrt{2\pi m k_B T}}$ is the de Broglie wavelength of a particle of mass m in a gas with temperature T. The internal energy of the system can be calculated as

$$U = -\frac{\partial}{\partial \beta}\left(\frac{PV}{k_B T}\right)_{z,V} = -\frac{\partial}{\partial \beta}\left(\frac{V}{\lambda_{\text{dB}}^3} g_{\frac{5}{2}}(z)\right)_{z,V} = \frac{3}{2} k_B T \frac{V}{\lambda_{\text{dB}}^3} g_{\frac{5}{2}}(z). \tag{5.16}$$

For $T \to \infty$, the internal energy is expected to approach to converge to the classical limit $U \to \frac{3}{2} N k_B T$, but for the BS, the inverse limit is of greater importance, namely when the temperature is finite. The reason why will be explained later; for the moment one works with equations (5.15a) and (5.16). The number of particles in excited states N_{e} can be written with the help of (5.15b) as

$$N_{\text{e}} = V \frac{(2\pi m k_B T)^{\frac{3}{2}}}{h^3} g_{\frac{3}{2}}(z)\,. \tag{5.17}$$

For a given volume and temperature, the number of particles in excited states is solely defined by the value of z. The fugacity is bounded as $0 \leq z \leq 1$ and, given that the Bose-Einstein function $g_{\frac{3}{2}}(z)$ increases monotonically with z, it translates into an upper bound $g_{\frac{3}{2}}(z) \leq g_{\frac{3}{2}}(1) = \xi(\frac{3}{2})$, where $\xi(\frac{3}{2})$ is the Riemann zeta function. So, the number of excited particles is also bounded:

$$N_{\text{e}} \leq V \frac{(2\pi m k_B T)^{\frac{3}{2}}}{h^3} \xi(\frac{3}{2}). \tag{5.18}$$

If the total number of particles in the system $N = N_{\text{e}} + N_0$ exceeds the limit above, then the excited states will receive as many particles as they can hold (taking the equality in equation (5.18)) and the non-excited states ($\varepsilon = 0$) will have a number

$$N_0 = N - N_e = N - V \frac{(2\pi m k_B T)^{\frac{3}{2}}}{h^3} \xi(\frac{3}{2}). \tag{5.19}$$

In this situation $z = 1$, which means that $1 = z = \frac{N_0}{N_0+1} = \frac{1}{1+\frac{1}{N_0}} \sim 1 - \frac{1}{N_0}$, that is $N_0 \to \infty$. A large number of particles accumulating in the single quantum state ($\varepsilon = 0$) is the phenomenon of Bose condensation, and by the lines above, the condition for its onset is

$$N \geq V T^{\frac{3}{2}} \frac{(2\pi m k_B)^{\frac{3}{2}}}{h^3} \xi(\frac{3}{2}), \tag{5.20}$$

or if N and V are held constant

$$T \leq \left[\frac{N}{V} \frac{h^3}{(2\pi m k_B)^{\frac{3}{2}}} \frac{1}{\xi(\frac{3}{2})} \right]^{\frac{2}{3}} := T_{\mathrm{c}}, \tag{5.21}$$

where T_{c} is defined as the critical temperature below which the system of particles begins to form a Bose condensate. Rewritten in a more compact notation, it is

$$T_{\mathrm{c}} := \frac{2\pi\hbar^2}{m k_B} \left(\frac{n}{\xi(\frac{3}{2})} \right)^{\frac{2}{3}}, \tag{5.22}$$

where $n = \frac{N}{V}$ is the number density. This means that the number of excited and non-excited particles can be expressed as a function of the temperature of the gas as

$$N_{\mathrm{e}} = N \begin{cases} \left(\frac{T}{T_{\mathrm{c}}}\right)^{\frac{3}{2}}, & \text{if } T \leq T_{\mathrm{c}}, \\ 1, & \text{if } T \geq T_{\mathrm{c}} \end{cases}, \tag{5.23}$$

$$N_0 = N \begin{cases} 1 - \left(\frac{T}{T_{\mathrm{c}}}\right)^{\frac{3}{2}}, & \text{if } T \leq T_{\mathrm{c}}, \\ 0, & \text{if } T \geq T_{\mathrm{c}} \end{cases}, \tag{5.24}$$

respectively. Now, for $T \leq T_{\mathrm{c}}$, the fugacity is unity and the internal energy of the gas may be written with the help of equation (5.16) as

$$U = \frac{3}{2} k_B T \frac{V}{\lambda_{\mathrm{dB}}^3} \xi(\frac{5}{2}), \tag{5.25}$$

from which the heat capacity may be obtained as

$$C_{\mathrm{v}} = \frac{dU}{dT} = \frac{15}{4} k_B V \frac{\xi(\frac{5}{2})}{\lambda_{\mathrm{dB}}^3} = \frac{15}{4} k_B N \frac{\xi(\frac{5}{2})}{\xi(\frac{3}{2})} \left(\frac{T}{T_{\mathrm{c}}} \right)^{\frac{3}{2}}. \tag{5.26}$$

For a BS, the critical temperature is

$$T_{\mathrm{c}} = (2.06 \times 10^{14}\ \mathrm{K}) \lambda^{-\frac{2}{3}} \left(\frac{m}{1\ \mathrm{GeV}} \right) \rho_*^{\frac{2}{3}}, \tag{5.27}$$

where ρ_* is a dimensionless variable as defined in Section 3.2.3. The temperature of the BS at its creation is $T_{\mathrm{initial}} = (1.17 \times 10^{13}\ \mathrm{K}) \left(\frac{m}{1\ \mathrm{GeV}} \right) \frac{p_*}{\rho_*}$, so the temperature ratio is

$$\frac{T_{\text{intial}}}{T_{\text{c}}} = (0.06)\lambda^{\frac{2}{3}} \frac{p_*}{\rho_*^{5/3}}, \tag{5.28}$$

which is much smaller than unity and confirms the previous assumption that the limit when the temperature is finite is of greater importance than the behavior when $T \to \infty$. By means of equation (5.24) the number of non-excited particles (assuming $\lambda, p_*, \rho_* = 1$) is

$$N_0 > N(1-(0.06)^{\frac{3}{2}}) = 0.985N, \tag{5.29}$$

so one can assume that all particles are in the ground state and that the whole BS is a Bose-Einstein condensate.

There is one subtlety about this assumption. The problem of the formation of the BS is not treated in this work, but if the mechanism for the BS's formation was similar to the one for normal stars, then it would be expected that, before the star's formation, its DM particles would form a cloud with low densities and high temperatures. Then, during this time, the cloud's temperature could be greater than the critical temperature and the ensemble would not be a Bose-Einstein condensate. In the course of the cloud's evolution towards a compact object, its density would increase and its temperature would decrease, so it would then transition to a condensate state. In what follows, it will be assumed that the star is already in this state, the heat capacity is given by equation (5.26) and it remains this way throughout the star's evolution.

5.4. Boson Star's Time Evolution

Given the star's heat capacity calculated in Section 5.3 and the mechanisms for its energy loss mentioned in Section 5.2, the temperature evolution can be expressed as the differential equation

$$\frac{dT}{dt} = -\frac{L_{D\gamma}+L_{L\gamma}}{C_{\text{v}}}, \tag{5.30}$$

whose solutions have been numerically calculated for different values of the dark photon mass. They are presented in Figure 5.1, where each dark photon mass is color-coded. The left vertical axis presents the solutions in terms of the dimensionless temperature introduced in Section 3.2.3, while the right one shows the values in Kelvin assuming $\lambda = 1$ and $m = 1$ GeV. This choice of parameter values is maintained throughout the section.

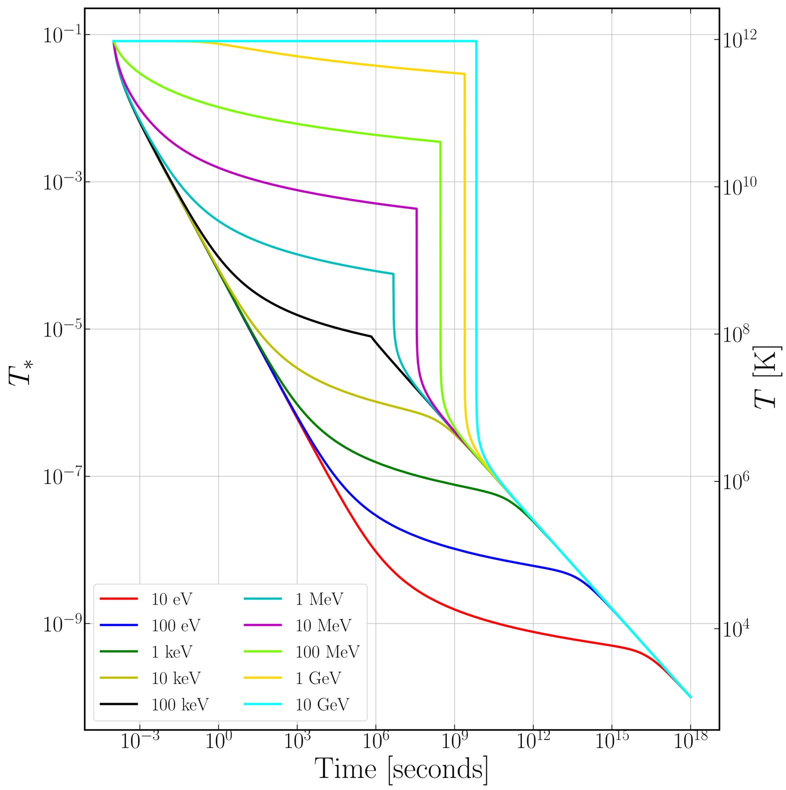

Figure 5.1.: Temperature evolution for different dark photon masses.

There are several points that can be extracted from the previous Figure. The first is that the late-time behavior of the temperature is independent of the initial conditions, namely all curves approach the attractor given by the solution of the equation

$$\frac{dT}{dt} = -\frac{L_{L\gamma}}{C_{\rm v}} = -\frac{4\pi r_{\rm th}^2 \sigma_{\rm SB} T^4}{C_{\rm v}}, \tag{5.31}$$

which can be expressed analytically as

$$T_{\rm late}(t) = T_0 \left(1 + \frac{5}{2} S(t - t_0) T_0^{\frac{5}{2}}\right)^{-\frac{2}{5}}, \tag{5.32}$$

where $S = 2\sigma_{\rm SB} \frac{\xi(\frac{3}{2})}{\xi(\frac{5}{2})} \frac{T_c^{\frac{3}{2}}}{G\rho_{\rm core} m_{\rm p} N_{\rm DS}}$. The reason for this is the exponential suppression of the dark photon emission. As noted from Figure 5.1, the star cools considerably in a timescale of decades to hundreds of years and today it would be cold with a temperature of the order of 1000 K.

Secondly, the beginning of cooling dominated by visible photon emission, marked by the sharp drops in the curves, happens later for an increase in the dark photon's mass, going from a couple of days to hundreds of years. This is better shown by Figure 5.2, where the thermal radius and the visible photon's mean free path are plotted for the two limiting cases of the dark photon mass. The moment when the visible photons thermalize, namely when both lengths are the same is denoted with points.

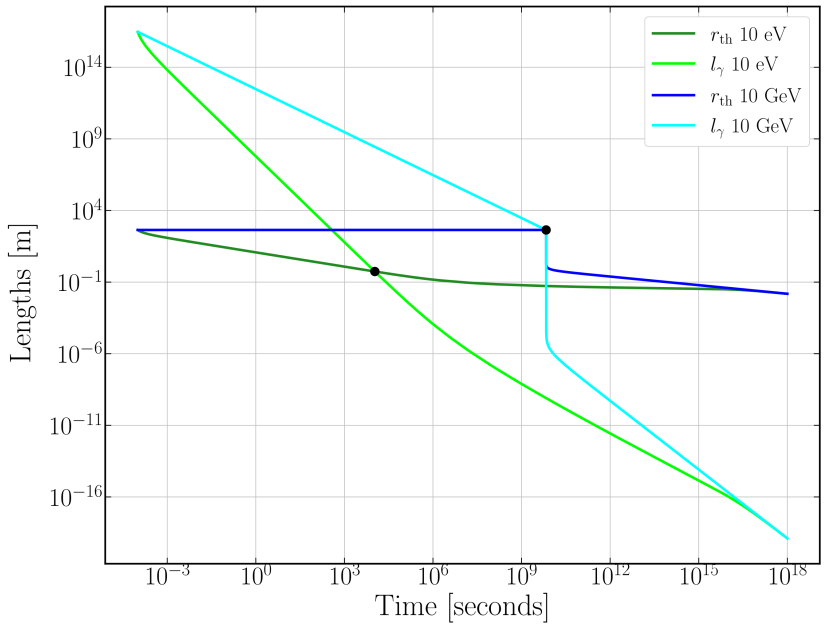

Figure 5.2.: Thermal radius and photon mean free path evolution for two different dark photon masses.

From the temperature's behavior with time, the luminosity evolution can also be obtained, as shown in Figure 5.3:

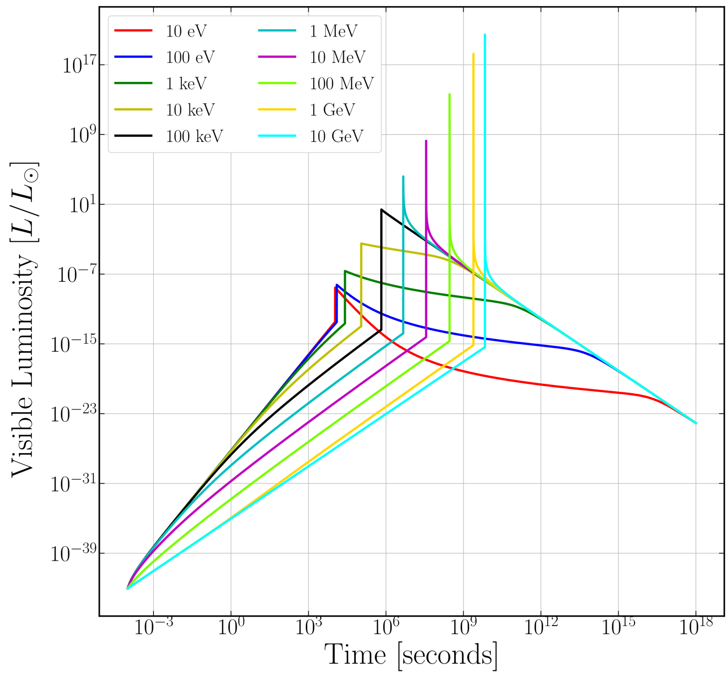

(a) Visible luminosity.

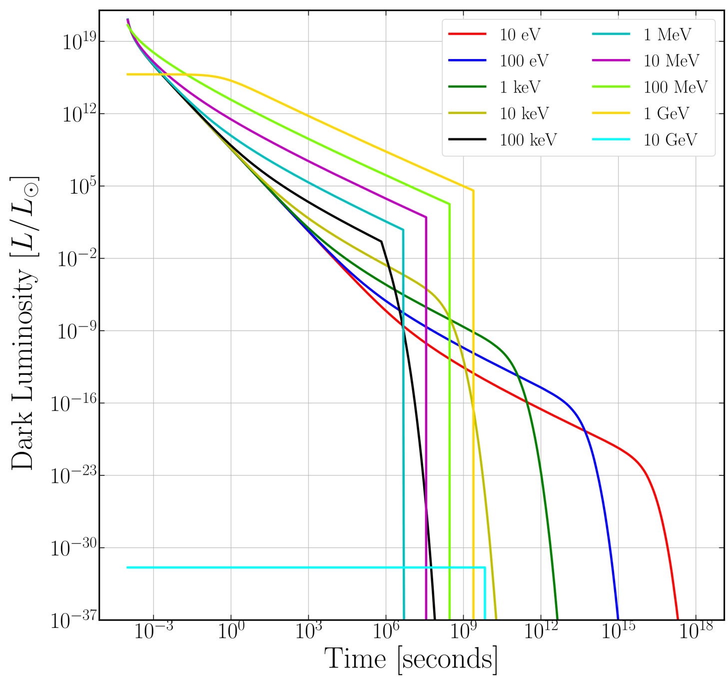

(b) Dark photon luminosity.

Figure 5.3.: Visible and dark photon luminosities evolution for different dark photon masses.

As can be observed from Figure 5.3a, for large dark photon masses the visible luminosity of the star upon entering the blackbody regime peaks abruptly and may reach values several orders of magnitude above the Sun's luminosity ($L_\odot = 3.828 \times 10^{26}$ W). Taking the scenario represented by a dark photon mass of 10 GeV, an object with such a luminosity at a redshift of $z = 1$ would lead to an observed flux of

$$F_{\text{obs}} = \frac{L}{4\pi D_{\text{L}}} = \left(7.24 \times 10^{-8} \, \frac{\text{erg}}{\text{s cm}^2}\right) \lambda \left(\frac{m}{1 \text{ GeV}}\right), \tag{5.33}$$

where D_{L} is the luminosity distance, which was calculated for a cosmology with $H_0 = 69.6 \, \frac{\text{km}}{\text{s Mpc}}$, $\Omega_{\text{m}} = 0.3$, $\Omega_\Lambda = 0.7$. Such a signal would exhibit a blackbody spectrum with a peak at the redshifted wavelength given by Wien's law

$$\lambda_{\text{peak}} = (1+z)\frac{2898 \, \mu\text{m K}}{T} = (4.97 \times 10^{-8} \text{ nm}) \left(\frac{1 \text{ GeV}}{m}\right)^{-1}. \tag{5.34}$$

This would correspond to a photon with an energy of approximately $(25 \text{ GeV}) \left(\frac{1 \text{ GeV}}{m}\right)$. According to Figure 5.4, for $\lambda = 1$ and $m = 1$ GeV, such a signal could be detected by Fermi-LAT.

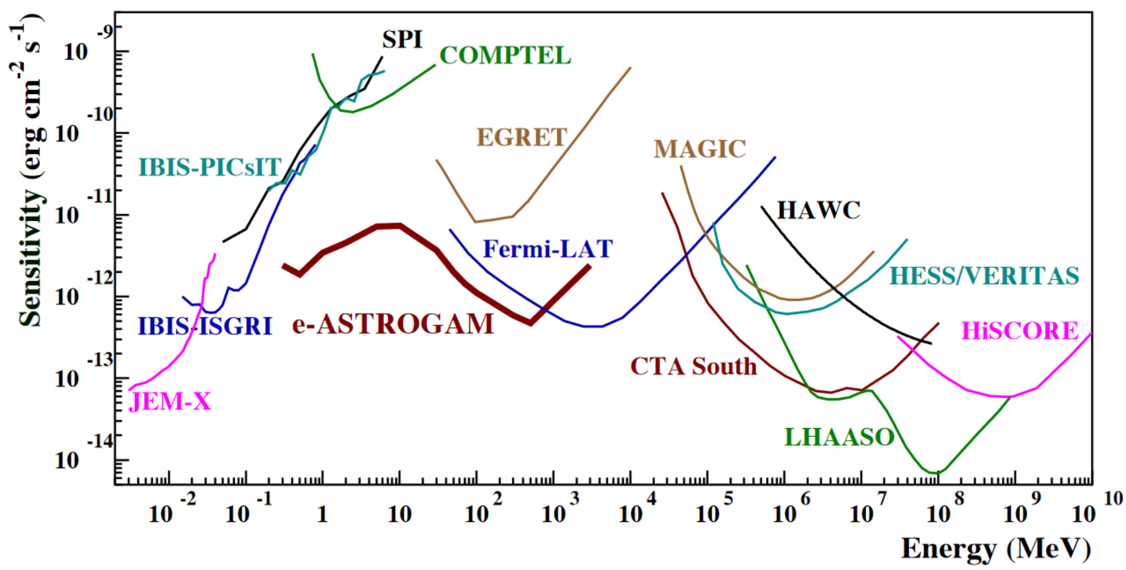

Figure 5.4.: Point source sensitivity of different instruments for an effective exposure of one year (de Angelis *et al.*, 2018).

For this choice of parameters the observed flux would fall several orders of magnitude above the experiment's sensitivity, so it leads to the speculation that some detected unidentified point sources could be, in fact, BSs that had captured enough protons, as described in this thesis. Nevertheless, it is crucial to remember that this result comes from the best-case scenario for the production of a signal, that is:

- The BS solution and the DM-proton interaction cross-section were chosen so that the star's capture rate was maximized. This means in turn that the amount of protons and electrons needed within the thermal radius for the emitted photons to thermalize is reached faster. The faster this point is reached, the greater is the star's temperature, as it had less time to cool down. Consequently, the emitted photons' blackbody spectrum is centered at higher energies.

- The number density of the medium surrounding the BS was taken to be $n = 1\ \text{cm}^{-3}$, which corresponds to an average value of the ISM in the Milky Way, but at redshift $z = 1$, which takes place outside of the galaxy, this could be several orders of magnitude smaller. A smaller number density would lead to a smaller rate of capture.

- The dark photon mass was picked to be greater than the star's mass, which meant that practically no dark photons were emitted, as their luminosity was exponentially suppressed. As such, the peak in the luminosity when the visible radiation is thermal is maximized, as exemplified by the 10 GeV curve in Figure 5.3. For smaller dark photon masses, the maximum luminosity drops substantially and would lead to much smaller observed fluxes.

- Finally, the choice of the fundamental parameters of the model $\lambda = 1$ and $m = 1$ GeV have been arbitrary. A variation of these values would change all calculations starting from the BS's structure all the way to the observed flux. An example of such changes is shown in Figure 5.5, where the evolution of the star's temperature and visible luminosity are plotted for $m = 100$ GeV. Upon comparison with Figures 5.1 and 5.3 key differences can be noted, such as a much larger peak in the luminosity, which is around 20 orders of magnitude larger than the Sun's luminosity, or that the thermalization of photons happens much later than in the case of $m = 1$ GeV.

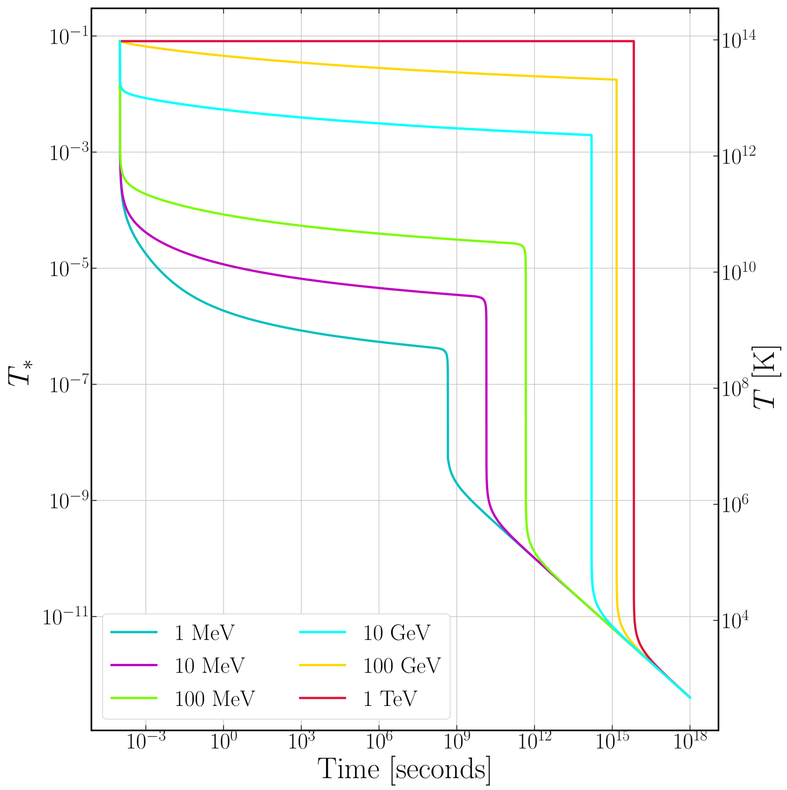

(a) Temperature evolution.

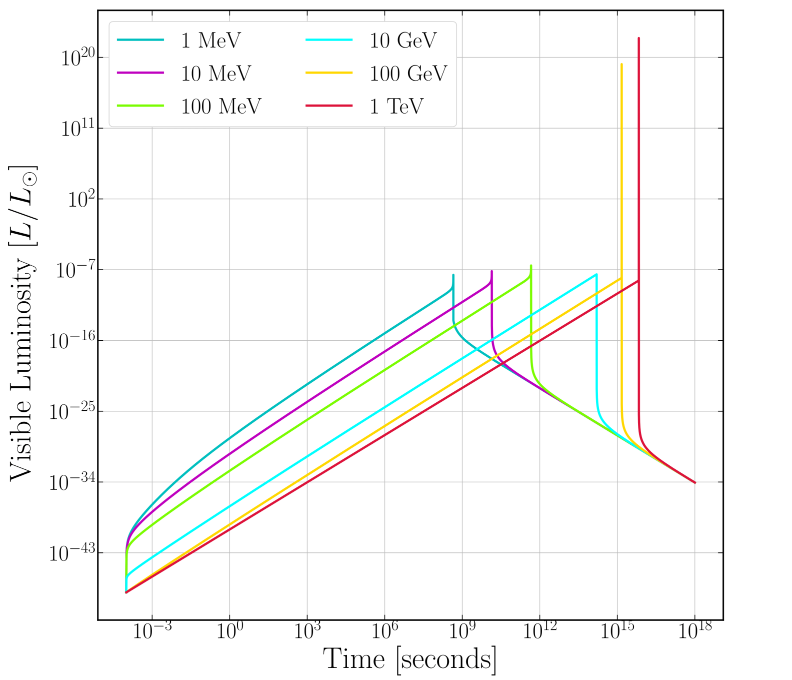

(b) Normal luminosity evolution.

Figure 5.5.: Temperature and visible luminosity evolution for a DM particle mass of $m = 100$ GeV.

The work done for this thesis is relevant as it shows that the possibility exists for compact objects made up of DM to emit detectable radiation by means of the protons and electrons that it captures, which opens a new avenue for their detection other than microlensing. However, as exposed in previous lines, the model is dependent on three parameters, namely the dark boson and dark photon masses and the boson self-interaction coupling constant. While the conclusion that BSs will produce signals is independent of their values, they do greatly influence their strength, which is crucial for their detection. As such, it is important to constrain the model's parameters to determine its validity. This should be possible through microlensing observations, as only model parameters that could explain the lack of visible signals would be valid.

6. Summary and Outlook

6.1. Summary

This thesis offered a brief historical overview on the theoretical and experimental efforts towards the understanding of DM. With this background, the work undertaken in this study was motivated. Setting out from the assumptions that DM is a particle which can form compact objects, in particular self-interacting BSs, and that it couples to protons, it was hypothesized that BSs may capture enough protons and electron such that they could emit radiation according to known mechanisms.

The first step to tackle this question was to understand the structure of self-interacting BSs. This was done in the formalism of General Relativity with an energy-momentum tensor provided by the theory of a complex scalar field with a quartic self-interaction. The only parameters entering this model are the self-coupling and the boson's mass. The equations of stellar structure were derived and numerically solved. Radial profiles of the BS's mass, pressure, density and temperature were derived and analyzed, in particular, in the limit of strong self-interactions. The total mass-radius relation was obtained and the stable configuration with the largest mass was calculated.

After the determination of the BS's profile, its capture of protons was tackled. As this is dependent on the star's surroundings, a brief introduction to the ISM and its components was provided. Subsequently, some calculations of the amount of baryons captured per time by a general compact object, the so-called capture rate, were preformed assuming only gravitational effects. This computation was later improved with the formalism introduced by Andrew Gould and applied to the particular case of BSs gathering protons. It was found that the stable BS solution that maximizes capture is the one with the largest mass and the smallest radius. This solution was assumed for subsequent calculations.

Given the BS's radial profiles and rate of capture of protons, the consequences of the baryon population in terms of detectable signals was focused on. First, it was determined that captured protons reach thermal equilibrium with the star in a matter of nanoseconds and that they gather within a length defined as the thermal radius. Correspondingly, the energy dissipation mechanisms available were then determined to be thermal, namely bremsstrahlung and blackbody radiation. As an analogue to visible stars, evacuation of energy through dark photons was also invoked and presented. Afterwards it was determined that the BS forms a Bose-Einstein condensate and its heat capacity was calculated accordingly. With the previous estimates, the star's temperature evolution was calculated, which in turn allowed for the computation of the luminosity evolution in terms of visible and dark photons. It was then determined that, for a particular choice of parameters, a sudden high-luminosity flash could be produced in the star, which could be detected by current gamma-ray experiments.

Finally, the validity of this result and the assumptions that went into it were discussed. The work done in this thesis shows the possibility of observing compact objects made up of DM through non-gravitational means, namely through gamma-ray emission. Given this new path of detection, I consider that this prospect deserves further study.

6.2. Outlook

This work has shown that it is possible for dark compact objects to be detected through gamma-ray observations. However, it can also be applied to constrain parameters, namely the DM particle's mass. Microlensing searches have not coincided with gamma-ray observations, therefore, if the observed compact object was a BS, this would mean that the boson's mass should be small enough such that the star's radiative signal was too weak to be detected. This sets constraints on this particular parameter and can help in the construction of DM models.

On the other hand, the calculations and results of this work can be extended and refined in several ways.

In the first place, the next logical extension after studying self-interacting BSs in the context of this thesis is to ascertain if similar conclusions may also be derived for the case of self-interacting fermion stars. The effect of the Pauli exclusion principle on the structure and heat capacity of the star may lead to strikingly contrasting results.

In terms of refining the calculations in this study, one possible path is to drop the static assumption for the structure of the BS. In this work it was assumed that from the moment the star is formed, its mass and radius remain constant, only its temperature changes due to the energy loss on account of radiation from the captured protons and electrons. A correct treatment would be to evolve the system of ordinary differential equations governing the structure of the star to a system of partial differential equations which includes both radial distance and time. This new system should also couple the star's luminosity with the other dependent variables, that is, the mass, pressure and density.

Another possible line of work would be a more careful treatment of capture and loss of SM particles by the star. This formalism should consider not only capture, but also escape, annihilation, decay, and perhaps higher order processes. The assumption made in this present work was that all protons that got close enough to the star would be captured and would never escape, but this is not necessarily the case and a more precise calculation could lead to interesting changes in the star's time evolution.

Yet another aspect that could be improved would be the calculation of the heat capacity of the BS. Previous authors have concluded that for high temperatures, the ideal case of free, non-interacting bosons would suffice, as the differences due to self-interaction and gravitational effects are only apparent in extremely low temperatures. Regardless, given the exotic nature of BSs and the fact that they form a Bose-Einstein condensate even at high temperatures, which is outside the scope of any Earth-based experiments, a precise treatment of a SIBEC could perhaps lead to different timescales for the star's evolution and the luminosity that can be expected from its gathered SM particles.

A. Conversion of Units

The problem of compact objects made from DM involves results from quantum theory, thermodynamics and gravity. As such, the appearance of the fundamental constants of nature such as the speed of light c, the Planck constant $\hbar$, the gravitational constant G and the Boltzmann constant k_B is to be expected in all equations. In order to simplify the results it is customary to set these constants to 1 and restore them on the grounds of dimensional analysis when a computation is performed. In the case of this thesis, only c and $\hbar$ are set to 1, so the restoration of units is not as simple as in the case of works using (Planckian) natural units, where all fundamental constants are set to unity. As such, I write how to convert units to serve as a reference for the work in this thesis.

As a convention, I will use expressions like $A|\mathrm{u}$. This means quantity A expressed in units u (just the number value, no units attached). The mass and distance conversions read

$$M|_{\mathrm{kg}} = M_* \frac{\Lambda^{\frac{1}{2}} M_{\mathrm{Pl}}^2}{m} = \frac{(M_{\mathrm{Pl}}|_{\mathrm{GeV}})^2 (M_{\mathrm{Pl}}|_{\mathrm{kg}})}{\sqrt{4\pi}} \lambda^{\frac{1}{2}} \left(\frac{1\ \mathrm{GeV}}{m}\right)^2 M_*, \tag{A.1a}$$

$$r|_{\mathrm{m}} = x_* \frac{\Lambda^{\frac{1}{2}}}{m} = \frac{(M_{\mathrm{Pl}}|_{\mathrm{GeV}})^2 (l_{\mathrm{Pl}}|_{\mathrm{m}})}{\sqrt{4\pi}} \lambda^{\frac{1}{2}} \left(\frac{1\ \mathrm{GeV}}{m}\right)^2 x_*, \tag{A.1b}$$

where M_* is the mass in dimensionless units ($\mathscr{M}_*$) and x_* is defined as in Section 3.2.

To find the density transformation, the calculation is longer and it uses the two results above. First one considers:

$$\begin{aligned} 4\pi \int_0^R r^2 \rho(r) dr = M &= \frac{(M_{\mathrm{Pl}}|_{\mathrm{GeV}})^2 (M_{\mathrm{Pl}}|_{\mathrm{kg}}\ \mathrm{kg})}{\sqrt{4\pi}} \lambda^{\frac{1}{2}} \left(\frac{1\ \mathrm{GeV}}{m}\right)^2 M_* \\ &= \frac{(M_{\mathrm{Pl}}|_{\mathrm{GeV}})^2 (M_{\mathrm{Pl}}|_{\mathrm{kg}}\ \mathrm{kg})}{\sqrt{4\pi}} \lambda^{\frac{1}{2}} \left(\frac{1\ \mathrm{GeV}}{m}\right)^2 \left[4\pi \int_0^{x_{*\max}} x_*^2 \rho_*(x_*) dx_*\right]. \end{aligned} \tag{A.2}$$

By the conversion from x_* to r given by (A.1b), one can write

$$x_* = \frac{\sqrt{4\pi}}{(M_{\mathrm{Pl}}|_{\mathrm{GeV}})^2 (l_{\mathrm{Pl}}|_{\mathrm{m}}\ \mathrm{m})} \lambda^{-\frac{1}{2}} \left(\frac{1\ \mathrm{GeV}}{m}\right)^{-2} r, \tag{A.3}$$

and

$$x_{*\max} = \frac{\sqrt{4\pi}}{(M_{\mathrm{Pl}}|_{\mathrm{GeV}})^2 (l_{\mathrm{Pl}}|_{\mathrm{m}}\ \mathrm{m})} \lambda^{-\frac{1}{2}} \left(\frac{1\ \mathrm{GeV}}{m}\right)^{-2} R. \tag{A.4}$$

Then, one can change variables in the dimensionless integral above as

$$\int_0^{x_{*\max}} x_*^2 \rho_*(x_*) dx_* = \int_0^R \left[\frac{\sqrt{4\pi}}{(M_{\mathrm{Pl}}|_{\mathrm{GeV}})^2 (l_{\mathrm{Pl}}|_{\mathrm{m}}\ \mathrm{m})} \lambda^{-\frac{1}{2}} \left(\frac{1\ \mathrm{GeV}}{m}\right)^{-2}\right]^3 r^2 \rho_*(r) dr. \tag{A.5}$$

Inserting into the expression for M in (A.2), one obtains

$$\begin{aligned}\int_0^R r^2 \rho(r) dr =& \frac{(M_{\mathrm{Pl}}|_{\mathrm{GeV}})^2 (M_{\mathrm{Pl}}|_{\mathrm{kg}}\ \mathrm{kg})}{\sqrt{4\pi}} \lambda^{\frac{1}{2}} \left(\frac{1\ \mathrm{GeV}}{m}\right)^2 \\ &\times \left[\frac{\sqrt{4\pi}}{(M_{\mathrm{Pl}}|_{\mathrm{GeV}})^2 (l_{\mathrm{Pl}}|_{\mathrm{m}}\ \mathrm{m})} \lambda^{-\frac{1}{2}} \left(\frac{1\ \mathrm{GeV}}{m}\right)^{-2}\right]^3 \int_0^R r^2 \rho_*(r) dr.\end{aligned} \tag{A.6}$$

Upon simplification:

$$\int_0^R r^2 \rho(r) dr = \frac{4\pi (M_{\mathrm{Pl}}|_{\mathrm{kg}}\ \mathrm{kg})}{(M_{\mathrm{Pl}}|_{\mathrm{GeV}})^4 (l_{\mathrm{Pl}}|_{\mathrm{m}}\ \mathrm{m})^3} \lambda^{-1} \left(\frac{1\ \mathrm{GeV}}{m}\right)^{-4} \int_0^R r^2 \rho_*(r) dr, \tag{A.7}$$

which implies

$$\int_0^R r^2 \rho(r) dr = \int_0^R r^2 \left[\frac{4\pi (M_{\mathrm{Pl}}|_{\mathrm{kg}}\ \mathrm{kg})}{(M_{\mathrm{Pl}}|_{\mathrm{GeV}})^4 (l_{\mathrm{Pl}}|_{\mathrm{m}}\ \mathrm{m})^3} \lambda^{-1} \left(\frac{1\ \mathrm{GeV}}{m}\right)^{-4} \rho_*(r)\right] dr, \tag{A.8}$$

so, one obtains the transformation

$$\rho|_{\frac{\mathrm{kg}}{\mathrm{m}^3}} = \frac{4\pi (M_{\mathrm{Pl}}|_{\mathrm{kg}})}{(M_{\mathrm{Pl}}|_{\mathrm{GeV}})^4 (l_{\mathrm{Pl}}|_{\mathrm{m}})^3} \lambda^{-1} \left(\frac{1\ \mathrm{GeV}}{m}\right)^{-4} \rho_*. \tag{A.9}$$

From here it is simple to obtain the transformation for the pressure, by noticing that ρc^2 has the correct units. As such, the pressure transforms as

$$p|_{\mathrm{Pa}} = \frac{4\pi (M_{\mathrm{Pl}}|_{\mathrm{kg}}) (c|_{\frac{\mathrm{m}}{\mathrm{s}}})^2}{(M_{\mathrm{Pl}}|_{\mathrm{GeV}})^4 (l_{\mathrm{Pl}}|_{\mathrm{m}})^3} \lambda^{-1} \left(\frac{1\ \mathrm{GeV}}{m}\right)^{-4} \rho_*. \tag{A.10}$$

Also, for the number density, one divides by the DM mass and obtains

$$n|_{\frac{1}{\mathrm{m}^3}} = \frac{4\pi(M_{\mathrm{Pl}}|_{\mathrm{kg}})}{(M_{\mathrm{Pl}}|_{\mathrm{GeV}})^4(l_{\mathrm{Pl}}|_{\mathrm{m}})^3(1\ \mathrm{GeV})|_{\mathrm{kg}}}\lambda^{-1}\left(\frac{1\ \mathrm{GeV}}{m}\right)^{-3}\rho_*. \tag{A.11}$$

Furthermore, given the pressure and density conversions, the temperature transformation may also be obtained, as hinted by the relation $T = \frac{m}{k_B}\frac{p}{\rho}$ and the definition of the dimensionless quantity $T_* := \frac{p_*}{\rho_*}$, as

$$T = \left(\frac{1\ \mathrm{GeV}}{m}\right)^{-1}\frac{1}{k_B}\frac{p}{\rho}(1\ \mathrm{GeV}) = \frac{(1.79\times 10^{-27}\ \mathrm{kg})}{k_B}c^2\left(\frac{1\ \mathrm{GeV}}{m}\right)^{-1}T_*. \tag{A.12}$$

Computing and simplifying all expressions, the rule for the conversion of relevant quantities is:

$$M = (9.15\times 10^{29}\ \mathrm{kg})\lambda^{\frac{1}{2}}\left(\frac{1\ \mathrm{GeV}}{m}\right)^2 M_*, \tag{A.13a}$$

$$r = (678.48\ \mathrm{m})\lambda^{\frac{1}{2}}\left(\frac{1\ \mathrm{GeV}}{m}\right)^2 x_*, \tag{A.13b}$$

$$\rho = \left(2.92\times 10^{21}\ \frac{\mathrm{kg}}{\mathrm{m}^3}\right)\lambda^{-1}\left(\frac{1\ \mathrm{GeV}}{m}\right)^{-4}\rho_*, \tag{A.13c}$$

$$p = \left(2.62\times 10^{38}\ \mathrm{Pa}\right)\lambda^{-1}\left(\frac{1\ \mathrm{GeV}}{m}\right)^{-4}p_*, \tag{A.13d}$$

$$n = \left(1.63\times 10^{48}\ \frac{1}{\mathrm{m}^3}\right)\lambda^{-1}\left(\frac{1\ \mathrm{GeV}}{m}\right)^{-3}\rho_*, \tag{A.13e}$$

$$T = \left(1.17\times 10^{13}\ \mathrm{K}\right)\left(\frac{1\ \mathrm{GeV}}{m}\right)^{-1}T_*. \tag{A.13f}$$

Bibliography

Aguilar, M. *et al.* (Apr. 2013). "First Result from the Alpha Magnetic Spectrometer on the International Space Station: Precision Measurement of the Positron Fraction in Primary Cosmic Rays of 0.5-350 GeV". In: *Physical Review Letters* 110.14, 141102, p. 141102. DOI: 10.1103/PhysRevLett.110.141102 (cit. on p. 49).

Alpher, Ralph A. and Robert Herman (Nov. 1948). "Evolution of the Universe". In: *Nature* 162.4124, pp. 774–775. DOI: 10.1038/162774b0 (cit. on p. 11).

Aprile, E. *et al.* (Apr. 2019). "Constraining the Spin-Dependent WIMP-Nucleon Cross Sections with XENON1T". In: *Physical Review Letters* 122.14, 141301, p. 141301. DOI: 10.1103/PhysRevLett.122.141301. arXiv: 1902.03234 [astro-ph.CO] (cit. on p. 61).

Babcock, Horace W. (Jan. 1939). "The rotation of the Andromeda Nebula". In: *Lick Observatory Bulletin* 498, pp. 41–51. DOI: 10.5479/ADS/bib/1939LicOB.19.41B (cit. on p. 6).

Balberg, Shmuel, Stuart L. Shapiro, and Shogo Inagaki (Apr. 2002). "Self-Interacting Dark Matter Halos and the Gravothermal Catastrophe". In: *The Astrophysical Journal* 568.2, pp. 475–487. DOI: 10.1086/339038. arXiv: astro-ph/0110561 [astro-ph] (cit. on p. 45).

Begeman, K. G., A. H. Broeils, and R. H. Sanders (Apr. 1991). "Extended rotation curves of spiral galaxies : dark haloes and modified dynamics." In: *MNRAS* 249, p. 523. DOI: 10.1093/mnras/249.3.523 (cit. on p. 5).

Bekenstein, Jacob D. (Oct. 2004). "Relativistic gravitation theory for the modified Newtonian dynamics paradigm". In: *Phys. Rev. D* 70.8, 083509, p. 083509. DOI: 10.1103/PhysRevD.70.083509. arXiv: astro-ph/0403694 [astro-ph] (cit. on p. 9).

Bertone, Gianfranco and Dan Hooper (Oct. 2018). "History of dark matter". In: *Reviews of Modern Physics* 90.4, 045002, p. 045002. DOI: 10.1103/RevModPhys.90.045002. arXiv: 1605.04909 [astro-ph.CO] (cit. on p. 4).

Bertone, Gianfranco, Dan Hooper, and Joseph Silk (Jan. 2005). "Particle dark matter: evidence, candidates and constraints". In: *Phys. Rep.* 405.5-6, pp. 279–390. DOI: 10.1016/j.physrep.2004.08.031. arXiv: hep-ph/0404175 [hep-ph] (cit. on p. 10).

Buchmueller, Oliver, Caterina Doglioni, and Lian-Tao Wang (Mar. 2017). "Search for dark matter at colliders". In: *Nature Physics* 13.3, pp. 217–223. DOI: 10.1038/nphys4054. arXiv: 1912.12739 [hep-ex] (cit. on p. 17).

Burbidge, G. R. and E. Margaret Burbidge (Sept. 1959). "The Hercules Clusters of Nebulae." In: *The Astrophysical Journal* 130, p. 629. DOI: 10.1086/146752 (cit. on p. 4).

Chavanis, Pierre-Henri (2015). "Self-gravitating Bose-Einstein Condensates". In: *Quantum Aspects of Black Holes*, pp. 151–194. DOI: 10.1007/978-3-319-10852-0_6 (cit. on p. 69).

Chavanis, Pierre-Henri and Tiberiu Harko (Sept. 2012). "Bose-Einstein condensate general relativistic stars". In: *Phys. Rev. D* 86.6, 064011, p. 064011. DOI: 10.1103/PhysRevD.86.064011. arXiv: 1108.3986 [astro-ph.SR] (cit. on p. 69).

Clowe, Douglas, Anthony Gonzalez, and Maxim Markevitch (Apr. 2004). "Weak-Lensing Mass Reconstruction of the Interacting Cluster 1E 0657-558: Direct Evidence for the Existence of Dark Matter". In: *The Astrophysical Journal* 604.2, pp. 596–603. DOI: 10.1086/381970. arXiv: astro-ph/0312273 [astro-ph] (cit. on p. 15).

Clowe, Douglas *et al.* (Sept. 2006). "A Direct Empirical Proof of the Existence of Dark Matter". In: *ApJ* 648.2, pp. L109–L113. DOI: 10.1086/508162. arXiv: astro-ph/0608407 [astro-ph] (cit. on pp. 9, 14).

Colpi, Monica, Stuart L. Shapiro, and Ira Wasserman (Nov. 1986). "Boson stars: Gravitational equilibria of self-interacting scalar fields". In: *Physical Review Letters* 57.20, pp. 2485–2488. DOI: 10.1103/PhysRevLett.57.2485 (cit. on p. 29).

Conrad, Jan and Olaf Reimer (Mar. 2017). "Indirect dark matter searches in gamma and cosmic rays". In: *Nature Physics* 13.3, pp. 224–231. DOI: 10.1038/nphys4049. arXiv: 1705.11165 [astro-ph.HE] (cit. on pp. 10, 19).

de Angelis, A. *et al.* (Aug. 2018). "Science with e-ASTROGAM. A space mission for MeV-GeV gamma-ray astrophysics". In: *Journal of High Energy Astrophysics* 19, pp. 1–106. DOI: 10.1016/j.jheap.2018.07.001. arXiv: 1711.01265 [astro-ph.HE] (cit. on p. 77).

Dicke, R. H. *et al.* (July 1965). “Cosmic Black-Body Radiation.” In: *The Astrophysical Journal* 142, pp. 414–419. DOI: 10.1086/148306 (cit. on p. 11).

Dine, Michael, Willy Fischler, and Mark Srednicki (Aug. 1981). “A simple solution to the strong CP problem with a harmless axion”. In: *Physics Letters B* 104.3, pp. 199–202. DOI: 10.1016/0370-2693(81)90590-6 (cit. on p. 8).

Editor NASA HEASARC (Sept. 2020). *The Einstein Observatory (HEAO-2)*. Last checked on April 17th, 2021. URL: https://heasarc.gsfc.nasa.gov/docs/einstein/heao2.html (cit. on p. 13).

Einasto, Jaan, Ants Kaasik, and Enn Saar (July 1974). “Dynamic evidence on massive coronas of galaxies”. In: *Nature* 250.5464, pp. 309–310. DOI: 10.1038/250309a0 (cit. on p. 6).

Ellis, John *et al.* (June 1984). “Supersymmetric relics from the big bang”. In: *Nuclear Physics B* 238.2, pp. 453–476. DOI: 10.1016/0550-3213(84)90461-9 (cit. on p. 7).

Ferrière, Katia M. (Oct. 2001). “The interstellar environment of our galaxy”. In: *Reviews of Modern Physics* 73.4, pp. 1031–1066. DOI: 10.1103/RevModPhys.73.1031. arXiv: astro-ph/0106359 [astro-ph] (cit. on p. 47).

Freeman, K. C. (June 1970). “On the disks of spiral and SO Galaxies”. In: *The Astrophysical Journal* 160, pp. 811–830. DOI: 10.1086/150474 (cit. on p. 6).

Gamow, G. (1948). “The Evolution of the Universe”. In: *Nature* 162.4122, pp. 680–682. DOI: 10.1038/162680a0 (cit. on p. 11).

Gershtein, S. S. and Ya. B. Zel’dovich (Sept. 1966). “Rest Mass of Muonic Neutrino and Cosmology”. In: *Soviet Journal of Experimental and Theoretical Physics Letters* 4, pp. 120–122 (cit. on p. 7).

Giagu, Stefano (May 2019). “WIMP Dark matter searches with the ATLAS detector at the LHC”. In: *Frontiers in Physics* 7, 75, p. 75. DOI: 10.3389/fphy.2019.00075 (cit. on p. 16).

Goldman, Itzhak and Shmuel Nussinov (Nov. 1989). “Weakly interacting massive particles and neutron stars”. In: *Phys. Rev. D* 40 (10), pp. 3221–3230. DOI: 10.1103/PhysRevD.40.3221 (cit. on p. 55).

Gould, Andrew (Apr. 1992). “Cosmological Density of WIMPs from Solar and Terrestrial Annihilations”. In: *The Astrophysical Journal* 388, p. 338. DOI: 10.1086/171156 (cit. on p. 56).

Gould, Andrew (Oct. 1987). "Resonant Enhancements in Weakly Interacting Massive Particle Capture by the Earth". In: *The Astrophysical Journal* 321, p. 571. DOI: 10.1086/165653 (cit. on p. 56).

Griest, K. (2002). "WIMPs and MACHOs". In: *Encyclopedia of Astronomy and Astrophysics*. Ed. by P. Murdin, E2634. DOI: 10.1888/0333750888/2634 (cit. on p. 8).

Harvey, David *et al.* (Mar. 2015). "The nongravitational interactions of dark matter in colliding galaxy clusters". In: *Science* 347.6229, pp. 1462–1465. DOI: 10.1126/science.1261381. arXiv: 1503.07675 [astro-ph.CO] (cit. on p. 15).

Hawkins, M. R. S. (Mar. 2015). "A new look at microlensing limits on dark matter in the Galactic halo". In: *A&A* 575, A107, A107. DOI: 10.1051/0004-6361/201425400. arXiv: 1503.01935 [astro-ph.GA] (cit. on p. 8).

Hegyi, Dennis J. and Keith A. Olive (June 1983). "Can galactic halos be made of baryons?" In: *Physics Letters B* 126.1-2, pp. 28–32. DOI: 10.1016/0370-2693(83)90009-6 (cit. on p. 8).

Holmberg, Erik (Sept. 1940). "On the Clustering Tendencies among the Nebulae." In: *The Astrophysical Journal* 92, p. 200. DOI: 10.1086/144212 (cit. on p. 4).

Hu, Wayne and Scott Dodelson (Jan. 2002). "Cosmic Microwave Background Anisotropies". In: *ARA&A* 40, pp. 171–216. DOI: 10.1146/annurev.astro.40.060401.093926. arXiv: astro-ph/0110414 [astro-ph] (cit. on p. 13).

Kalberla, P. M. W. and L. Dedes (Sept. 2008). "Global properties of the H I distribution in the outer Milky Way. Planar and extra-planar gas". In: *A&A* 487.3, pp. 951–963. DOI: 10.1051/0004-6361:20079240. arXiv: 0804.4831 [astro-ph] (cit. on pp. 50, 51).

Kalberla, Peter M. W. and Jürgen Kerp (Sept. 2009). "The Hi Distribution of the Milky Way". In: *ARA&A* 47.1, pp. 27–61. DOI: 10.1146/annurev-astro-082708-101823 (cit. on p. 50).

Kaup, David J. (Aug. 1968). "Klein-Gordon Geon". In: *Physical Review* 172.5, pp. 1331–1342. DOI: 10.1103/PhysRev.172.1331 (cit. on p. 28).

Kim, Jihn E. (July 1979). "Weak-interaction singlet and strong CP invariance". In: *Physical Review Letters* 43.2, pp. 103–107. DOI: 10.1103/PhysRevLett.43.103 (cit. on p. 8).

Kouvaris, Chris and Peter Tinyakov (Apr. 2011). "Constraining asymmetric dark matter through observations of compact stars". In: *Phys. Rev. D* 83.8, 083512, p. 083512. DOI: 10.1103/PhysRevD.83.083512. arXiv: 1012.2039 [astro-ph.HE] (cit. on p. 65).

Markevitch, M. *et al.* (Mar. 2002). "A Textbook Example of a Bow Shock in the Merging Galaxy Cluster 1E 0657-56". In: *ApJ* 567.1, pp. L27–L31. DOI: 10.1086/339619. arXiv: astro-ph/0110468 [astro-ph] (cit. on p. 14).

Markevitch, M. *et al.* (May 2004). "Direct Constraints on the Dark Matter Self-Interaction Cross Section from the Merging Galaxy Cluster 1E 0657-56". In: *The Astrophysical Journal* 606.2, pp. 819–824. DOI: 10.1086/383178. arXiv: astro-ph/0309303 [astro-ph] (cit. on p. 15).

Maselli, Andrea, Chris Kouvaris, and Kostas D. Kokkotas (May 2019). "The Photon Spectrum of Asymmetric Dark Stars". In: *arXiv e-prints*, arXiv:1905.05769, arXiv:1905.05769. arXiv: 1905.05769 [astro-ph.CO] (cit. on p. 68).

Masuda, Kota, Tetsuo Hatsuda, and Tatsuyuki Takatsuka (Feb. 2016). "Hadron-quark crossover and hot neutron stars at birth". In: *Progress of Theoretical and Experimental Physics* 2016.2, 021D01, p. 021D01. DOI: 10.1093/ptep/ptv187. arXiv: 1506.00984 [nucl-th] (cit. on p. 45).

McKellar, Andrew (Jan. 1941). "Molecular Lines from the Lowest States of Diatomic Molecules Composed of Atoms Probably Present in Interstellar Space". In: *Publications of the Dominion Astrophysical Observatory Victoria* 7, p. 251 (cit. on p. 11).

Milgrom, M. (July 1983a). "A modification of the Newtonian dynamics - Implications for galaxies." In: *The Astrophysical Journal* 270, pp. 371–383. DOI: 10.1086/161131 (cit. on p. 9).

– (July 1983b). "A modification of the newtonian dynamics : implications for galaxy systems." In: *The Astrophysical Journal* 270, pp. 384–389. DOI: 10.1086/161132 (cit. on p. 9).

– (July 1983c). "A modification of the Newtonian dynamics as a possible alternative to the hidden mass hypothesis." In: *The Astrophysical Journal* 270, pp. 365–370. DOI: 10.1086/161130 (cit. on p. 9).

Mróz, Przemek *et al.* (Jan. 2019). "Rotation Curve of the Milky Way from Classical Cepheids". In: *ApJ* 870.1, L10, p. L10. DOI: 10.3847/2041-8213/aaf73f. arXiv: 1810.02131 [astro-ph.GA] (cit. on p. 51).

Ostriker, J. P., P. J. E. Peebles, and A. Yahil (Oct. 1974). "The Size and Mass of Galaxies, and the Mass of the Universe". In: *ApJ* 193, p. L1. DOI: 10.1086/181617 (cit. on p. 6).

Peccei, R. D. and Helen R. Quinn (June 1977). "CP conservation in the presence of pseudoparticles". In: *Physical Review Letters* 38.25, pp. 1440–1443. DOI: 10.1103/PhysRevLett.38.1440 (cit. on p. 8).

Peebles, P. J. and Bharat Ratra (Apr. 2003). "The cosmological constant and dark energy". In: *Reviews of Modern Physics* 75.2, pp. 559–606. DOI: 10.1103/RevModPhys.75.559. arXiv: astro-ph/0207347 [astro-ph] (cit. on p. 3).

Peebles, P. J. E. (June 1984). "The Origin of Galaxies and Clusters of Galaxies". In: *Science* 224.4656, pp. 1385–1391. DOI: 10.1126/science.224.4656.1385 (cit. on p. 7).

Peek, J. E. G. and S. E. Clark (Nov. 2019). "Small-scale H I Channel Map Structure Is Cold: Evidence from Na I Absorption at High Galactic Latitudes". In: *ApJ* 886.1, L13, p. L13. DOI: 10.3847/2041-8213/ab53de. arXiv: 1909.09647 [astro-ph.GA] (cit. on p. 52).

Penzias, A. A. and R. W. Wilson (July 1965). "A Measurement of Excess Antenna Temperature at 4080 Mc/s." In: *The Astrophysical Journal* 142, pp. 419–421. DOI: 10.1086/148307 (cit. on p. 11).

Planck Collaboration *et al.* (Sept. 2020a). "Planck 2018 results. I. Overview and the cosmological legacy of Planck". In: *A&A* 641, A1, A1. DOI: 10.1051/0004-6361/201833880. arXiv: 1807.06205 [astro-ph.CO] (cit. on pp. 12, 13).

Planck Collaboration *et al.* (Sept. 2020b). "Planck 2018 results. VI. Cosmological parameters". In: *A&A* 641, A6, A6. DOI: 10.1051/0004-6361/201833910. arXiv: 1807.06209 [astro-ph.CO] (cit. on p. 3).

Poincaré, H. (Oct. 1906). "The Milky Way and the Theory of Gases". In: *Popular Astronomy* 14, pp. 475–488 (cit. on p. 4).

Raen, Troy J. *et al.* (June 2021). "The effects of asymmetric dark matter on stellar evolution - I. Spin-dependent scattering". In: *MNRAS* 503.4, pp. 5611–5623. DOI: 10.1093/mnras/stab865. arXiv: 2010.04184 [astro-ph.GA] (cit. on p. 20).

Reeves, Hubert *et al.* (Feb. 1973). "On the Origin of Light Elements". In: *The Astrophysical Journal* 179, pp. 909–930. DOI: 10.1086/151928 (cit. on p. 9).

Roberts, M. S. and A. H. Rots (Aug. 1973). "Comparison of Rotation Curves of Different Galaxy Types". In: *A&A* 26, pp. 483–485 (cit. on p. 6).

Rubin, V. C., Jr. Ford W. K., and N. Thonnard (June 1980). "Rotational properties of 21 SC galaxies with a large range of luminosities and radii, from NGC 4605 (R=4kpc) to UGC 2885 (R=122kpc)." In: *The Astrophysical Journal* 238, pp. 471–487. DOI: `10.1086/158003` (cit. on p. 6).

Rubin, Vera C. and Jr. Ford W. Kent (Feb. 1970). "Rotation of the Andromeda Nebula from a Spectroscopic Survey of Emission Regions". In: *The Astrophysical Journal* 159, p. 379. DOI: `10.1086/150317` (cit. on p. 6).

Ruffini, Remo and Silvano Bonazzola (Nov. 1969). "Systems of Self-Gravitating Particles in General Relativity and the Concept of an Equation of State". In: *Phys. Rev.* 187 (5), pp. 1767–1783. DOI: `10.1103/PhysRev.187.1767` (cit. on p. 28).

Rybicki, George B. and Alan P. Lightman (1986). *Radiative Processes in Astrophysics* (cit. on p. 67).

Schumann, Marc (Oct. 2019). "Direct detection of WIMP dark matter: concepts and status". In: *Journal of Physics G Nuclear Physics* 46.10, p. 103003. DOI: `10.1088/1361-6471/ab2ea5`. arXiv: `1903.03026 [astro-ph.CO]` (cit. on pp. 18, 19).

Schwarzschild, M. (Sept. 1954). "Mass distribution and mass-luminosity ratio in galaxies". In: *AJ* 59, p. 273. DOI: `10.1086/107013` (cit. on p. 6).

Skordis, Constantinos (June 2008). "Generalizing tensor-vector-scalar cosmology". In: *Phys. Rev. D* 77.12, 123502, p. 123502. DOI: `10.1103/PhysRevD.77.123502`. arXiv: `0801.1985 [astro-ph]` (cit. on p. 9).

Szalay, A. S. and G. Marx (June 1976). "Neutrino rest mass from cosmology." In: *A&A* 49.3, pp. 437–441 (cit. on p. 7).

Tisserand, P. *et al.* (July 2007). "Limits on the Macho content of the Galactic Halo from the EROS-2 Survey of the Magellanic Clouds". In: *A&A* 469.2, pp. 387–404. DOI: `10.1051/0004-6361:20066017`. arXiv: `astro-ph/0607207 [astro-ph]` (cit. on p. 9).

Tucker, W. *et al.* (May 1997). "1E0657-56: A Contender for the Hottest Known Cluster". In: *American Astronomical Society Meeting Abstracts #190*. Vol. 190. American Astronomical Society Meeting Abstracts, 52.02, p. 52.02 (cit. on p. 13).

Tucker, W. H., H. Tananbaum, and R. A. Remillard (May 1995). “A Search for “Failed Clusters” of Galaxies”. In: *The Astrophysical Journal* 444, p. 532. DOI: `10.1086/175627` (cit. on pp. 9, 13).

Widrow, Lawrence M. (Jan. 2002). “Origin of galactic and extragalactic magnetic fields”. In: *Reviews of Modern Physics* 74.3, pp. 775–823. DOI: `10.1103/RevModPhys.74.775`. arXiv: `astro-ph/0207240 [astro-ph]` (cit. on p. 48).

Wilczek, F. (Jan. 1978). “Problem of strong P and T invariance in the presence of instantons”. In: *Physical Review Letters* 40.5, pp. 279–282. DOI: `10.1103/PhysRevLett.40.279` (cit. on p. 8).

Wittman, David, Nathan Golovich, and William A. Dawson (Dec. 2018). “The Mismeasure of Mergers: Revised Limits on Self-interacting Dark Matter in Merging Galaxy Clusters”. In: *The Astrophysical Journal* 869.2, 104, p. 104. DOI: `10.3847/1538-4357/aaee77`. arXiv: `1701.05877 [astro-ph.CO]` (cit. on p. 15).

Zwicky, F. (Jan. 1933). “Die Rotverschiebung von extragalaktischen Nebeln”. In: *Helvetica Physica Acta* 6, pp. 110–127 (cit. on p. 4).

Declaration of Authenticity

This thesis is my original work and has not been previously submitted for an examination that has led to the award of a degree.

To the best of my knowledge and belief, this thesis contains no material previously published or written by another person except where due reference is made.

Munich, September 24th, 2021